

Systematic Framework for Teleoperation with Haptic Shared Control

Smisek, Jan

DOI

[10.4233/uuid:e7d8b0d5-8d7a-4d68-b106-c37f30d455a4](https://doi.org/10.4233/uuid:e7d8b0d5-8d7a-4d68-b106-c37f30d455a4)

Publication date

2017

Document Version

Final published version

Citation (APA)

Smisek, J. (2017). *Systematic Framework for Teleoperation with Haptic Shared Control*. [Dissertation (TU Delft), Delft University of Technology]. <https://doi.org/10.4233/uuid:e7d8b0d5-8d7a-4d68-b106-c37f30d455a4>

Important note

To cite this publication, please use the final published version (if applicable).
Please check the document version above.

Copyright

Other than for strictly personal use, it is not permitted to download, forward or distribute the text or part of it, without the consent of the author(s) and/or copyright holder(s), unless the work is under an open content license such as Creative Commons.

Takedown policy

Please contact us and provide details if you believe this document breaches copyrights.
We will remove access to the work immediately and investigate your claim.

Systematic Framework for Teleoperation with Haptic Shared Control

Jan Smíšek



SYSTEMATIC FRAMEWORK FOR TELEOPERATION WITH HAPTIC SHARED CONTROL

SYSTEMATIC FRAMEWORK FOR TELEOPERATION WITH HAPTIC SHARED CONTROL

Proefschrift

ter verkrijging van de graad van doctor
aan de Technische Universiteit Delft,
op gezag van de Rector Magnificus prof. ir. K. C. A. M. Luyben,
voorzitter van het College voor Promoties,
in het openbaar te verdedigen op woensdag 12 april 2017 om 15:00 uur

door

Jan SMÍŠEK

Master of Science in Systems and Control,
Czech Technical University in Prague, Tsjechische Republiek,
Master of Science with a Major in Space Technology,
Luleå University of Technology, Zweden,
geboren te Městec Králové, Tsjechische Republiek.

Dit proefschrift is goedgekeurd door de

promotor: Prof.dr.ir. M. Mulder

copromotor: Dr.ir. M.M. van Paassen en Dr.ir. A. Schiele

Samenstelling promotiecommissie:

Rector Magnificus,

Prof.dr.ir. M. Mulder,

Dr.ir. M.M. van Paassen,

Dr.ir. A. Schiele,

voorzitter

Technische Universiteit Delft, promotor

Technische Universiteit Delft, copromotor

Technische Universiteit Delft, copromotor

Onafhankelijke leden:

Prof.Dr.-Ing. F. Flemisch,

Prof.dr. A.M.L. Kappers,

Prof.dr. H. Nijmeijer,

Prof.dr. F.C.T. van der Helm,

Fraunhofer FKIE

Vrije Universiteit Amsterdam

Technische Universiteit Eindhoven

Technische Universiteit Delft

Reservelid:

Prof.dr.ir. J.A. Mulder,

Technische Universiteit Delft



This thesis was carried out to large parts and conceptualized jointly with the Telerobotics and Haptics Lab of the European Space Agency.

This research was supported by the Dutch Technology Foundation STW (H-Haptics research project 12161), which is part of the Netherlands Organization for Scientific Research (NWO), and which is partly funded by the Ministry of Economic Affairs.

Keywords: Teleoperation, shared control, communication delay, haptics

Printed by: Ipskamp Printing

Front: ESA Interact demonstrator rover operating on an engineering model of the Schiaparelli EDM Mars lander (design by Emiel den Exter).

Back: The author using the Haptics-1 setup (ESA Telerobotics and Haptics Lab) inside the ISS Columbus module mockup.

Copyright © 2017 by J. Smisek

ISBN 978-94-028-0612-0

An electronic version of this dissertation is available at
<http://repository.tudelft.nl/>.

SUMMARY

Systematic Framework for Teleoperation with Haptic Shared Control

Jan Smíšek

Teleoperation – performing tasks remotely by controlling a robot – permits the execution of many important tasks that would otherwise be infeasible for people to carry out directly. Nuclear accident recovery, deep water operations, and remote satellite servicing are just three examples. Remote task execution principally offers two extremes for control of the teleoperated robot: *direct telemanipulation*, which provides flexible task execution, but requires continuous operator attention, and *automation*, which lacks flexibility but offers superior performance in predictable and repetitive tasks (where the human assumes a supervisory role). This dissertation explores a third option, termed *haptic shared control*, which lies in-between these two extremes, and in which the control forces exerted by the human operator are continuously merged with ‘guidance’ forces generated by the automation. In a haptic shared control system, the operators continually contribute to the task execution, keeping their skills and situational awareness. It is common practice to design the haptic shared control systems heuristically, by iteratively adjusting them to the satisfaction of the system designer, primarily based on human-in-the-loop experiments.

In this dissertation, we aim to improve this design and evaluation process. Our goal is to follow a system-theoretic approach and formalize the design procedures of haptic shared control systems applied to teleoperation. Such a formalization should provide designers of future HSC systems with a better understanding and more control over the design process, with the ultimate goal of making the HSC systems safer, easier and more intuitive to use, and overall to perform better.

The research goal of this dissertation has been divided into three parts:

- (1) *Develop methods to allow coping with operator-related uncertainties associated with operator reaction to human-machine goal conflicts and external disturbances.*

Throughout the dissertation, the response of operators on the haptic guidance forces was found to be of significant influence. The operator and the automatic system share control over the task on a common control interface. Consequently, the effects of the haptic forces applied on the master device strongly depend on the neuromuscular admittance setting of the operator’s limb holding the interface, and a systematic method was sought to select an optimal scaling of the haptic guidance forces. To accomplish

this, a new methodology to identify the desired neuromuscular setting of an operator and use it for haptic shared control design was presented and validated. The proposed system minimizes the required operator physical workload and also improves situation awareness, compared to haptic settings that ignore the neuromuscular system.

Scaling of the haptic guidance forces determines the level of control authority that the automatic guidance system has over tasks. In real cases, tasks can change, in reaction to external disturbances, or internally, due to goal conflicts between the support system and the human operator. Therefore, one fixed level of the guidance scaling will likely be insufficient, and adaptation of the control authority is necessary to better facilitate this variability. To this end, an adaptable authority guidance scheme, based on the operator's grip force, has been proposed, and two opposite approaches to trade the control authority are tested – increasing versus decreasing guidance strength with operator grip force. Results show that the novel grip-adaptable method allows operators to increase their performance over manual control, and over a haptic shared control system with weak guidance force scaling. At the same time, the method substantially reduces the operator physical control effort required to cope with conflicts and disturbances.

- (2) *Reduce the teleoperation system-related uncertainties caused by inaccurate knowledge of the remote environment geometry and communication delays.*

In teleoperated contact tasks, the task environment naturally constrains the operation. Haptic shared control systems base their provided support on the available geometrical models of these task environments. However, in practice, these models can be an inaccurate representation of the actual task and objects, resulting in error modes. So far, this research direction, although extremely relevant, has been relatively neglected, with only a few empirical works analyzing the effects of these inaccuracies using human-in-the-loop experiments. Therefore, a system-theoretic method is developed in this thesis, to study the consequences of these inaccuracies on the teleoperation system itself. A novel system description – extending a widely used framework presented by Dale Lawrence – is proposed to quantify the effects of the inaccuracies on task safety and performance. Interaction of the natural force feedback (e.g., feedback force based on the slave end-effector force sensor) with the haptic guidance force was analyzed. It was found that this interaction is nontrivial and possibly of a large practical importance.

A second aim was to design a shared control system that would support operators in the execution of a teleoperated contact task with severe time delays in the communication channel. To prevent unsafe interactions with the remote environment, the stability of the system has to be ensured, while also mitigating the need for the operator to anticipate the delayed slave reaction. A novel extension of the model-mediated teleoperation principle for rate-controlled systems is proposed, to provide delay robustness especially for extended time delays, between 0.1 and 2 seconds. Instead of directly exchanging the commands and feedback between master and slave, a model of the remote environment is created and continuously updated on the master side. The force feedback information to the operator is then based on this local model, which is by its definition not delayed.

(3) *Develop a unifying framework for analysis of haptic shared control systems.*

In its third part, this thesis concentrates more on the ‘machine’ side of the haptic shared control design problem. Here it aims to formalize haptic shared control to study the effects the operator, the communication channel, and the possible task model inaccuracy can have on the complete system. A unified framework is proposed to address these challenges. The framework allows the analysis of haptic shared control systems applied to all conventional teleoperation architectures, and offers ways to study the effects of the operator and teleoperation system on the overall performance. Theoretical results are supported by numerical simulations and are experimentally verified on a real 6-DOF haptic teleoperation setup.

In this dissertation, experimentally-verified systematic methodologies have been developed to study haptic shared control systems applied in teleoperation.

The main conclusions are:

- (1) The approach of tuning the strength of the haptic feedback on the basis of the ‘relax task’ setting of the neuromuscular system, led to tuning settings that were appreciated by the operators, maintaining satisfactory task performance, with both physical and mental workload reduction.
- (2) An operator grip force-based, adaptable-authority haptic shared controller can increase task performance over an ‘under-tuned’ fixed-authority guidance system. Moreover, the effort of the operator necessary to overcome an incorrect guidance can be significantly reduced with respect to the fixed-authority systems.
- (3) The HSC system guidance forces and the natural feedback forces interact with each other in a nontrivial way, effectively masking potential inaccuracies of the guidance system from the operator, which can be unsafe.
- (4) The presented systematic methods can indeed be used to make accurate predictions about the performance of the studied teleoperator systems with the addition of haptic guidance, as the predictions were confirmed by both numerical simulations and experimental trials.

The following recommendations can be made for future research:

- (a) The currently presented methods should be extended beyond haptic shared control towards an even more general shared control framework, for example by including approaches described in the literature that let the automation directly alter the inputs to the controlled system.
- (b) The applicability of presented findings should be investigated further, in real-life tasks and on the fringes of HSC systems design scope.
- (c) A next step should be to move from the systematic analysis towards ‘systematic design’, i.e., the insights obtained using the presented methods should be applied directly in the design stage to tune the haptic shared controllers.

PREFACE

The motivation for the presented work is to develop haptic shared control support systems for teleoperation that might be used for future robotic space exploration missions. Haptic shared control is an attractive human-machine paradigm applicable to a wide range of fields. This dissertation was created as part of the larger program called Human-centered Haptics (H-Haptics), that explored applying similar principles to other application domains, such as lane keeping systems for car driving, minimally invasive surgical robots, or sub-sea mining. Within this program, the dissertation contributes to the ‘Multimodal Space Robotics Teleoperation for Uncertainty Robustness in Human-Robot and Robot-Environment Variations’ project, which was conceived jointly by Dr. André Schiele and Dr. René van Paassen (dissertation co-promoters). The dissertation was supervised by Prof. Max Mulder (promotor).

The work presented in this dissertation was developed at, and benefited greatly from the expertise, facilities, and support of the Telerobotics and Haptics Lab at the European Space Research and Technology Centre (ESTEC) of the European Space Agency (ESA), and of the Control and Simulation Department, Faculty of Aerospace Engineering, Delft University of Technology.

Parts of the work constituted integral components of the ESA METERON flight project, in which technologies to safely teleoperate a robot located on the ground by an astronaut operator from on-board of the International Space Station were developed and successfully validated.

CONTENTS

Summary	v
Preface	ix
1 Introduction	1
1.1 Introduction to teleoperation	1
1.1.1 Stability and performance of teleoperation systems	3
1.1.2 A shifting view of teleoperation system performance	4
1.1.3 Shared control	5
1.2 Open problems	7
1.2.1 Uncertainty in the operator	7
1.2.2 Uncertainty in the teleoperation system	9
1.2.3 Systematic approach.	9
1.3 Motivation, goal, and research approach	10
1.4 Dissertation outline.	12
1.5 Research contributions and limitations	14
I Operator related uncertainty	19
2 Neuromuscular system based tuning of haptic shared control	21
2.1 Introduction	23
2.2 Neuromuscular based tuning of HSC systems.	24
2.2.1 UAV collision avoidance system and previous work	24
2.2.2 Properties of the human neuromuscular system	25
2.2.3 Neuromuscular admittance based tuning method	27
2.2.4 NMS related tuning choices	27
2.2.5 Identifying intrinsic neuromuscular system admittance	28
2.3 Neuromuscular identification experiment	28
2.3.1 Method	28
2.3.2 Results	31
2.4 UAV teleoperation experiment	32
2.4.1 UAV Teleoperation	32
2.4.2 Method	36
2.4.3 Results	40
2.5 Discussion	45
2.6 Conclusion and recommendations	47

3	Adaptable HSC based on operator grip force	49
3.1	Introduction	51
3.2	HSC system with grip-adaptable authority	52
3.2.1	Formalizing the grip-adaptable HSC system	53
3.3	Method	56
3.3.1	Subjects	56
3.3.2	Procedure and task instructions	56
3.3.3	Experimental trial	56
3.3.4	Apparatus	57
3.3.5	Experiment design and Independent variables.	58
3.3.6	Dependent measures	61
3.3.7	Hypotheses	62
3.3.8	Data analysis and visualization	63
3.4	Results	63
3.4.1	Task performance: mean off-track excursion.	64
3.4.2	Operator control effort: steering force	64
3.4.3	Operator control effort: grip force	65
3.4.4	HSC effectiveness: haptic guidance disagreement	65
3.4.5	HSC effectiveness: mean HSC stiffness.	66
3.5	Discussion	67
3.6	Conclusions.	70
II	Teleoperation system related uncertainty	71
4	Geometrical goal uncertainties in a teleoperated contact task	73
4.1	Introduction	75
4.2	HSC in common teleoperation architectures	77
4.3	Theoretical performance evaluation	79
4.3.1	Effects of guidance inaccuracy in constrained task.	79
4.3.2	Effects of operator's arm impedance	80
4.4	Simulation results.	81
4.5	Experimental results	82
4.5.1	Experimental setup	82
4.5.2	Task and results	83
4.6	Discussion	84
4.7	Conclusions.	86
5	Contact task HSC system robust to time delay	87
5.1	Introduction	89
5.2	Approach	90
5.2.1	Decoupling for interaction with unknown environment	90
5.2.2	Master input device and Operator model	91
5.2.3	Slave robot.	91
5.2.4	Slave robot and Environment models	92
5.2.5	Wall position detector	92

5.3	Stability and reference tracking analysis	92
5.3.1	Master-side system	93
5.3.2	Slave-side system	94
5.3.3	Tuning guidelines	96
5.4	Experimental validation on a 1-DOF setup	96
5.5	Conclusion	99

III Framework 101

6	Systematic framework for analysis of HSC systems	103
6.1	Introduction	105
6.2	HSC in a general teleoperation architecture.	106
6.2.1	Teleoperation system model	107
6.2.2	Slave-based and Master-based type HSCs	110
6.2.3	Note on controller structure of the Lawrence scheme	111
6.3	Performance metrics for a HSC system	111
6.3.1	Operator interaction with the HSC system	111
6.3.2	System performance metrics.	113
6.4	Theoretical system performance analysis	113
6.4.1	Steady-state theoretical system performance	114
6.4.2	Discussion of the steady-state performance results	115
6.5	Numerical simulation.	116
6.5.1	Method	116
6.5.2	Simulation results	117
6.6	Experimental validation.	120
6.6.1	Method	121
6.6.2	Experimental results	124
6.7	Discussion	126
6.7.1	Using the master-based guidance increases performance, especially for ‘slow’ and/or distant slave robots.	127
6.7.2	Teleoperation architecture affects the HSC system.	127
6.7.3	Comparison of theoretical vs. experimental values	128
6.7.4	Implications for other application domains	128
6.8	Conclusions.	129
7	Discussion and Conclusions	131
7.1	Recapitulation of research goals	131
7.2	Discussion	131
7.2.1	Scaling of the guidance forces	132
7.2.2	Geometrical goal uncertainties	133
7.2.3	Robustness to communication time delay	135
7.2.4	Towards a unifying systematic approach.	136
7.3	Conclusions.	140
7.4	Recommendations	141

Bibliography	143
Abbreviations	157
Samenvatting	159
Acknowledgements	163
Curriculum Vitæ	165
List of Publications	167

1

INTRODUCTION

In an increasingly complex world of growth, development, expansion and exploration, there are many tasks that are too dangerous, challenging or simply too far away for people to perform directly. Nuclear accident recovery, deep water operations and remote satellite servicing are just three examples. Many of these tasks need to be executed by individuals with special knowledge and skills, however it can be impossible or prohibitively expensive to place these individuals on site. Instead, these tasks can be conducted by robots, which are often stronger, faster, more durable to adverse conditions and more resistant to fatigue than human beings.

However, with the current state of technology, robots unfortunately still lack human problem solving capabilities [1]. Unlike robotic manipulators used on production lines in factories, where the tasks are generally well defined and repetitive, robots involved in maintenance and exploration tasks at distant locations often face unforeseen challenges that cannot yet be reliably automated. One of the limiting factors can be the fact that the available knowledge of the remote environment is insufficient or invalid. For example, a robot used in a nuclear accident recovery task may not be able to reliably operate solely based on pre-accident models of the environment. Parts of the environment that must be interacted with to finish the task (e.g., door knobs, valves) might be damaged to an extent that is beyond the current capabilities of automatic systems. Programming automation for these badly specified tasks would be too costly, possibly error-prone, and simply highly impractical [2].

To overcome this problem, trained human operators can perform the task by remotely teleoperating the robot, using their skills, knowledge, intuition, and talents for improvisation to find a solution. A typical teleoperation system is illustrated in Figure 1.1. The system consists of a master device, which the operator uses as a control input interface, and a controlled slave robot. Commonly, the operator is also provided with visual feedback of the remote scene. These two systems are typically connected through computer-based control systems over a communication channel.

Examples of some existing teleoperation systems are shown in Figure 1.2. The presented systems were developed to carry out very diverse tasks, such as remote area

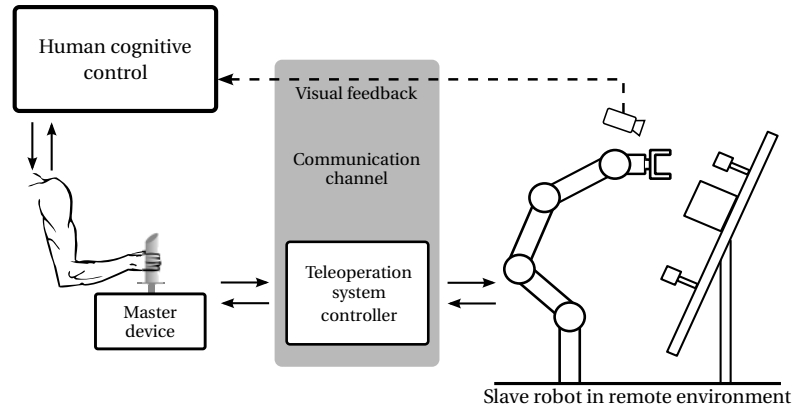


Figure 1.1: Schematic depiction of a teleoperation system. A *human operator* uses the *master device* to issue commands over the *communication channel* to the *slave robot* that interacts with the *task environment*. The human operator is provided with *visual feedback* of the environment and with natural force feedback that is facilitated through the communication channel on the master device (adapted from [3]).

surveillance, in Figure 1.2(a); teleoperated assembly, in Figure 1.2(b); or planetary exploration and remote maintenance, in Figure 1.2(c).

From the operator's perspective, a teleoperation system should ideally behave transparently. In other words, operators should be able to interact with the remote environment as if they were physically there, performing the task directly. This implies that the operators should be, via the teleoperation system, immersed in the remote environment, preferably to such an extent that their perception (at least in modalities relevant for the task) should be unchanged.

This dissertation focuses on the haptic feedback modality of teleoperation systems. For example, if the task at hand involves physical contact with the remote environment, such as in a teleoperated connector mating task, the operator benefits from the addition of (high fidelity) force feedback [4]. The forces exerted by the slave robot on the remote environment need to be accurately fed back to the master side and accurately controlled by the operator. Systems that provide such communication in both directions are referred to as bilateral.

Current control interfaces, however, still have severe practical limitations, and a steep contrast exists between performing a task directly and performing it through a teleoperation system. Considering first the perception of the tele-operators, they mainly have to rely on the visual feedback of the task. The camera view is commonly only provided on a monoscopic display with a restrictive update rate, field of view and resolution. To fully reproduce the feedback forces to the operator, the teleoperation system needs to transmit these forces over the communication channel with a high sampling rate (1000 Hz is often considered as the rule of thumb [5, 6]). Unfortunately, such a high sampling rate is still hard to achieve in distributed scenarios over practical networks [7, 8].

On the remote site, the actions that the tele-operator can perform are dictated by the construction of the slave robot. The dexterity and versatility of a human hand is still superior to current robotic end-effectors. However, robotic end-effectors can contribute

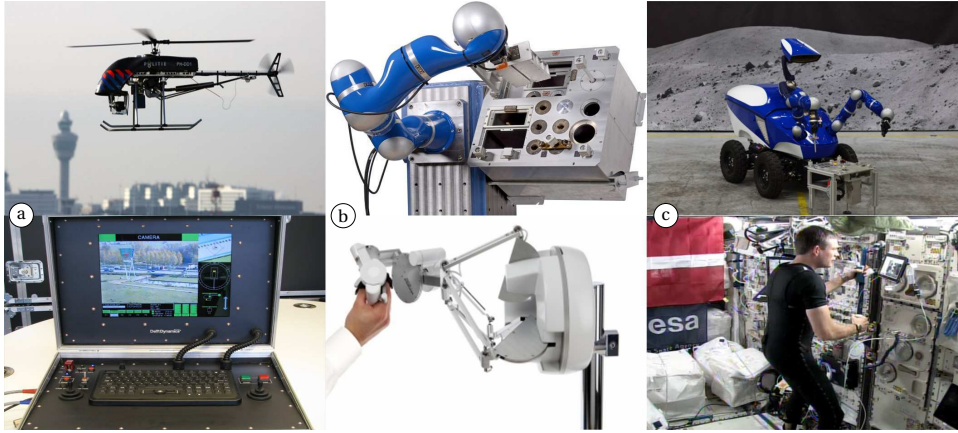


Figure 1.2: Examples of some existing master-slave teleoperation systems: a) a teleoperated unmanned aerial vehicle for surveillance tasks (Delft Dynamics); b) KUKA Lightweight Robot controlled by a Sigma 7 force feedback master device (Force Dimensions and Telerobotics & Haptics Laboratory, ESA); c) Astronaut from on-board the International Space Station controlling the Interact rover on the ground (Telerobotics & Haptics Laboratory, ESA).

capabilities that human hands cannot; motion scaling and vibration suppression can for example offer increased precision. For some specialized tasks, such as laparoscopic surgery, teleoperated task execution is preferred as it is less invasive and more gentle on the patient [9].

Some of these limitations are quickly being eliminated with advancing technology. For instance, fast high-resolution stereoscopic cameras as well as high-quality head-mounted displays are now commercially available and attract attention from the teleoperation community [10, 11]. The bandwidth of the communication channel is also improving rapidly, allowing the transmission of richer visual and force feedback information. However, the communication delay will always remain a fundamental limitation.

In the next section, the performance of teleoperation systems will be discussed in more detail and formalized.

1.1.1. STABILITY AND PERFORMANCE OF TELEOPERATION SYSTEMS

Since the first teleoperated systems were introduced in the field of nuclear research [12], their designers have been striving to improve the fidelity of how the system can represent the remote environment to the operator, i.e., how well the operator can haptically perceive the environment through the teleoperation system [13]. A general teleoperation system is visualized in Figure 1.3. Transparency is one of the widely accepted ways to assess the fidelity of a teleoperated system [14]. Ideal transparency is achieved when there exists equal operator and environment forces $F_h(s) = -F_e(s)$ (the negative sign originates from a customary direction definition) and also equal velocities of the hand and the end-effector on both sides $V_h(s) = V_e(s)$, where s is the Laplace operator. This transparency requirement is traditionally expressed as the equality between the impedance rendered by the master device towards the operator $Z_t(s)$ and the impedance of the re-

mote environment $Z_e(s)$, where:

$$Z_t(s) = \frac{F_h(s)}{V_h(s)}, \quad Z_e(s) = \frac{-F_e(s)}{V_e(s)} \quad (1.1)$$

In 1993, Dale Lawrence proposed a framework to optimize the transparency of a teleoperated system [14], which was later adopted and extended by other researchers in the field [15, 16]. Unfortunately, the achievable level of the system transparency [17], is limited practically due to imperfections of the teleoperation system, such as: practical limitations of the hardware [18], the control methods employed [17], and time delays in the communication channel [18, 19]. Despite progress in the field, teleoperation still remains associated with high workload and sub-optimal situational awareness and safety [20].

1

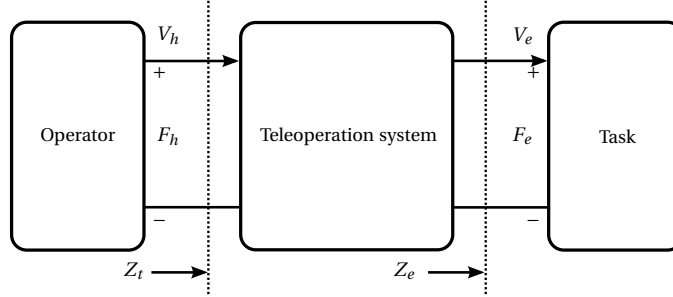


Figure 1.3: General two-port model of a bilateral teleoperation system. A two-port model of a bilateral teleoperation system shows the concept of perfect transparency as the equality of $Z_t = Z_e$ (figure adapted from [14]).

1.1.2. A SHIFTING VIEW OF TELEOPERATION SYSTEM PERFORMANCE

In recent years, the focus has started to shift from improving the teleoperation system itself to improving the performance of the complete teleoperated task. It has been observed that, for a range of practical tasks, once the teleoperation system is reasonably good, further improvements in transparency only provide marginal benefits to the actual task execution. For example, when operators try to insert an electrical connector plug into its counterpart, they need to be able to recognize the initial contact of the plug and the possible misalignment during the insertion. Adding richer feedback information, however, was found (in a simplified experimental setup) to make the insertion neither significantly safer nor faster, nor did it reduce the workload of the operator [20–22].

In line with these findings, teleoperation systems can be viewed not only as fully general systems (where system transparency would be the only metric of interest), but rather as systems used for solving some specific, and at least partially known, tasks. Consequently, teleoperation system designers have started to look for methods that would improve the overall task performance of practical teleoperation scenarios.

The very definition of good task performance is task specific, and so are the various task-optimized methods to achieve it [5, 13]. However, some general concepts can be abstracted, e.g., if the task involves following a reference trajectory, like in car driving, we

can calculate the error between the reference and the actual trajectory, and assess how well the trajectory was actually followed. A practical system should facilitate conducting a task in a timely and safe manner. For instance, in tasks directly involving contact with the environment, such as the aforementioned electrical connector mating, the system should allow careful manipulation with the fine parts, which can be assessed based on the magnitudes of the contact forces. Last but not least, keeping the operators aware of the environment and minimizing their workload, both physical and mental, is of high importance for any practical human-machine system.

A promising approach to achieve higher task performance, through combining the robustness and problem solving capabilities of a human operator with the precision and repeatability offered by automatic control systems –shared control– is described next.

1.1.3. SHARED CONTROL

This dissertation explores an emerging human-machine paradigm, termed *shared control* [23–25], which conceptually lies in between direct telemanipulation and automation. Very much like automatic systems, shared control systems require (some) knowledge of the task to be effective in guiding the operator. If our understanding of the complete task would be perfect, then it might be more desirable to fully automate the task. However, by moving the operators to a supervisory control position, outside the control loop, it becomes more difficult for them to recognize a possible inadequacy of the task model and/or correct any errors the automation might make [26].

In a shared control system, the operators continuously contribute to the task execution, keeping their skills and situational awareness [23]. Moreover, shared control systems can rely on the operator's knowledge of the task, which makes them more robust to changes in the task and environment and often more practically feasible to design than an automated system. For instance, consider an unmanned aerial vehicle (UAV) surveillance tasks in an urban, obstacle-laden environment. Designing a control system that navigates through the environment autonomously, reacting quickly to possible changes of the environment, would be significantly more difficult than providing a shared control system that merely measures the distance to the nearest obstacle and helps the operator steer away from a possible collision. Yet such a simple system has been shown to provide increased safety and operator's situational awareness during the task [27–31].

So far, shared control systems have been shown to offer many benefits in diverse tasks, such as improved car driving precision with reduced workload [32], faster task execution with reduced contact forces exerted on the remote environment and reduced operator workload in assembly tasks [22], and safer UAV teleoperation [33].

In *haptic shared control* – the shared control approach explored in this dissertation, the actions of the automatic system are implemented as additional guidance forces that are added on the master device. With addition of the guidance forces and adaptation of the master device properties, a continuous transfer of control authority between the human operator and the automation is achieved [34]. This is in contrast to the common interaction with automation, in which the operator acts as a supervisor of automation, instructing or permitting automated task execution [1, 35]. This traditional supervisory role of the operator produces a more discrete interaction with automation, with associ-

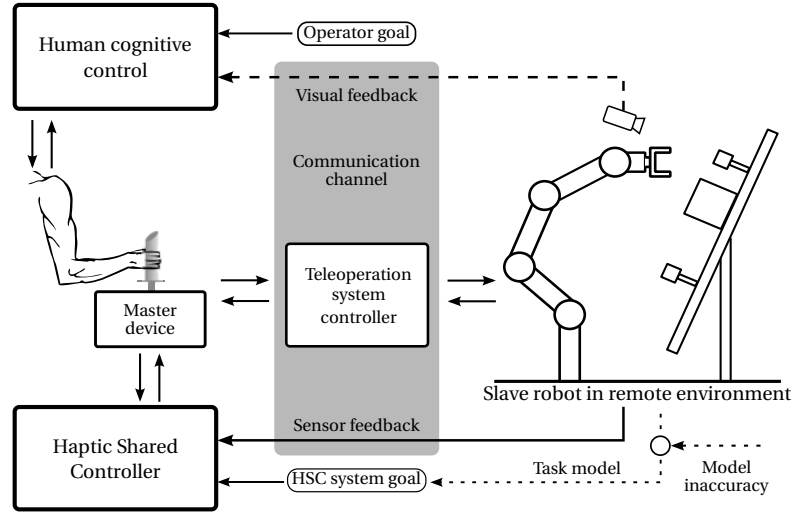


Figure 1.4: Teleoperation system supported by a Haptic Shared Controller. The *Haptic shared controller* provides support in performing the *HSC system goal* based on the available *task model* (that can suffer from *model inaccuracy*). For effective operation the *HSC system goal* has to be in line with the *operator goal*. Figure has been adapted from [22].

ated mode confusion problems (e.g., why does my car slow down?, is the cruise control on or off?).

Haptic shared control (HSC) provides the operator with support in task execution from an automatic system by addition of guidance forces on the master device [36]. Conceptually, it follows the shift from seeking an improvement in how well the operator can sense the environment, to improving how well the operator can actually execute the task. There are many examples of HSC systems applied across different fields which also makes the term definitions rather broad. Within the scope of this dissertation, haptic shared control is understood as *addition of computer-generated forces that are commanded to the master device during teleoperation to facilitate execution of a specific task*.

The control action of the haptic shared controller can be conceptualized as a virtual force field that calculates the guidance force based on the state of the slave robot. Depending on the task, the force field can be designed to provide either attractive or repulsive forces. An example of three tasks is given in Figure 1.5, where the teleoperator is supported in three different ways depending on the slave robot position, as:

- a) *Attractive guidance*. The HSC can take the form of an attractive force field, i.e., of a haptic equivalent of a ‘snap-to-grid’ feature, known from computer graphic programs, and support the operator in aligning perfectly with the object to be grasped [24] (under the absence of model inaccuracies or external disturbances). The same principle was applied in different areas to support lane keeping during car driving [37], and following a flight path using a haptic flight director [38].

- b) *Protected region.* The HSC system can provide operators with a protected region repulsive force field, that makes them aware of the regions of the remote environment that the slave robot should not enter, e.g., fragile electronic modules. This approach is also applied in other application domains, such as UAV and ground vehicle collision avoidance [27, 39].
- c) *Mediated contact.* The virtual force field is programmed to coincide with the environment and provide the operator with forces based on a pre-programmed model (instead of natural feedback forces), essentially mediating the contact through this model. In teleoperation literature this principle is classified as model-mediated or virtual reality-based force feedback [40]. A conceptually similar approach can be applied in telesurgical systems to provide the surgeon with higher ‘haptic contrast’ between tissues with similar degrees of stiffness [41].

In all three examples, the operator is in full control of the robot, while the automatic part aims to improve the task performance by providing support with ‘details’ of the task execution. The distinctive feature of the haptic shared control paradigm is that all inputs of the automatic system are implemented as additional forces on the master device, i.e., the master device position remains the only control command for the slave robot, but is also moved by the haptic shared control system [42]. In this way, the operator can generally be more aware of the actions of the automatic system. Moreover, if the guidance forces are designed to be ‘weaker than the operator’, the guidance can be overruled, leaving the final authority to the operator at all times [34]. By carefully selecting the scaling of the guidance forces, a wide variety of authority trade-offs between the human operator and the automatic system can be realized. On the one hand, very weak guidance forces can, for example, serve as additional information to the operator, merely suggesting what action should be taken according to the automatic part of the system. Conversely, using strong scaling of the guidance force practically creates a fully automatic system, which can work without any inputs from the operator (and the operator would be required to use increased physical effort to overrule it [36]).

1.2. OPEN PROBLEMS

In standard teleoperation system design literature, the system stability and transparency are the predominant focal points. Assumptions about the operator, the environment, and the communication channel are only considered in the system design phase, to ensure system stability and the highest achievable level of transparency for an assumed ‘worst case’ operator, environment and time delay models [13]. The challenge addressed in this dissertation is to utilize these models even further and use them to design optimized haptic shared control systems in a more systematic way.

1.2.1. UNCERTAINTY IN THE OPERATOR

Within the scope of this dissertation, two uncertainties, that originates from the operator executing a teleoperated task with support of an HSC system, are considered:

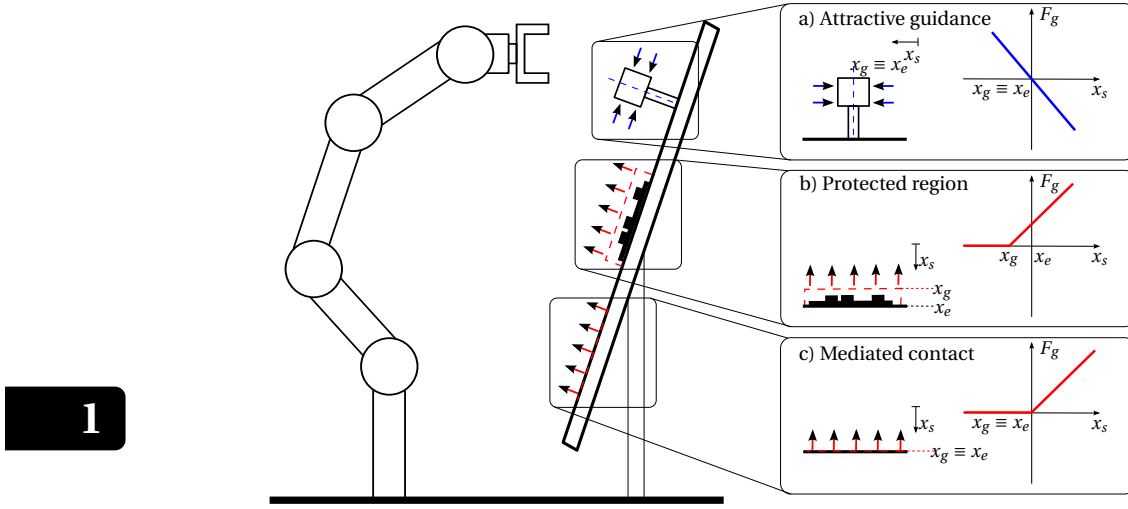


Figure 1.5: Haptic shared control facilitating three conceptually different tasks. The arrows visualize the guidance forces that are calculated based on the slave robot position x_s with respect to the guidance reference x_g and applied as additional guidance forces F_g on the master device. In (a) the attractive force (in blue) supports fine alignment of the robot gripper with the center-line of the object in the remote environment x_e ; in (b) the repulsive force (in red) creates a protected area in a safe distance from x_e , where the slave robot should not enter; in (c) the repulsive force is located on the edge of the environment (at position x_e), essentially providing a model-mediated alternative for the natural force feedback.

UNCERTAINTY IN THE OPERATOR'S NEUROMUSCULAR SYSTEM

The operator and the automatic system share control over the task on a common control interface. Consequently, the effects of the haptic forces applied on this control interface (i.e., the displacement of the master device) strongly depend on the neuromuscular admittance setting of the operator's limb holding the interface and thus an HSC ideally needs to be designed to match this setting. Operators can achieve a wide range of neuromuscular settings [43]. For instance, the operator can follow the guidance force by holding the master device compliantly, or in contrast, the operator can resist the guidance by stiffening up the arm to enforce his/her control inputs. Both situations can be expressed and investigated as (extreme) adaptations of the **operator neuromuscular system**.

UNCERTAINTY IN THE OPERATOR'S GOAL

For a haptic shared control system to be effective, the higher-level *operator goal* needs to be in accordance with the *HSC system goal*, otherwise a **goal conflict** occurs. In other words, providing support to the operator can become counterproductive if the operator has a very different preference on how the teleoperated task should be executed (or even which task is desired).

For example, in HSC systems designed to support lane keeping while driving a car, the automatic system's goal might be to help the driver to follow the centerline of the road [37]. However, it is worth asking, how would the whole human-car system react, if the automation sensor would suddenly malfunction and 'pick-up' a parallel lane? Such

conflicts in the control goals are detrimental to task performance and often lead to lower user acceptance of the system due to increased workload [34, 37, 44].

1.2.2. UNCERTAINTY IN THE TELEOPERATION SYSTEM

In addition, two uncertainties that relate to the teleoperation system are considered:

UNCERTAINTY IN THE TASK MODEL

If haptic guidance is used to support a contact task, like mating an electrical connector, its efficiency strongly depends on the quality of the reference trajectory that an operator is supposed to follow. The guidance system should support the operator with fine alignment prior and during the mating task. However, if the reference is based on an inaccurate *task model* of the real environment elements, for example due to incorrect sensor calibration, the effectiveness of the guidance provided to the operator is reduced, severely limiting the achievable performance of the teleoperated task [45, 46]. In this dissertation, such discrepancies between the real environment and its model are referred to as the **geometrical goal uncertainty**.

UNCERTAINTY IN THE COMMUNICATION CHANNEL

If the operator and the controlled robot are physically located far apart, the teleoperation becomes more difficult due to associated time delays. The time delays faced by current distributed teleoperation systems can range from tens of milliseconds for terrestrial applications within one country to hundreds of milliseconds when a satellite relay network is used [8, 47]. In shared communication channels, such as the Internet or GSM-based connections, varying communication delays are common. Dedicated ‘point-to-point’ communication channels can be used to keep the communication delay at least constant, however, these point-to-point connections are expensive and rare [48].

The **time delay** in bilateral teleoperation is challenging on two levels. First, from the system point of view, even a small time delay in the order of tens of milliseconds in the closed loop feedback system jeopardizes the system stability, and needs to be accounted for by an appropriate controller design method [18, 19]. The majority of current methods essentially adds damping in some way to the system and lowers the scaling of the feedback forces reflected to the operator. Unfortunately, this degrades the perceived realism of the remote environment, e.g., stiff objects are perceived as ‘spongy’ [14].

Second, the operator, in order to compensate for the delay, needs to anticipate the reaction of the teleoperated system on the input commands. Often the operator needs to rely on the visual feedback and control the robot in a ‘move-and-wait’ fashion, which increases operator workload and leads to longer task completion times [1]. This problem becomes even more challenging if the task involves contact, like mating a connector. The visual information is then often insufficient and the operator has to control the robot based on the delayed force feedback. It becomes difficult to correctly judge and control the amount of force the slave robot exerts on the environment, risking damage to the environment or to the robot [49].

1.2.3. SYSTEMATIC APPROACH

Currently, methods to design HSC systems are mainly heuristic and there are no systematic methods that explicitly take the uncertainties outlined in the previous section into

account. The majority of available research on the topic provides rather ad hoc solutions for specific problems and relies on adjusting the haptic shared control system design parameters in a trial-and-error fashion, often based on experimental human factors studies for specific tasks. This is a costly and time-exhausting method.

The main aim of this dissertation is therefore to formalize the design process of HSC systems and to provide a more systematic methodology, as an alternative to the heuristic design approach, newly based on the knowledge of the operator, the environment, and the communication channel. The *systematic approach* is based on using control-theoretic models of the aforementioned elements in a generic teleoperation system. Such an approach would allow the analysis and design of HSC systems with a reduced need to conduct human-in-the-loop experiments as a part of the design process.

1

1.3. MOTIVATION, GOAL, AND RESEARCH APPROACH

The open problems outlined above are reflected by the main research question:

Main research question

How to systematically analyze and design a haptic shared control system for bilateral teleoperation that is operating in the presence of uncertainties in the operator, in the environment and in the communication channel?

The main research question is addressed by considering the following sub-questions, each of which is directly motivated by the research challenges outlined in the previous section. The sub-questions are then discussed in more detail, together with the corresponding research approach and related literature. For easier navigation in the dissertation the sub-questions are listed together with corresponding dissertation chapters.

Research sub-questions

- (1) How can the knowledge of an operator's **neuromuscular system** be used in the design of a haptic shared controller? (Chapter 2)
- (2) How can we systematically model, address, and mitigate possible **goal conflicts** between the operator and the automatic part of a shared control system? (Chapter 3)
- (3) What systematic description allows to analyze **geometrical goal uncertainties** hindering haptic shared control in bilateral teleoperation? (Chapter 4)
- (4) How to design a shared control system to be robust against severe **time delays** in the communication channel? (Chapter 5)

The **first sub-question** is related to finding a systematic method to select an optimal tuning of the haptic shared control system based on the knowledge of the **operator neuromuscular system**. Knowledge of the neuromuscular system setting can be used

to understand and optimize the interaction between the operator and the haptic shared control system [50–53]. Some of these settings are of special significance and offer advantages, such as ensuring that the operator is still actively involved in the task execution by designing the system to provide only relatively weak support [34].

Here, a two-stage approach was followed. First, we seek a formal methodology to identify the desired neuromuscular admittance setting of an operator. The design objective is a system that minimizes the required physical workload of the operator, by making the system function correctly when the operator limb is relaxed. Second, a way of how to include this knowledge into the HSC system architecture is proposed and validated in a human-in-the-loop experiment.

The **second sub-question** is related to addressing the **goal conflict**, in other words, the possible goal disagreement between the operator and the HSC system.

In this dissertation, a system-theoretical approach is offered to study these goal-related conflicts. Moreover, the aim is to provide a way for the operator to resolve the conflict and allow a smooth shift of control authority between the operator and the HSC system. To this end, an architecture based on using the operator's grip force as an additional control input is presented and validated in a human-in-loop study.

The **third sub-question** focuses on creating a systematic description of **geometrical goal uncertainties** impeding haptic guidance systems employed in bilateral teleoperation. So far, the practical effects of these inaccuracies have only been studied in human-in-the-loop experiments [45], however, without a formalization in clear control-theoretic terms.

A system-theoretical approach is used for the teleoperation system itself. A new system description (extending the Lawrence's framework [14]) is proposed and used to quantify the effects of the inaccuracies on task safety and performance. Furthermore, interaction of the natural force feedback with the haptic guidance force is analyzed. The theoretical predictions are compared with simulations and experimentally validated.

The **fourth sub-question** focuses on providing robustness to the **time delay** in the communication channel (especially in cases of long delays, in range from 0.1 to 2 seconds). The envisioned teleoperation system needs to: 1) ensure system stability while maintaining high transparency; 2) alleviate the need of the operator to anticipate the delayed slave reaction; 3) prevent unintended interaction of the slave robot with the remote environment.

These aforementioned requirements are, in this dissertation, addressed by following the concept of model-mediated teleoperation [40]. Instead of directly exchanging the commands and feedback between master and slave, a model of the remote environment is created and continuously updated at the master side. The force feedback information to the operator is based on this local model and is, by its nature, not delayed.

Revisiting the **main question** – it is stated that a novel system-theoretical view is needed to facilitate the analysis and design of haptic shared control systems in the presence of the challenges mentioned above. All four sub-questions are focused on different aspects of the overall problem and offer validated methods to address these. The remaining step is to bring the particular findings together into a systematic framework.

To take this step, in this dissertation, we extend Lawrence's general teleoperation framework [14] by the addition of haptic shared control. The challenges addressed by

the four sub-questions are treated uniformly, using the same system-theoretical description. The benefit of this innovative system description is threefold: First, it allows to explain and quantify the effects of the operator and the system uncertainties on the overall system behavior. Second, the proposed description allows assessing the interaction between the uncertainties themselves and also between the underlying teleoperation system and different methods how the HSC system can be implemented.

1.4. DISSERTATION OUTLINE

The chapters of this dissertation, except for the Introduction and the Discussion and Conclusions chapters, are all based on scientific publications that have been written separately and can, therefore, be read independently from each other. Every chapter starts with a short introduction: both to connect the chapter's content to the rest of the dissertation and to list the original publication(-s) that formed the chapter. The titles of the chapters were re-formulated to strengthen the consistency of the thesis. The sequence of the chapters reflects both the logical and the chronological order.

The dissertation consists of seven chapters and is divided into three parts, as illustrated in Figure 1.6. In **Part 1**, the dissertation describes the design and validation of haptic shared control systems taking the operator related uncertainties explicitly into account. In **Part 2**, the challenges associated with teleoperation system are described together with methods to increase system robustness against these uncertainties. In **Part 3** the findings of all previous chapters are conceptually combined into a systematic framework. Finally, **Chapter 7** provides a general discussion and conclusions.

PART 1: OPERATOR RELATED UNCERTAINTY

CHAPTER 2 - NEUROMUSCULAR-SYSTEM-BASED TUNING OF HSC SYSTEMS

The chapter describes the design, tuning and validation of a neuromuscular analysis based design method for haptic shared control systems on a case study of an unmanned aerial vehicle collision avoidance system. Conceptually, the system provides a *protected region* type HSC, see Figure 1.5(b). The aim of the chapter is to provide a systematic method to find an optimized haptic guidance system authority setting that requires the operator to apply only minimal physical effort during teleoperation. By doing so the chapter advocates the use of a neuromuscular system (NMS) analysis based tuning as opposed to 'heuristic tuning', i.e., tuning based on adjustment of the control gains to yield higher performance (e.g., increased safety in case of a collision avoidance system). The chapter reports results of a two-step human-in-the-loop experiment, when ten subjects participated in a NMS identification experiment and their data were used to calculate the HSC system tuning gains. After that, a different group of twelve subjects performed a simulated unmanned aerial vehicle control validation experiment.

CHAPTER 3 - ADAPTABLE HSC BASED ON OPERATOR GRIP FORCE

The chapter explores haptic guidance systems beyond using only one fixed setting (as is the case in Chapter 2), namely by making the HSC system adaptable based on the operator grip force. The problem is studied on a trajectory following task supported with *attractive guidance* type HSC, see Figure 1.5(a). The chapter describes how this proposed

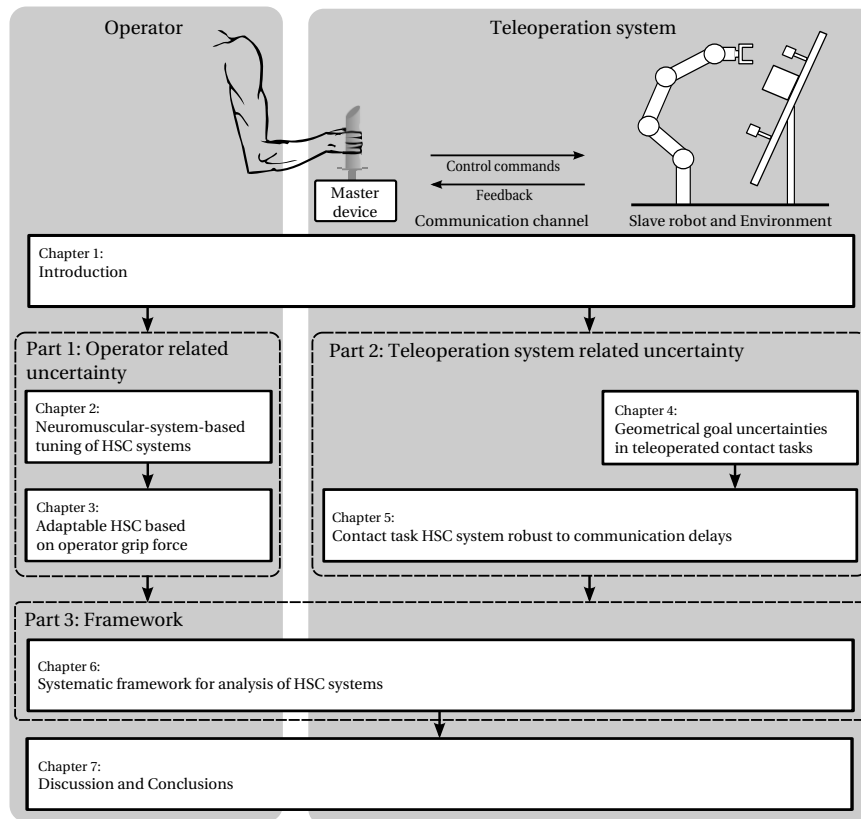


Figure 1.6: Visualized outline of the dissertation.

system behaves in situations in which there is a disagreement between the human operator and the automatic system, and makes theoretical predictions how operators could efficiently use this additional control input to the system. The proposed adaptable HSC system is evaluated in a human-in-the-loop study and compared with a traditional ‘fixed-setting’ controller.

PART 2: TELEOPERATION SYSTEM RELATED UNCERTAINTY

CHAPTER 4 - GEOMETRICAL GOAL UNCERTAINTIES IN A TELEOPERATED CONTACT TASK

The chapter describes the specific challenges related to using a position reference based haptic guidance to provide support in a contact task, specifically to support peg-in-hole insertion with *attractive guidance* type HSC, see Figure 1.5(a). Such an HSC system is used to support the operator to precisely align the peg prior and during the insertion into the hole. It is highlighted how the inevitable geometrical inaccuracies of the guidance reference models negatively interacts with the natural force feedback in bilateral teleoperation. The chapter offers a system-theoretical analysis of the problem by ex-

tending the Lawrence framework [14]. The findings are confirmed by simulation and also experimentally on a 6-DOF master-slave teleoperation system.

CHAPTER 5 - CONTACT TASK HSC SYSTEM ROBUST TO TIME DELAY

The chapter introduces a haptic shared control method created specifically to provide support in contact tasks, by providing *mediated contact*, see Figure 1.5(c). Using a force sensor on the slave robot, the system continuously searches for contact with the remote environment and updates the environment model based on this measurement. The proposed method is designed to be robust against guidance model geometrical inaccuracies that were described in Chapter 4. Moreover, by communicating the task model instead of the force measurements directly, the proposed method is inherently robust to delays in the communication channel. The stability and performance of the proposed method is theoretically analyzed and compared against measurements on a practical 1-DOF master - slave teleoperation system with a simulated time delay of 2 seconds.

1

PART 3: FRAMEWORK

CHAPTER 6 - SYSTEMATIC FRAMEWORK FOR ANALYSIS OF HSC SYSTEMS

The chapter aims to connect the previous chapters into one system-theoretical framework. An extension of Lawrence's general teleoperation architecture [14] developed in Chapter 4 (here termed *slave-based* guidance) is further extended in this chapter by an additional haptic shared controller channel that is conceptually based on the model-mediated teleoperation principles studied in Chapter 5 (termed *master-based* guidance). The presented system-theoretical framework can be used to study teleoperation systems with an *attractive* HSC. It can be used to explore the effects of operator's neuromuscular setting (Chapter 2), operator's authority in case of goal conflicts (Chapter 3), geometrical goal uncertainties (Chapter 4) and communication time-delays (Chapter 5), using one systematic description. The theoretical findings are supported by numerical simulations and experimentally verified on a 6-DOF master-slave teleoperation system.

CHAPTER 7 - DISCUSSION AND CONCLUSIONS

In the final chapter, the findings presented in the preceding chapters are discussed and an attempt is made to connect them together and draw unified conclusions and recommendations.

1.5. RESEARCH CONTRIBUTIONS AND LIMITATIONS

This dissertation focuses on developing a system-theoretical approach to derive a generic bilateral control framework that includes haptic shared control as an additional channel in the system description. We build on, and add to, a body of literature that addresses the challenges related to the aims of this dissertation by means of human factor studies. The proposed framework allows to identify and systematically address practical challenges that reduce the performance and user acceptance of a teleoperated system. Strategies were investigated to mitigate the influence of HSC controller model inaccuracies and communication time delays, enhancing user performance over time-delayed and error-prone systems, by implementing static and flexible user authority schemes. The main contributions of this dissertation are as follows:

- We present a novel neuromuscular analysis-based design method for haptic shared control systems, on a case study of an unmanned aerial vehicle collision avoidance system. The presented approach is the first HSC design method that considers a 2-DOF NMS setting model (roll and pitch) and explicitly accounts for the effects that a spring-centered control interface has on the operator's NMS setting. The method is validated in a human-in-the-loop experiment.
- We present an HSC system that is the first to allow its control authority to be adaptable based on the operator grip force. Two methods to modulate the control authority depending on the grip force are given. The dissertation describes how to stimulate disagreement between the human operator and the automatic system, and offers a novel methodology to make predictions on how operators could efficiently use the novel adaptability of the HSC system to resolve the disagreement. The method is validated in a human-in-the-loop experiment, and the theoretically developed predictions match the experimental results.
- We propose a new extension of the Lawrence general teleoperation framework to allow system-theoretical analysis of geometrical goal uncertainties of HSC systems supporting teleoperated contact tasks. To the best of our knowledge, this is the first systematic method to study the effects of these geometrical uncertainties. The method can be directly applied to a large set of common teleoperation architectures. The findings are confirmed by simulation and validated experimentally on a 6-DOF master-slave teleoperation system.
- We present a novel extension of the model-mediated teleoperation approach to rate input commands. The stability and performance of the proposed method are theoretically analyzed, and design trade-offs with corresponding tuning guidelines are provided. The method is experimentally validated in 1-DOF.
- We present a systematic framework to study attractive guidance HSC systems applied in teleoperation, which can be used to analyze all common teleoperation architectures that can be modeled using Lawrence's framework [14]. We identify and formalize two HSC implementations prevalent in the literature, and coin them by terms *slave-* and *master-based* guidance types. The presented framework is the first to systematically compare those guidance types and quantify the control authority retained by the operator and the remaining system transparency. The findings are confirmed by simulation and validated experimentally on a 6-DOF master-slave teleoperation system.

Furthermore, the research findings described in this dissertation were directly applied in two space flight projects conducted by the Telerebotics and Haptics Laboratory of the European Space Agency (ESA). The projects led to several teleoperation experiments conducted by selected astronauts from on-board the International Space Station (ISS). The experiments aimed to explore the limits of state-of-the-art teleoperation systems. A geostationary satellite relay link 'Tracking and Data Relay Satellite System' (TDRSS), with an average round-trip time delay of 850 ms, served as a communication channel between Earth and ISS. The *mediated contact* HSC method developed in Chapter 5 was successfully used in the Interact experiment [54] to aid a peg-in-hole insertion

task. The Interact demonstration of an end-to-end robot control with force-feedback from space took place between the ISS and the ESA European Space Research and Technology Centre (ESTEC) at Noordwijk, NL on the 7th of September 2015 (astronaut Andreas Mogensen, ESA). In parallel, an extension of that method was used in the Haptics-2 experiment [8], to facilitate a high fidelity force feedback teleoperation, evaluated during a stiffness discrimination task. The Haptics-2 demonstration of advanced teleoperation between space and ground took place at several dates during June and August 2015 (with astronauts Terry Virts, NASA and Kimiya Yui, JAXA).

The scope of the dissertation, however, could not capture all elements related to a complete teleoperation system. In the following we list some relevant challenges that were not addressed in this dissertation:

1

- (1) The dissertation focuses on the haptic modality (i.e., on the feedback forces). A functional visual feedback was assumed in the whole dissertation and it was present in all human-in-the-loop experiments. However, the effects of visual feedback (or the option of using other modalities, e.g., audio feedback) on task performance were not studied. For an example experimental investigation of the visual feedback influence on task performance, the reader can refer to [55, 56].
- (2) In Chapter 5, where the presence of time delays in the communication channel are considered explicitly, for the sake of simplifying the analysis, the time delay was assumed to be constant, with no packet loss, packet re-ordering etc. Nevertheless, the feasibility of the proposed methods was demonstrated on practical real-life communication channels (e.g., standard Internet, TDRSS satellite relay link) which exhibited packet loss and re-ordering during the Interact [54] and Haptics-2 experiments [8].
- (3) Conflicts between the operator and the HSC system were, in this dissertation, studied as either originating from an incorrect scaling of the haptic cues or from goal-related conflicts. However, another possible source of conflicts lies on the task execution level. In other words, both parties are in agreement on which goal should be executed but they differ in *how*. In Rasmussen's 'Skills, Rules, Knowledge' framework [57], this type of conflict would fall into the 'rules' category. In the car driving example, this task execution conflict could manifest as the HSC system supporting a different path through a curve than is the driver's preference. The reader should refer to [58] for recent insights on this topic and for a possible solution [59].
- (4) The haptic shared control approach can also be used as a training tool to prepare future operators for their tasks [60, 61], but also in non-teleoperated context, e.g., as a calligraphy trainer [62] or to teach general dynamical systems control strategies [63]. However, this function of the HSC systems is not explored.
- (5) Some of the methods presented in this dissertation were described on One-Degree-Of-Freedom examples. For Chapters 2, 3, and 4 this was done merely to simplify the exposition and the presented methods could be directly scaled to higher-DOFs. However, for Chapter 5, extension to a higher-DOF case is not straightforward. Besides a few exceptions [64] this is in line with the available literature on model-mediated teleoperation. However, both methods (directly in their one-DOF implementation)

successfully facilitated their intended tasks during the Haptics-2 and Interact flight experiments conducted by the ESA.

- (6) The model-mediated [40] approach was used to maintain stability of the teleoperation system despite time delay in the communication channel. This approach was not directly compared with other, more traditional, approaches (e.g., time domain passivity [18, 65], wave variables [19], or using energy-based controllers [66]). However, the focus here was on providing high performance feedback over long time delays (0.1 - 2 seconds), which is beyond the capabilities of these traditional methods.
- (7) The aim of this dissertation is to provide a better understanding of haptic shared control systems employed in bilateral teleoperation, specifically in the presence of the aforementioned practical challenges related to the operator, the environment, and the communication channel. The developed methods allow the analysis of HSC systems while taking these challenges into consideration, and proposes some possible techniques to address them.

The analytic methods in Chapters 3, 4, and 6 all constitute novel and successful attempts to address the respective challenges in a general and systematic way. In Chapters 2, 3, 5, and 6, methods providing particular solutions to these challenges are presented and validated in laboratory experiments. However, the dissertation does *not* claim to provide a complete and fully general procedure to overcome all these challenges (developing such a procedure is left for future research).

I

OPERATOR RELATED UNCERTAINTY

2

NEUROMUSCULAR SYSTEM BASED TUNING OF HAPTIC SHARED CONTROL

*The chapter describes the design, tuning and validation of a neuromuscular analysis based design method for haptic shared control systems, on a case study of an unmanned aerial vehicle collision avoidance system (a **protected region** type HSC). The aim of the chapter is to provide a systematic method to find an optimal haptic guidance system authority setting; with the system being optimal in the sense that it requires the operator to apply only minimal physical effort during teleoperation. To this end, the chapter advocates the use of a neuromuscular system analysis based tuning as opposed to 'heuristic tuning', i.e., tuning based on adjustment of the control gains to yield higher performance (increased safety of the collision avoidance system).*

This chapter is based on the following publications:

- Jan Smisek, Emmanuel Sunil, Marinus M. van Paassen, David Abbink and Max Mulder, "Neuromuscular-System-Based Tuning of a Haptic Shared Control Interface for UAV Teleoperation", IEEE Transactions on Human-Machine Systems, 2016 (in press)
- Emmanuel Sunil, Jan Smisek, Marinus M. van Paassen and Max Mulder, "Validation of a Neuromuscular Analysis Based Tuning Method for Haptic Shared Control Systems", IEEE International Conference on Systems, Man, and Cybernetics, San Diego, 2014
- Jan Smisek, Marinus M. van Paassen, David Abbink and Max Mulder, "Neuromuscular analysis based tuning of haptic shared control assistance for UAV collision avoidance", IEEE World Haptics Conference, Daejeon, 2013

CHAPTER SUMMARY

Haptic guidance is a promising way to support Unmanned Aerial Vehicle (UAV) operators, but the design of haptic guidance forces is often heuristic. This chapter describes the design and experimental validation of a systematic neuromuscular analysis based tuning procedure for haptic guidance, here applied to haptic collision avoidance system for UAV tele-operation. This tuning procedure is hypothesized to reduce operator workload as compared to current heuristic tuning methods. The proposed procedure takes into consideration the estimated mechanical response of the neuromuscular system (NMS) to haptic cues. A ‘relax task’ setting of the NMS, for which reflexive and muscular activation is minimal, is chosen as the design point for tuning the haptic support, as this setting is expected to yield minimal physical workload. The chapter first presents a neuromuscular identification experiment, performed to estimate the ‘relax task’ admittance of an operator’s arm. The averaged admittance of a group of subjects ($n = 10$) was then used for tuning the haptic shared controller, which was subsequently evaluated in its ability to support different operators ($n = 12$) in a simulated unmanned aerial vehicle surveillance task. Results show that our novel tuning procedure indeed reduces operator workload and also improves situation awareness compared to haptic settings that ignore the neuromuscular system. In fact, it is shown that over-tuning, which frequently occurs for these heuristically tuned systems, leads to even lower user acceptance scores than interfaces without any haptic support.

2.1. INTRODUCTION

In Haptic Shared Control (HSC) systems, a human operator and an automatic controller share control of a dynamical process on a common control interface, that serves as the only input to the controlled system [67]. Such design ensures that the operator is continuously informed about the actions of the automation, allowing him/her to stay involved in the decision making process through intuitive haptic interactions [68]. In doing so, HSC has the potential to support operators while mitigating some of the human-machine interaction issues frequently associated with automated control systems, such as loss of skills and situational awareness [67–69].

Implementing the actions of the automatic system as additional guidance forces on the control interface allows the operator to decide how to react to these. The operator can do this in two ways: by consciously generating a force to give way or counteract the guidance forces, but also by intentionally changing the neuromuscular system (NMS) properties of the limb interacting with the control interface. In other words, if the operator agrees with the provided automatic's support, he/she can become compliant and give way to the haptic forces. In contrast, if the operator disagrees, he/she can stiffen up to resist the haptic force, effectively overruling the automation. In this manner, the operator can dynamically interact with the automation during the operation [68].

The advantageous adaptability of the operator's neuromuscular system also makes HSC systems challenging to design. To cause the desired control interface position, thereby providing the correct inputs to the controlled system, the HSC system force needs to be correctly scaled to match the instantaneous 'setting' of the operator's arm NMS (i.e., whether the operator's arm is compliant, stiff or in between). Although it may be feasible to estimate the NMS admittance in real-time [70], adapting the HSC system based on adaptation of the operator might lead to undesirable outcomes. For instance, if the operator, by stiffening-up, aims to regain control authority over the controlled system, the automation could adapt to this change by increasing the force scaling, and effectively over-ruling the operator [34]. Therefore, we explored tuning the HSC system to one fixed scaling, that corresponds to a specific (and beneficial) setting of the NMS system. When the operator matches his/her neuromuscular behavior to this expected stiffness, the haptic forces will then cause correctly scaled inputs to the human-in-the-loop system.

It is common practice to heuristically tune this scaling to the satisfaction of the system designer [71]. However, we aim to improve and formalize the tuning process. In our preliminary studies we presented an identification method to measure relax task admittance on realistic haptic control interfaces [53] and then tested its utility in a UAV collision avoidance system [52].

The aim of the chapter is twofold: First, we provide a complete systematic and experimentally validated tuning method that uses the operator's arm relax task setting as the design stiffness. Second, expanding upon our previous studies [52, 53], this research will provide more insight into the interaction of the operators with the haptic cues by investigating the agreement of operators with the provided haptic support and analyzing how this agreement changes based on specific situation during the flight.

We first introduce a haptic collision avoidance system that relies on an artificial force field and explain the available HSC tuning choices based on the attainable settings of

the human NMS, in Section 2.2. Motivation for the relax-task setting based tuning is discussed in detail. We then identify the challenges associated with obtaining (relax task) neuromuscular admittance measurement on a spring-centered control interface and present an appropriate experimental identification procedure in Section 2.3. In Section 2.4, relax task tuning, using the average data from the first experiment, is used in a human-in-the-loop experiment simulating UAV teleoperation, to judge user acceptance of the novel tuning procedure. The chapter concludes with a comprehensive discussion of the results and summarizes the main conclusions, in Sections 2.5 and 2.6.

2.2. NEUROMUSCULAR BASED TUNING OF HSC SYSTEMS

This section introduces a human-centered tuning approach for haptic cues that is based on properties and measurements of the operator's arm NMS. First, the UAV collision avoidance system is introduced. Second, neuromuscular properties relevant to the tuning approach are presented together with the theoretical rationale of the tuning method.

2

2.2.1. UAV COLLISION AVOIDANCE SYSTEM AND PREVIOUS WORK

An interesting application of HSC in aviation is the use of haptic feedback to improve the safety of Unmanned Aerial Vehicles (UAVs) [72]. Previously presented studies augmented the visual feedback from onboard cameras with haptic guidance moments applied on a control interface to help teleoperators in steering a UAV away from obstacles [27, 29–31, 73]. All these studies have indicated that such a system improves the safety of teleoperation, but at the cost of increased workload [27, 74]. Similar issues were also reported from systems implemented in car driving domain [67].

These previous HSC systems were designed heuristically, i.e., the HSC force scaling was found by testing different values in a human-in-the-loop study, until satisfactory performance was achieved. For instance, the primary objective of one of the studies was to improve system safety over pure manual control [75]. To realize this goal, the haptic controller was typically tuned to generate very strong haptic guidance moments. While 'over-tuning' haptic cues improved safety, it also biased control authority towards the automation [74]. Recent research has shown that heuristic tuning can result in disagreements between the human operator and the automation on a the neuromuscular level [50].

The difficulty with heuristic tuning has been attributed to the large adaptation range of the neuromuscular system. It was observed that operators are able to adapt their NMS properties such that performance and overall system stability are satisfactory, regardless of the specific tuning used. However, adaptations to non-optimal settings of the NMS, as is often the case with heuristic tuning methods, causes the haptic cues to be perceived as too strong, resulting in increased user discomfort and workload over time [76].

As a objective for the current study, it was hypothesized that in order to improve user acceptance of HSC systems, it is necessary to tune haptic cues such that workload is reduced, but without sacrificing system safety or human control authority over the automation. The motivation was, building on our preliminary studies [53, 77], to provide a systematic and validated tuning method that would achieve the aforementioned objective, without relying on heuristic tuning.

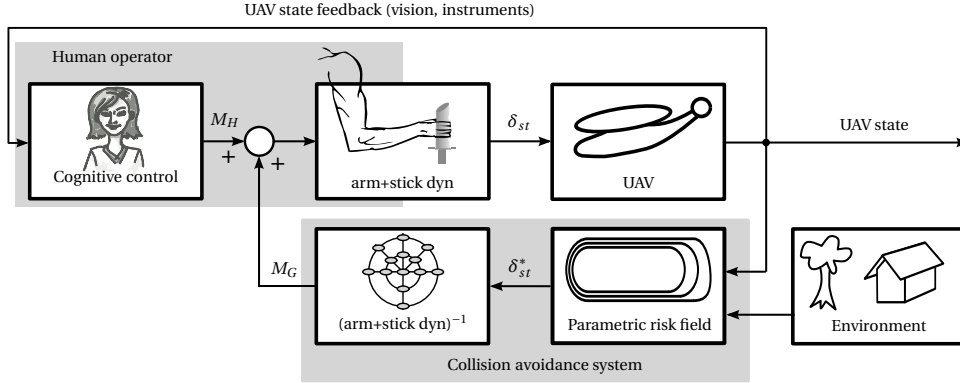


Figure 2.1: UAV teleoperation with a haptic *Collision avoidance system*. Based on the UAV state in the environment, the *Parametric risk field* calculates an optimal collision avoidance maneuver, that is scaled by the inverse arm/stick dynamics to a haptic cue on the control side-stick (based on [53]). A method to appropriately chose this scaling is the focus of the current chapter.

2

A teleoperated UAV scenario, with addition of the collision avoidance system, is illustrated in Figure 2.1. An outer feedback loop to the UAV teleoperator is complemented with an inner haptic feedback loop generated by the collision avoidance system. The operator controls the UAV through the side-stick position δ_{st} . The haptic guidance moment, M_G , and the moment generated by the teleoperator, M_H , act together on the side-stick. The resulting position of the side-stick, δ_{st} , constitutes the sole steering command issued to the UAV.

The collision avoidance system becomes effective only if the UAV flies into a close vicinity of an obstacle. The parametric risk field system scans the environment for obstacles and computes the risk of collision with the corresponding optimal avoidance maneuver [75]. The ‘optimal’ collision avoidance (in the sense of a ‘best’ collision avoidance vector [75]) is achieved with the optimal side-stick position δ_{st}^* . To yield the desired δ_{st}^* , it has to be converted to a properly scaled haptic guidance moment, M_G . The appropriate choice of this particular scaling is the focus of this chapter.

2.2.2. PROPERTIES OF THE HUMAN NEUROMUSCULAR SYSTEM

Neuromuscular system admittance of the operator arm to external (haptic) forces, i.e., the displacement caused by an external force, is an important parameter for designing HSC systems [78]. The intrinsic NMS properties are formed by the contribution of the skeleton (mainly the inertia) and by the contribution of different muscles (the inertia, stiffness and damping) [43]. However, the NMS is highly adaptive, Figure 2.2a, and admittance can be varied over a wide range of values through two physiological mechanisms: fast subconscious spinal reflexes and muscle pair co-contraction [43]. The neuromuscular system uses several sensors located in and near the muscles for its feedback mechanism, such as the muscle spindles and the Golgi Tendon Organs (GTO). The muscle spindles feedback muscle length and muscle velocity and the GTO feed back the force measured in the muscle tendons. The NMS adaptation is achieved by changing the reflex

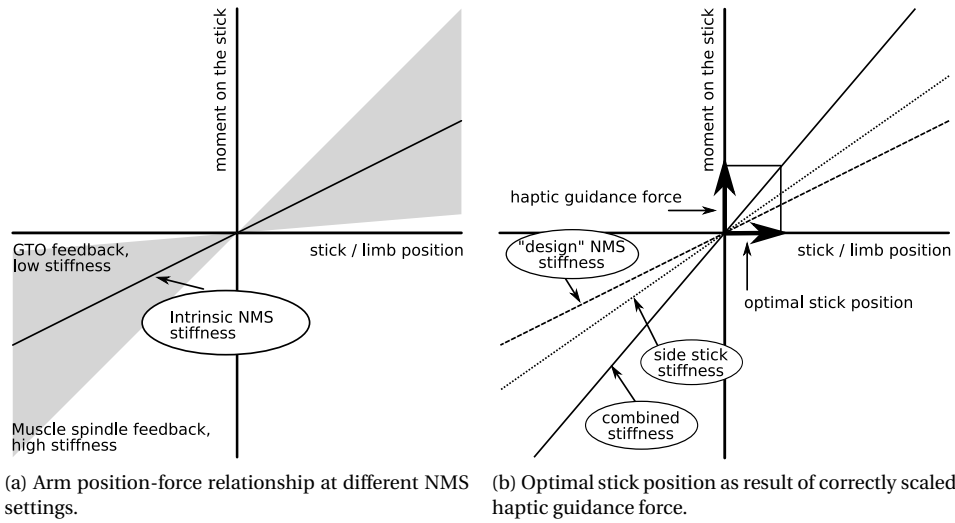


Figure 2.2: Neuromuscular based tuning rationale. Figure (a) illustrates the wide range of arm admittance settings the operator can adopt. The intrinsic stiffness corresponds to relax task situation, when operators do not exert any forces or change their admittance. In (b) the shared control system is tuned to a *design stiffness* which, together with the *side stick stiffness*, forms the *combined stiffness* of the whole system. Figure adapted from [53].

path strength. Stronger muscle spindle feedback produces a position feedback loop that generates a lower admittance (stiffer NMS). The reverse is also possible, stronger GTO feedback produces a higher admittance (less stiff NMS). Effectively, the stiffness of the neuromuscular system can be raised or lowered through the neural feedback [43, 78, 79]. To evoke different NMS admittance settings, humans can be instructed to respond to ex-

Table 2.1: Description of the three neuromuscular task instructions.

Task	Admittance	Description
Force Task (FT)	High	Yield to haptic moments and the motion of control interface
Relax Task (RT)	Medium	Do not react to haptic moments and follow motion of control interface
Position Task (PT)	Low	Resist haptic moments and maintain position of control interface

ternal moments in three distinct ways known in literature as the force, the relax and the position tasks [78], see Table 2.1.

2.2.3. NEUROMUSCULAR ADMITTANCE BASED TUNING METHOD

Haptic guidance moments applied on the control interface are transmitted to the human operator via his/her NMS. Therefore it is necessary to include the response of the NMS to haptic cues when tuning the haptic controller [50, 76]. Effectively, this approach uses the inverse of the combined dynamics of the NMS and of the control interface to compute the haptic guidance force, see Figure 2.2b. Applying this specific haptic guidance force, assuming the operator keeps the same NMS setting, will result in optimal stick position and consequently in a successful avoidance maneuver. Here, the HSC provides mostly low frequency inputs [75, 77] and so the stick/arm inverse dynamics can be considered as stiffness, yielding a guidance control law:

$$\begin{bmatrix} M_{G_p} \\ M_{G_r} \end{bmatrix} = \underbrace{[\mathbf{K}_{\text{NMS}}(\delta_{\text{st}}) + \mathbf{K}_{\text{st}}]}_{\text{combined stiffness}} \begin{bmatrix} \delta_{st_p}^* \\ \delta_{st_r}^* \end{bmatrix}, \quad (2.1)$$

where \mathbf{K}_{NMS} is the stiffness of the NMS and \mathbf{K}_{st} is the stiffness of the side-stick control interface. The \mathbf{K}_{NMS} and \mathbf{K}_{st} are defined separately along the pitch (p) and roll (r) hand/stick axes. The optimal side-stick input δ_{st}^* in Eq. (2.1) represents the output of the parametric risk field (described in more detail in Section 2.4.1). Note that the tuning law accounts for the dependence of \mathbf{K}_{NMS} on the magnitude and direction of manual control inputs applied on the side-stick, δ_{st} . To implement the control law described above, a value for \mathbf{K}_{NMS} has to be selected. Three available, NMS inspired, design options are described next.

2.2.4. NMS RELATED TUNING CHOICES

The following choices for neuromuscular stiffness, and thereby the tuning of the haptic feedback, can be distinguished:

INTRINSIC (RELAX TASK) STIFFNESS

The haptic feedback is tuned to match the intrinsic stiffness of the operator's NMS, i.e., the haptic feedback moment is scaled such that when applied, it will move the operator's relaxed arm holding the stick to the 'optimal stick position'. The haptic feedback will result in the correct stick response, unless the operator stiffens up, *actively disagreeing* with the guidance. The advantage of this tuning is that the physical work of the operator is minimized; for the intrinsic stiffness the Golgi tendon organ and muscle spindle feedback paths are not used. In many cases the spring stiffness of the stick will be higher than the intrinsic stiffness of the human operator. Consequently, the stick stiffness alone will not be too different from the combined stiffness of the stick and hand, and so the this tuning will also produce an acceptable response for a hands-off control.

LOWER THAN INTRINSIC STIFFNESS

The haptic feedback is tuned to match a lower than intrinsic stiffness of the NMS of the operator [76] (with force task stiffness being the lower limit). Such tuning keeps the operator more involved in the control loop by requiring active NMS adaptation towards the force task, which can be described as requiring *active agreement*. Interestingly, even negative stiffness tuning has been used in literature: to encourage fast evasive maneuvers in a car driving support system [80].

HIGHER THAN INTRINSIC STIFFNESS

The haptic feedback is tuned to match a higher than intrinsic stiffness of the NMS (with position task stiffness being the upper limit). The haptic guidance moment would result in correct stick position if the operator maintains increased arm stiffness, otherwise the stick position response to the haptic guidance will be too large, leading to overshoots during the avoidance maneuvers [50]. Depending on the actual tuning, it can be difficult for the operator to overrule the haptic feedback.

In this chapter, we advocate the choice of using intrinsic stiffness as the reference in tuning the collision avoidance HSC, for three reasons. First, intrinsic stiffness based tuning ensures that the physical workload of the operator is minimized, since no muscular activity is required to maintain intrinsic stiffness. Second, the system prevents colliding, unless the operator *actively disagree* by stiffening up the arm. And third, this setting has the attractive property that when the stick is released, the UAV will steer away from nearby obstacles.

2

2.2.5. IDENTIFYING INTRINSIC NEUROMUSCULAR SYSTEM ADMITTANCE

The NMS properties of human subjects are typically determined in three fundamental tasks, Table 2.1 [81]. The intrinsic stiffness of the neuromuscular system can be directly determined in the relax task, in which the reflexes are not used and the arm dynamics are dominated by its visco-elastic properties. However, the UAV control stick is normally spring centered, requiring the operator, in order to command UAV motion, to deflect the stick by applying force on it. The intrinsic NMS properties therefore need to be determined in presence of a bias force. Unfortunately, it is unattainable for subjects to maintain the required bias force and simultaneously suppress their neural reflexes to correctly execute the relax task. A method to overcome this practical challenge and identify the intrinsic NMS in a force task is described in the next section.

2.3. NEUROMUSCULAR IDENTIFICATION EXPERIMENT

The identification of human neuromuscular properties traditionally relies on using multisine signals to provide excitation forces on a range of frequencies. However, the distribution of power over the frequencies influences the reflexive action of the NMS [82]. A novel identification method, described in detail in a previous study [53], uses a disturbance signal with a wide-band spectrum, to suppress the arm's natural reflexes. In this manner the adaptation range of the NMS is effectively limited to the intrinsic visco-elastic properties.

2.3.1. METHOD

SUBJECTS AND TASK INSTRUCTIONS

Ten subjects (three female), all staff or graduate students of TU Delft, with an average age of 28.6 years ($\sigma = 2.4$) performed the experiment. All subjects were right-handed, none reported injuries or any other disorder in the upper extremities. The experiment was approved by the Delft University of Technology Human Research Ethics Committee. Subjects gave their informed consent prior to the experiment and no monetary compensation was offered.

The subjects were seated in an adjustable chair, Figure 2.3, such that the right forearm was parallel with the roll axis of the stick. The stick's hardware casing served as a rest for the forearm. Subjects were asked to perform force task, Table 2.1, keeping constant grip and hand position during the experiment.

EXPERIMENT DESIGN AND PROCEDURE

Three levels of bias moment magnitude were tested, 0, 0.7 and 1.4 Nm, in six directions: 0° , 45° , 90° , 135° , 180° , and 270° ; constituting thirteen test conditions $C_{1..13}$. A wide-band test signal (Section 2.3.1), applied as an additional moment on the stick, was used. Both, as a means of excitation to be able to identify the NMS, and to ensure that the reflex feedback action is suppressed. The experiment lasted approximately 1.5 hours, including briefing, debriefing, familiarization runs, and breaks.

The experiment started with performing multiple training runs to familiarize the subjects with the tasks. After that three experimental runs were done for all 13 conditions. Each individual run lasted 60 seconds, consisting of 10 seconds run-in time and of approximately 50 seconds measurement time, resulting in 9 full periods of the test signal for every condition.

APPARATUS

The electro-hydraulic side stick with armrest (A), in Figure 2.3, is located to the right of an adjustable chair. An 18 inch display, (B), was located at a distance of 80 cm in front of the subject. The side stick could move with two degrees of freedom, in pitch and roll rotation. The effective length, from axis of rotation to the center of the hand, between the middle and index finger, was 0.09m and the motion range was $\pm 22^\circ$ for pitch and $\pm 30^\circ$ for roll motion. The side stick measured the stick angular displacement $\underline{\delta}_{st}(t) = [\delta_{stp}(t), \delta_{str}(t)]^T$, the handling moment $\underline{m}(t) = [m_p(t), m_r(t)]^T$ applied by the subject on the stick, and the disturbance moment $\underline{d}(t) = [d_p(t), d_r(t)]^T$ imposed on it, for both roll and pitch respectively. Signals were sampled at 250 Hz. The active side stick was controlled in a closed-loop to behave as a mass-spring-damper system, as:

$$H_{st}(s) = \frac{\underline{\delta}_{st}(s)}{\underline{m}(s)} = \frac{1}{I_{st}s^2 + B_{st}s + K_{st}}, \quad (2.2)$$

where, for both the pitch and roll directions, inertia of $I_{st} = 0.02 \text{ kgm}^2$, damping coefficient $B_{st} = 0.2 \text{ Nmsrad}^{-1}$ and spring coefficient $K_{st} = 2 \text{ Nmrad}^{-1}$ were used, as in [27].

DISTURBANCE SIGNAL DESIGN

Two uncorrelated multi-sine signals $d_p(t)$ and $d_r(t)$ were designed in the frequency domain to excite the stick-arm dynamics in pitch and roll directions. Both signals contained power at 20 logarithmically distributed frequencies, $\underline{f} = [f_p, f_r]^T$, within a range of 0.4Hz and 20Hz, Figure 2.4a. The phases were selected to minimize the crest factor (peak-to-average amplitude ratio) [83]. Figure 2.4b shows one period (16.38s) of the disturbance signal in the time domain [84].

The signals had full power between 0.4Hz and 2.5Hz and 20% of the power above that frequency. A standard approach in human NMS admittance identification literature is

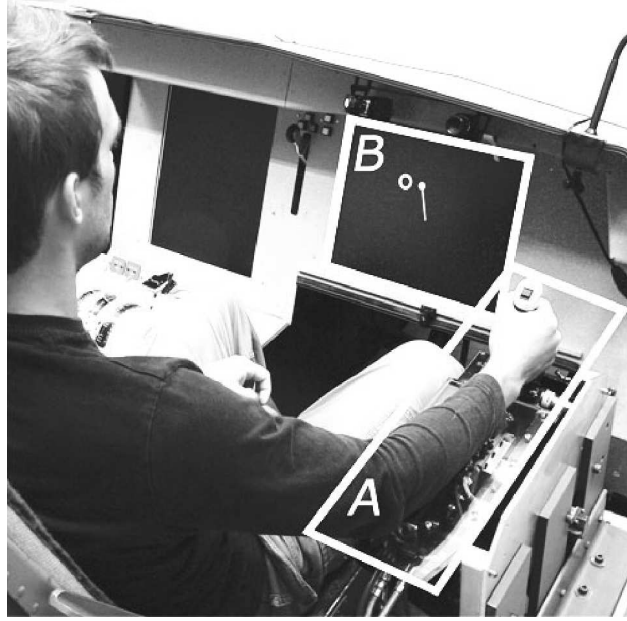


Figure 2.3: Neuromuscular identification experiment setup. The subject used the stick (A), to control position of a white dot on the display (B).

to use the full power signal only approximately below 1 Hz (reduced power method [82]). In contrast, in this work, the full power signal was intentionally applied above this frequency, to actually *suppress* the natural reflexes of the operator's arm, and allow the identification of intrinsic admittance. Alternatively, a uniform power distribution over all disturbance frequencies could have been used, or the higher frequencies could be omitted altogether in the future identification experiments, since these are not needed for the presented tuning method.

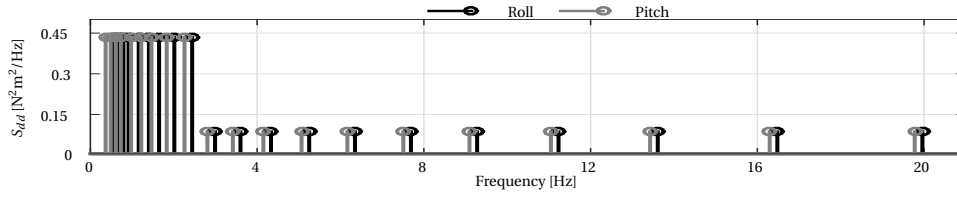
EXPERIMENTAL DATA PRE-PROCESSING

As a first step, mean values were subtracted from the measured time domain signals, ($\underline{d}(t)$, $\underline{\delta}_{st}(t)$ and $\underline{m}(t)$). Then the repetitions over the same condition were averaged in the time domain to reduce measurement noise and non-linear behavior of the NMS (e.g., voluntary inputs, muscle fatigue).

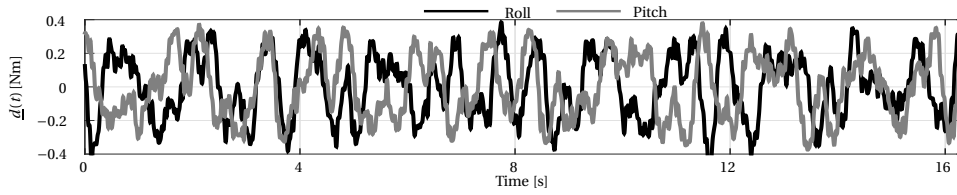
ADMITTANCE ESTIMATION USING SPECTRAL ANALYSIS

The moment input $\underline{m}(t)$, disturbance input $\underline{d}(t)$ and stick angle output $\underline{\delta}_{st}(t)$ were used to estimate auto- and cross-spectral densities $S_{\delta_{std}}(f)$ and $S_{md}(f)$ at the frequencies of the disturbance signal f . The NMS admittance is then obtained by using a closed-loop identification method [85].

Because the disturbance moment inputs are uncorrelated, the multiple-input and multiple-output admittance can be evaluated by using four separate single-input and



(a) Perturbation signal designed in frequency domain.



(b) One complete period (16.38s) of the disturbance signal.

Figure 2.4: Disturbance signal. Frequency and time domain content of the disturbance moment realizations for roll and pitch.

2

single-output spectral estimators [84, 86]. The admittance is calculated separately for all thirteen conditions ($C_{i=1..13}$):

$$\hat{G}_{C_i}(\underline{f}) = \begin{bmatrix} \frac{S_{\delta_{stp} dp}(\underline{f}_p)}{S_{m_p dp}(\underline{f}_p)} & \frac{S_{\delta_{stp} dr}(\underline{f}_r)}{S_{m_r dr}(\underline{f}_r)} \\ \frac{S_{\delta_{str} dp}(\underline{f}_p)}{S_{m_p dp}(\underline{f}_p)} & \frac{S_{\delta_{str} dr}(\underline{f}_r)}{S_{m_r dr}(\underline{f}_r)} \end{bmatrix} \quad (2.3)$$

ENDPOINT ADMITTANCE ELLIPSE

An intuitive way to visualize the 2-DOF dynamic characteristic of the endpoint admittance is using admittance ellipses [81]. The admittance ellipse displays the magnitude and direction of the response of the NMS to a unit moment input and is characterized by the size and direction of its major and minor axes. The major axis of the ellipse corresponds to the direction of the NMS with the least resistance to moment disturbances (highest admittance), and the minor axis to the direction with the largest resistance. The admittance ellipse can be evaluated at frequencies of the disturbances $f \in \underline{f}$ by:

$$\begin{bmatrix} \delta_{ell_r} \\ \delta_{ell_p} \end{bmatrix} = |\hat{G}_{C_i}(f)| \begin{bmatrix} \cos(\alpha) \\ \sin(\alpha) \end{bmatrix}, 0 \leq \alpha \leq 2\pi, \quad (2.4)$$

where δ_{ell_r} and δ_{ell_p} are the endpoint rotations for roll and pitch to unit moment disturbances, respectively.

2.3.2. RESULTS

The endpoint admittance ellipses at a low frequency ($f = 0.5\text{Hz}$) for all conditions averaged over all subjects are shown as in Figure 2.5 (standard deviation is displayed in

light gray). Data of one subject were discarded due to its very low admittance indicating incorrect execution of the requested task. Presented experimental data are available online [87].

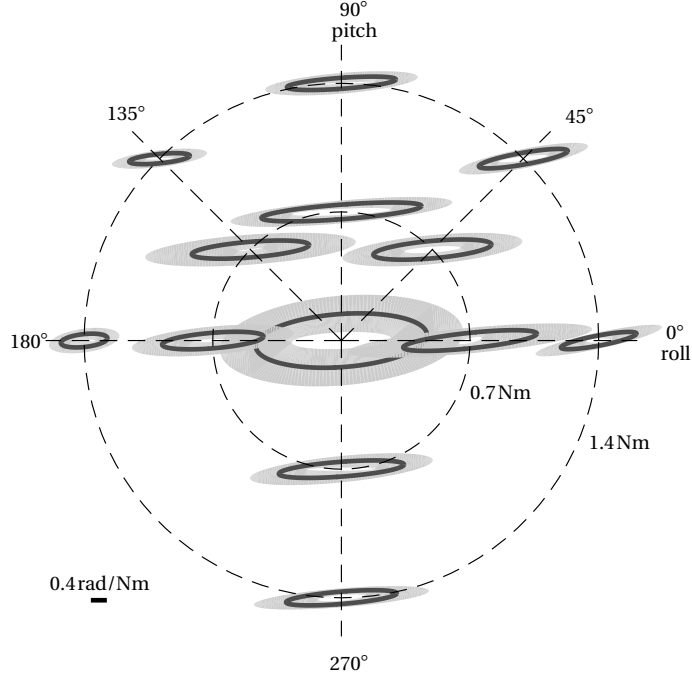


Figure 2.5: Mean estimated admittance ellipses over all subjects at $f = 0.5$ Hz. The standard deviation, shown in light gray, indicates relatively high consistency in responses among the group of subjects.

2.4. UAV TELEOPERATION EXPERIMENT

The set of NMS admittance measurements, previously obtained in Section 2.3, is in this section used as a reference for tuning a HSC collision avoidance system, and evaluated in a human study with a teleoperated UAV control task.

2.4.1. UAV TELEOPERATION

UAV MODEL

The UAV was modeled as an ‘easy-to-fly’, control-augmented, helicopter with a rotor diameter of 3 m [27]. Longitudinal side-stick inputs δ_p were mapped to forward velocity commands V_x , whereas lateral inputs δ_r were mapped to yaw rate commands $\dot{\psi}$, which

is not uncommon for, e.g., stabilized quadrotors:

$$\begin{aligned} H_{UAV_x}(s) &= \frac{V_x(s)}{\delta_p(s)} = \frac{1}{(0.3s+1)(0.18s+1)} \\ H_{UAV_y}(s) &= \frac{\dot{\psi}(s)}{\delta_r(s)} = \frac{1}{(0.2s+1)} \end{aligned} \quad (2.5)$$

In addition to the above dynamics, the UAV has a maximum velocity, V_{max} , and acceleration, a_{max} , of 5.0 m/s and 1.0 m/s² in the longitudinal direction, and a maximum yaw rate, $\dot{\psi}_{max}$, and yaw acceleration, $\ddot{\psi}_{max}$, of 0.32 rad/s and 2.0 rad/s² in the lateral direction. The UAV altitude was kept constant by an autopilot.

ENVIRONMENT

Six obstacles, modeled as buildings of different shapes, see Figure 2.6, made up the virtual environment of the remote sensing task (the environment was also used in previous studies [27]). Each obstacle was designed to evoke different control behavior. For instance, obstacle 3 required subjects to fly backwards into a U-shape building, with no visual cues in the direction of motion. Obstacles were re-arranged to create three different measurement and three training trajectories, to reduce boredom and learning effects.

2

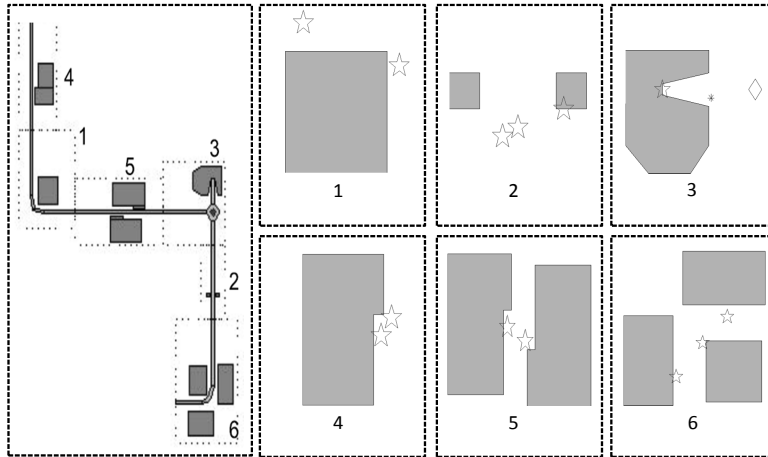


Figure 2.6: An example of a virtual environment composed of six obstacles; with waypoints (star symbols) to be flown through. A path to be flown backwards (diamond) ends inside the obstacle 3 opening (visually marked by an asterisk).

PARAMETRIC RISK FIELD

The parametric risk field (PRF) is the component of the automatic controller responsible for mapping obstacles in the environment to the optimal collision avoidance side-stick inputs, see Figure 2.1. The risk field is computed in the UAV reference frame, expressing the risk of collisions for obstacles detected within the scanned area. Subsequently, in

Section 2.4.1, the corresponding repulsive haptic moments are calculated and applied on the side-stick by the haptic controller to help the teleoperator to steer away from possible collisions. The PRF [75], was specifically designed for UAV teleoperation. It was found to generate more stable haptic moments, when compared to other haptic collision avoidance fields discussed in literature [39, 74, 75].

The shape and size of the risk field is proportional to the instantaneous UAV velocity, \mathbf{v} , and inversely proportional to its maximum deceleration, a_{max} . If the UAV is stationary, the field spans only a small circular region around the UAV. For non-zero velocities, the field extends in the direction of motion to provide sufficient time for the teleoperator to react to the haptic cues. Figure 2.7 displays the parameters and zones that define the PRF. Parameters d_{stop} and d_{ahead} are responsible for extending the size of the field when the UAV is moving and are defined as [27]:

$$d_{stop} = \frac{|\mathbf{v}|^2}{2a_{max}} \quad d_{ahead} = |\mathbf{v}| t_{ahead} \quad (2.6)$$

The risk field geometry is defined by four constant parameters: r_{pz} , d_{min} , t_{ahead} and a_{max} . The values of these parameters were refined through simulations for the UAV model used in this research by Lam et al. [75] and are listed in Table 2.2. The risk of collision, R , is based on the relative distance between the UAV and an obstacle, \mathbf{p} , also taking in account the instantaneous UAV velocity, \mathbf{v} :

$$R(\mathbf{p}, \mathbf{v}) = \begin{cases} 1 & \text{if } \mathbf{p} \text{ in Zone 1} \\ \cos\left(\frac{d}{d_0} \frac{\pi}{2} + \frac{\pi}{2}\right) + 1 & \text{if } \mathbf{p} \text{ in Zone 2} \\ 0 & \text{if } \mathbf{p} \text{ in Zone 3} \end{cases} \quad (2.7)$$

The cosine function for risk computation in Zone 2 enables a smooth transition in risk values between zones, consequently ensuring that there will be no sudden changes in the applied haptic moments. To evaluate the risk at point \mathbf{p} , distances d and d_0 need to be computed, see Figure 2.7.

The risk is used to compute an optimal side-stick input δ_{st}^* . First, the magnitude of the risk is calculated using Eq. (2.7), and its direction is defined from the obstacle to the center of the UAV. This allows for a straightforward implementation if a discrete sensor spanning the 360° area around the UAV is used [75]. If multiple obstacles are detected, the final collision avoidance steering vector is computed by vectorially summing the largest and smallest collision avoidance steering vectors, using the ‘max-min’ method [27]. Second, the resulting risk vector is scaled to the physical input limits of the side-sticks (for details see Section 2.3.1), i.e., the maximal risk value corresponded to the maximal deflection of the side-stick.

HAPTIC CONTROLLER IMPLEMENTATION

The haptic controller was implemented using the averaged admittance of ten subjects measured in Section 2.3, at a measurement/excitation signal frequency of 0.5 Hz. As discussed in Section 2.2, admittance depends on the magnitude and direction of manual control inputs [53, 88]. To account for this, the tuning was determined for 13 different conditions, as is shown in Figure 2.5. The control law relating the optimal side-stick

Table 2.2: Parametric risk field parameters.

Parameter	Value	Description
r_{pz}	1.5	Radius of protection zone [m]
d_{min}	1.5	Distance between zone 1 and zone 2 [m]
t_{ahead}	2	Maximum available reaction time [s]
a_{max}	1	Maximum UAV deceleration [m/s^2]

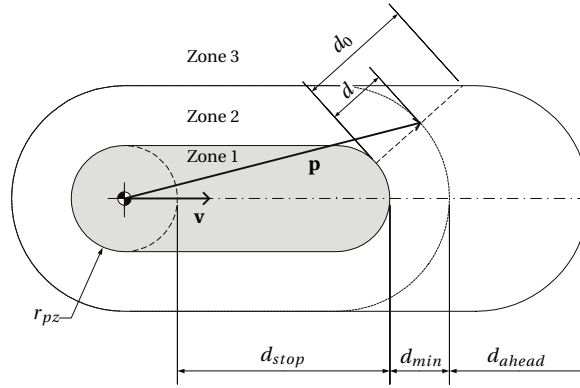


Figure 2.7: Parameters used to describe the shape of the Parametric Risk Field (based on [27]).

position δ_{st}^* (based on the risk calculated by Eq. (2.7) to the applied haptic moment, M_G , was implemented according Eq. (2.1).

The motions of the UAV with respect to the obstacles in the surroundings, and thereby the fluctuations in the haptic feedback, will produce signals from the collision avoidance system that are generally lower in bandwidth than 1 Hz [27]. Based on the estimated frequency responses, the combination of the NMS and the control interface can be for design purposes considered to be a constant gain [53]. The admittance at a low frequency ($f = 0.5$ Hz) over all conditions $C_{1..13}$ was transformed to stiffness:

$$\mathbf{K}_{NMS}(\delta_{st}) = (\hat{G}_{C_i}(f))^{-1} \quad (2.8)$$

To account for all permissible stick inputs δ_{st} , nearest neighbor interpolation was used to compute appropriate haptic cues (i.e., the closest available $\mathbf{K}_{NMS}(\delta_{st})$ to the instantaneous teleoperator manual control input is selected). The mapping of the instantaneous stick position δ_{st} to the $\mathbf{K}_{NMS}(\delta_{st})$ stiffness gains is visualized in Fig 2.8. It is hypothesized that this stick position-depended tuning approach will allow the haptic controller to better account for adaptation in NMS (in contrast to using only one constant NMS stiffness value), and as a consequence, improve the teleoperator's appreciation of the haptic cues.

By visual inspection of the identified admittance ellipses, Figure 2.5, a small roll-pitch and pitch-roll cross-term effect (i.e., rotation of the admittance ellipses) was ob-

served. However, it was deemed undesirable for the guidance forces to utilize this cross coupling and so to prevent it, the corresponding stiffness cross-term gains were set to zero, as: $\mathbf{K}_{\text{NMS}}(\delta_{st}) = \begin{bmatrix} K_{\text{NMS}p} & 0 \\ 0 & K_{\text{NMS}r} \end{bmatrix}$.

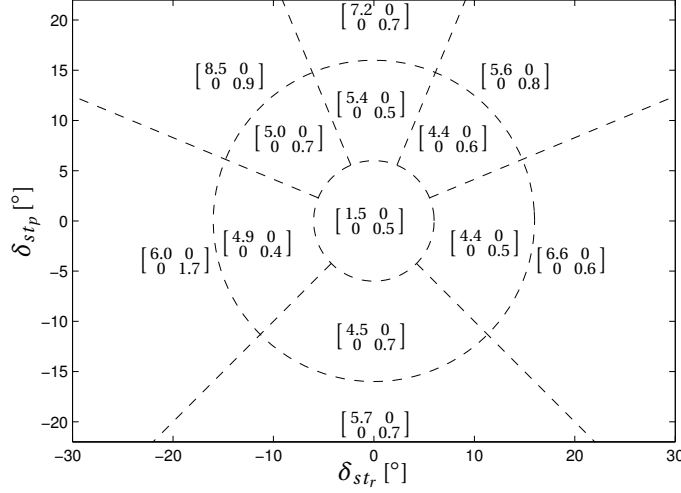


Figure 2.8: Mapping of actual stick position δ_{st} to the tuning gain $\mathbf{K}_{\text{NMS}}(\delta_{st})$ [Nm rad⁻¹].

2.4.2. METHOD

SUBJECTS AND TASK INSTRUCTIONS

Twelve right-handed male subjects, all graduate students of TU Delft, with an average age of 23.4 years ($\sigma = 0.7$), took part in the experiment. None of the subjects participated in the previous identification stage and none had any prior experience with haptic interfaces. Subject gave consent prior to the experiment and no monetary compensation was offered. The experiment was approved by the Delft University of Technology Human Research Ethics Committee.

During the experiment, subjects performed a UAV surveillance task in an obstacle laden urban environment. Subjects were instructed, in order of priority to: 1) avoid collisions, 2) fly as closely as possible through the center of waypoints (represented as smoke plumes), and 3) to perform the task as fast as possible. To improve experiment realism, each collision resulted in a 20 second time penalty during which the experiment was paused. Each trial took approximately 150 seconds to complete (when flown without collisions).

APPARATUS

A fixed-base flight simulator was used to perform the experiment, see Figure 2.9. Subjects were seated in a pilot chair (1) and used the same electro-hydraulic side-stick with the same dynamical parameters as in the preceding NMS admittance identification experiment. The side-stick (2) was used to manually control the UAV through the environment. The measurement signals were recorded at 250 Hz.

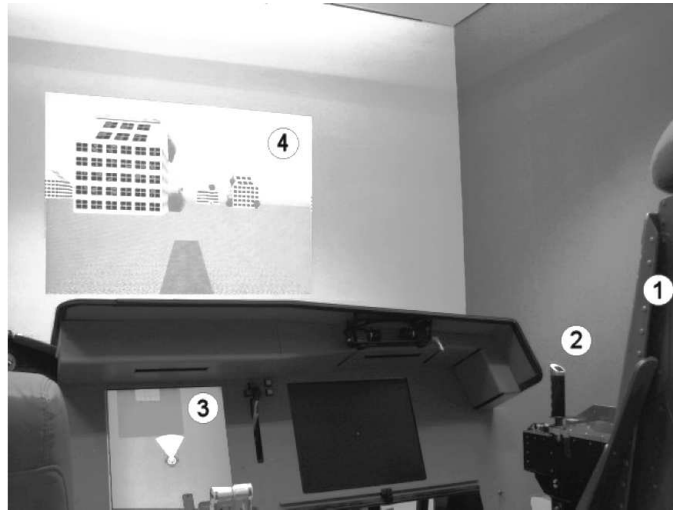


Figure 2.9: UAV teleoperation experiment setup. Fixed-base flight simulator with aircraft chair (1), hydraulic side-stick (2), navigation display (3) and onboard camera view (4).

2





Visual cues of the surroundings were projected on a wall in front of the subject, originating from a simulated onboard camera fixed to the longitudinal forward axis of the UAV (4). Additionally, a top-down view display was provided to aid the operator with navigating around obstacles (3).

INDEPENDENT MEASURES

Two categories of independent variables were studied in the experiment. The first category was concerned with the tuning profile (TP) of the haptic controller. A total of four TPs were tested, resulting in the four experiment conditions listed in Table 2.3. Here, UT and OT controllers represent TPs that are half and twice as strong as RT tuning, respectively. These two TPs were defined to study the sensitivity of the novel tuning procedure.

The second independent variable was obstacle (OB). Six different obstacles were tested during the experiment and the subjects were required to fly through all of them in every trial, for details see Section 2.4.1.

Table 2.3: UAV teleoperation experiment conditions and color coding.

Color	Symbol	Description
	NHF	No haptic feedback / pure manual control
	UT	HSC under-tuned relative to RT ($UT=0.5RT$)
	RT	HSC tuned based on relax task admittance data collected in Section 2.3
	OT	HSC over-tuned relative to RT ($OT=2RT$)

DEPENDENT MEASURES

The dependent measures used to compare the different haptic controllers can be divided into six categories: safety, performance, control activity, haptic activity, haptic controller agreement and subjective questionnaires. They are listed in Table 2.4. To assess the

Table 2.4: Experiment dependent measures.

Measure	Symbol	Description
Safety	$n_{collisions}$	Number of collisions [-]
Performance	\bar{V}	Mean velocity [m/s]
	d_{wp}	Minimum distance to waypoints [m]
Control Activity	$\sigma_{\dot{\delta}}$	Standard deviation of stick rate [rad/s], both roll and pitch
Haptic Activity	σ_{M_G}	Standard deviation of haptic guidance moment [Nm], both roll and pitch
Haptic Controller Agreement	M_{rms}	RMS error between the magnitude of human applied moment and the haptic guidance moment [Nm]
	M_{sgn}	Ratio of haptic guidance and human applied moments having the same sign [-]
Subjective	NASA TLX	Workload assessment survey
	SA	Situational awareness survey
	HA	Haptic feedback acceptance survey

agreement between the operator's voluntary moment inputs, M_H , and the haptic guidance moment, M_G , two separate metrics were calculated in discrete. The metrics were calculated in discrete time, for a total of n samples per trial when the haptic controller was active, i.e., for all k when $|M_G(k)| > 0$. Magnitude comparisons are based on the RMS error between the magnitudes of measured moment and the haptic moment as:

$$M_{rms} = \sqrt{\frac{1}{n} \sum_{k=1}^n (|M_G(k)| - |M_H(k)|)^2}, \quad (2.9)$$

with smaller values indicating higher magnitude agreement. Directional agreement is assessed as the ratio of haptic and measured moments having the same sign as:

$$M_{sgn} = \frac{1}{n} \sum_{k=1}^n \text{eq}(\text{sgn}(M_G(k)), \text{sgn}(M_H(k))), \quad (2.10)$$

where operator $\text{eq}(a, b)$ equals 1 if $a = b$, otherwise it equals 0. A M_{sgn} value of 1 indicates perfect agreement, whereas a value of 0 indicates total disagreement of moment directions.

The control activity, haptic activity, and haptic controller agreement were analyzed separately along the pitch (p) and the roll (r) axes to investigate the control strategy differences between the two directions observed during a pilot study.

Questionnaires were used to measure subjective workload, situational awareness (SA) and haptic feedback acceptance (HA). Workload is measured using the NASA Task Load Index (TLX) questionnaire [89]. The NASA TLX calculates workload as the weighted average of six subjective sub-scales: mental demand, physical demand, temporal demand, performance, frustration and effort. A higher weighted average (ranging between 0 and 100), suggests higher subjective workload. SA and HA are measured using questionnaires similar to the Eurocontrol SASHA method [90]. These questionnaires capture the teleoperators' awareness of their surroundings and whether haptic feedback was subjectively helpful in completing the task, respectively. The SA and HA questions are answered on a five point Likert type scale (ranging between 0 and 4), and the mean score of all the questions is taken as the measure of SA and HA, with higher scores indicating higher SA/HA.

HYPOTHESES

Three hypotheses were formulated for the validation experiment. Firstly, we hypothesized that task *safety*, in accordance with previous research [74, 75], will be increased with stronger *tuning profile* of the haptic controller.

Secondly, the task *performance* would remain unaffected by the *tuning profiles*, since the haptic cues should ideally not interfere with the task and only prevent collisions.

Thirdly, the *workload* associated with the task and the *acceptance of haptic feedback* should be optimal for the RT.

PROCEDURE

The experiment began with three initial training to allow subjects to practice controlling the UAV with and without the aid of haptic cues. Afterward, subjects flew one additional training run and four measurement runs for each TP. Experiment conditions were randomized and subjects had no prior knowledge of the conditions performed. At the end of each condition, subjective workload (using NASA TLX), situational awareness and haptic feedback acceptance were measured using questionnaires. The total duration of the experiment, including briefing, debriefing, familiarization runs, and breaks, was approximately 2 hours.

DATA ANALYSIS

All objective dependent measures were computed per obstacle to take into account the different order of obstacles in each trajectory. The effects of the independent variables (TP and OB) on the dependent measures were analyzed using two-way repeated-measures ANOVA, with pairwise Bonferroni corrected comparisons used as post-hoc tests. For non-spherical data the Greenhouse-Geisser corrections were applied to the degrees of freedom [91].

Ordinal dependent measures, $n_{collisions}$ and subjective questionnaires results, were evaluated using the Friedman test; with Bonferroni corrected Wilcoxon signed-rank test as post-hoc.

VISUALIZATION OF RESULTS

Results are shown using their means and the 95% confidence intervals of the mean. The color coding of tuning profiles follows Table 2.3. Questionnaire results are visualized as box-plots, showing the median, the 25th and 75th percentiles and the maximal and minimal values (excluding outliers) over all subjects.

Due to the low number of collisions, the $n_{collisions}$ were summed over all subjects; corresponding confidence intervals (95%) are bootstrapped using the bias-corrected and accelerated percentile method (BCa) with 5000 samples [91].

2.4.3. RESULTS

The experimental results are in this section presented separately for all studied dependent measures. Overall, after the initial training period, there were no learning effects observed in the experimental data.

SAFETY

Figure 2.10a shows that the total number of collisions, $n_{collisions}$, decreased with increasing strength of the haptic controller, and was the lowest for the OT condition. However, the Friedman test did not reveal a significant effect of TP on $n_{collisions}$ (TP: $\chi^2(3) = 7.48$, $p = 0.058$).

The Friedman test did show an effect of OB on $n_{collisions}$, Figure 2.10b, (OB: $\chi^2(5) = 17.31$, $p \leq 0.01$). Obstacle 5, which resulted in the highest number of collisions, was also reported by subjects to be the most difficult.

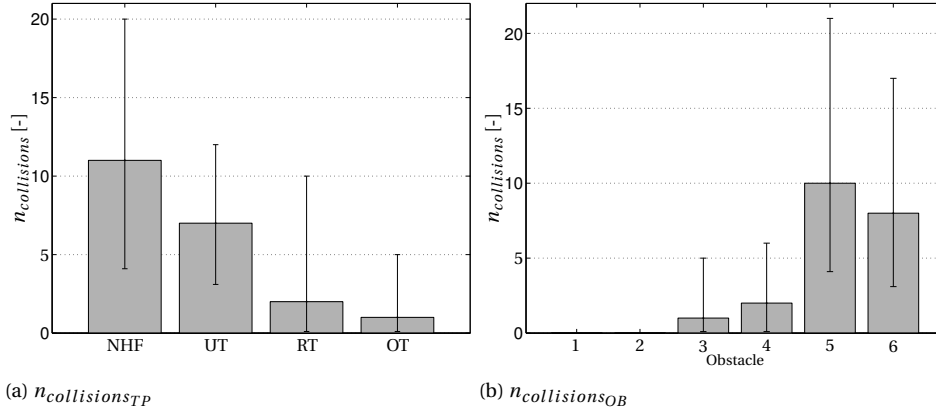


Figure 2.10: Task safety evaluated separately as a total number of collisions for all tuning profiles TP and obstacles OB over all subjects.

PERFORMANCE

The mean velocity of the UAV, \bar{V} , is shown in Figure 2.11a. Here it can be seen that for a particular obstacle, \bar{V} was relatively constant for all haptic controllers. On the other hand, \bar{V} did vary substantially with OB, a significant effect (OB: $F_{2.39,26.29} = 107.16$, $p \leq$

0.01). When comparing Figure 2.11a with Figure 2.10b, it can be seen that velocity tends to be lower for obstacles with a higher number of collisions. This indicates that subjects decreased UAV velocity in an attempt to follow the primary task instruction of avoiding collisions, particularly for difficult obstacles.

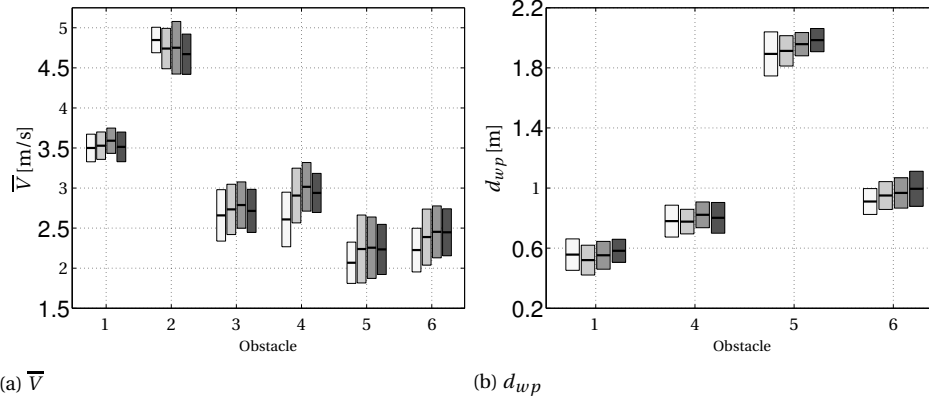


Figure 2.11: Task performance. Obstacles 2 and 3 did not have smoke plumes serving as waypoints. TP coding is described in Table 2.3.

Similar to \bar{V} , the minimum distance to waypoints, d_{wp} , was not influenced by TP, but affected by OB (OB: $F_{3,33} = 296.79, p \leq 0.01$), see Figure 2.11b. Moreover, it can be seen that d_{wp} followed the same trend as $n_{collisions_{OB}}$ and obstacles with more collisions had higher d_{wp} . This provides additional evidence that subjects employed a conservative control strategy when tackling difficult obstacles.

CONTROL ACTIVITY

The standard deviation of the longitudinal side-stick deflection rate, σ_{δ_p} , is shown in Figure 2.12a. For all obstacles, σ_{δ_p} was the smallest for NHF and the largest for OT (TP: $F_{1.33,14.59} = 19.56, p \leq 0.01$). The roll stick deflection rate σ_{δ_r} was the lowest for obstacle 2 (OB: $F_{1.93,21.27} = 42.80, p \leq 0.01$).

In the lateral direction, Figure 2.12b, σ_{δ_r} was the highest for the OT controller (TP: $F_{3,33} = 17.57, p \leq 0.01$). Similar to the longitudinal direction, post-hoc tests revealed no differences between UT and RT for σ_{δ_r} . Since turning was not necessary to complete obstacle 2, this obstacle resulted in the lowest σ_{δ_r} (OB: $F_{1.93,21.27} = 25.95, p \leq 0.01$).

HAPTIC ACTIVITY

The standard deviation of the longitudinal haptic guidance moment, $\sigma_{M_{Gp}}$, shown in Figure 2.12c, increased with increasing strength of the haptic controller (TP: $F_{1.35,14.87} = 75.88, p \leq 0.01$). Post-hoc tests showed differences between all three haptic controllers ($p \leq 0.01$). In terms of OB, variations increased from obstacle 1 to 6 (OB: $F_{2.66,29.24} = 6.50, p \leq 0.05$).

Standard deviation of the lateral haptic guidance moment, $\sigma_{M_{Gr}}$, are much greater for obstacles 4-6 when compared to obstacles 1-3 (OB: $F_{2,22} = 9.57, p \leq 0.01$), see

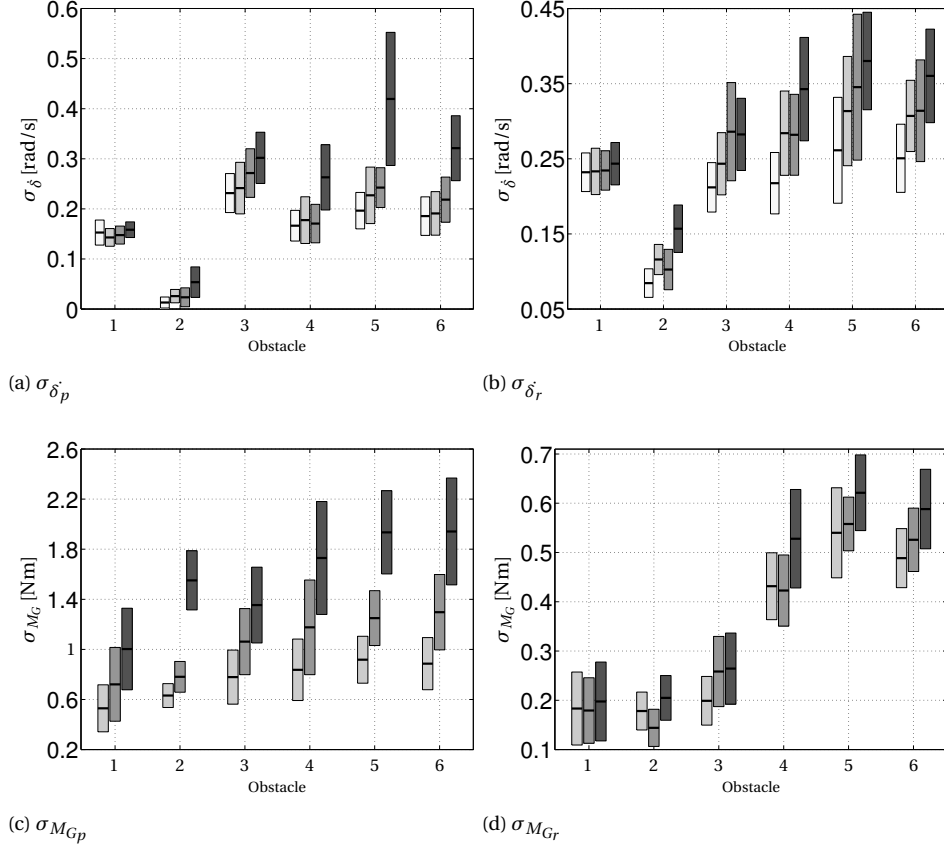


Figure 2.12: Control and haptic activity. Coding is described in Table 2.3.

Fig 2.12d. The OT tuning produced the largest $\sigma_{M_{Gr}}$ for all obstacles (TP: $F_{2,22} = 9.57, p \leq 0.01$). Post-hoc tests showed no differences between UT and RT controllers.

HAPTIC CONTROLLER AGREEMENT

Longitudinal agreement of the haptic moment magnitude, M_{rms_p} , is shown in Figure 2.13a. OT was found to have the highest value for M_{rms_p} , and consequently the lowest magnitude agreement of all controllers (TP: $F_{1,70,18.67} = 49.35, p \leq 0.01$). With respect to OB, obstacle 1 resulted in highest magnitude agreement while it was lowest for obstacle 6 (OB: $F_{2,24,24.55} = 5.45, p \leq 0.01$). As the differences between controllers is more evident for obstacles 4-6, a two-way interaction was also observed (TP×OB: $F_{3,59,39.53} = 10.99, p \leq 0.01$).

For the haptic moment magnitude agreement in the lateral direction, M_{rms_r} , in Figure 2.13b, OT had the lowest lateral magnitude agreement (TP: $F_{4,44} = 13.17, p \leq 0.01$). When compared to the longitudinal direction, magnitude agreement is higher for M_{rms_r} . However, variations between controllers increase for obstacle 4-6 yielding a significant

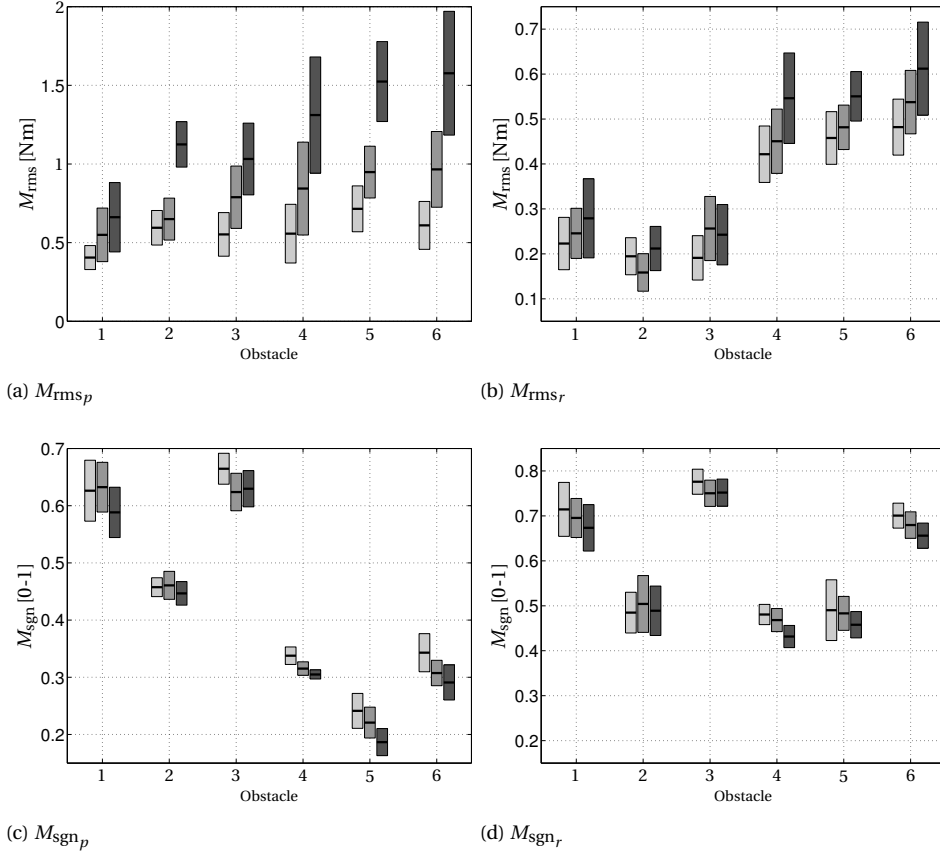


Figure 2.13: Haptic controller agreement. Coding is described in Table 2.3.

two-way interaction (TP \times OB: $F_{20,220} = 2.124, p \leq 0.01$), and as these three obstacle also caused lower magnitude agreement (SB: $F_{5,55} = 46.36, p \leq 0.01$).

Directional agreement of longitudinal haptic moments is assessed using M_{sgn_p} , in Figure 2.13c, with larger values implying greater agreement. Highest directional agreement was found for UT, and the lowest for OT, resulting in a significant effect of TP on M_{sgn_p} (TP: $F_{4,44} = 26.35, p \leq 0.01$). Obstacle 1 and 3 exhibited high directional agreement, but agreement was fell sharply for obstacles 4-6 (OB: $F_{5,55} = 231.75, p \leq 0.01$).

Lateral directional agreement, M_{sgn_r} , is shown in Figure 2.13d. It can be seen that lateral directional agreement is, on average, greater than for the longitudinal direction. Obstacle 3 resulted in the highest lateral directional agreement as the UAV was required to fly backwards, forcing subjects to rely on haptic cues to avoid obstacles outside their lateral field of view. Obstacles 1 and 6 also resulted in much higher directional agreements than other obstacle as these two obstacles involved sharp 90° turns which, while making the turn, obscured visual position of obstacles. These findings yield a significant effect of OB on M_{sgn_r} (OB: $F_{5,55} = 76.813, p \leq 0.01$). Concerning the relationship

with TP, lateral directional agreement deteriorated with increasing strength of the haptic controller (TP: $F_{4,44} = 10.38, p \leq 0.01$).

SUBJECTIVE QUESTIONNAIRES

Figure 2.14a displays overall workload, or Z-score, computed using the NASA TLX subjective questionnaire. Here a lower subjective rating symbolizes lower workload. The Friedman test showed that there was an effect of TP on overall workload (TLX: $\chi^2(3) = 18.10, p \leq 0.01$). Post-hoc analysis revealed that the differences were caused by the extreme conditions, NHF and OT, which had the highest workload levels. However, no substantial differences were recorded between UT and RT, and these two controllers led to the lowest measured workload. The six workload sources of the NASA TLX are pictured in

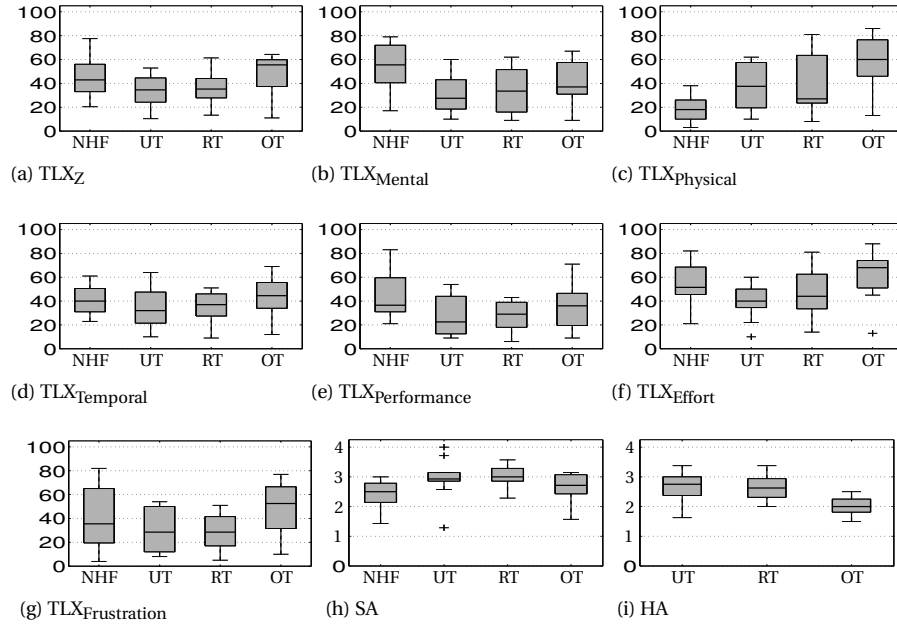


Figure 2.14: Subjective metrics: NASA TLX, Situational Awareness (SA), and Haptic Acceptance (HA).

Figs. 2.14b to 2.14g. Mental load (ML) and effort (EF) for UT/RT were reduced compared to NHF (ML: $\chi^2(3) = 16.20, p \leq 0.01$; EF: $\chi^2(3) = 15.91, p \leq 0.01$). However, physical load (PL) continued to be higher for the novel tuning method, and increased with the strength of the haptic controller, a significant effect (PL: $\chi^2(3) = 25.23, p \leq 0.01$). Despite improvements in performance, frustration and temporal load for UT/RT, TP effects were not significant.

Box plots for subjective situational awareness (SA) and haptic feedback acceptance (HA) are given in Figs. 2.14h and 2.14i. Here, higher subjective ratings imply better SA and HA. A Friedman test showed an effect of TP on SA, with the highest and lowest median SA recorded for RT and NHF respectively (SA: $\chi^2(3) = 11.58, p \leq 0.01$). A similar

trend was found for HA, with the highest acceptance for UT and RT, and the lowest for OT (HA: $\chi^2(2) = 8.21$, $p \leq 0.05$).

2.5. DISCUSSION

The main objective of this study is to provide a systematic and validated approach for tuning Haptic Shared Control (HSC) systems based on estimated admittance of the neuromuscular system (NMS), and – more specifically – to advocate the choice of the relax task admittance as the setting with the minimal required operator workload. To this end, a human-in-the-loop experiment simulating UAV teleoperation was performed to validate the tuning procedure. The following effects were observed:

NMS BASED TUNING WORKS AS A SYSTEMATIC METHOD

In general, subjective workload and situational awareness improved significantly for the under-tuned and the relax-task tuned haptic controllers when compared to manual control. Additionally, over-tuning the haptic controller, as is might be the case for heuristic tuning methods optimizing for safety [27], yields lower user acceptance than the condition with no haptic support. These results indicate that including UT/RT neuromuscular response in the HSC tuning procedure indeed improves overall user acceptance.

2

OVER-TUNING INCREASES WORKLOAD EVEN OVER NO HAPTIC FEEDBACK

The results of the three subjective questionnaires indicate that acceptance of haptic cues increased for UT and RT haptic controllers, supporting the third hypothesis. The reduction of overall NASA TLX workload for UT/RT compared to NHF can be traced back to a reduction of mental load and effort. This is in sharp contrast to earlier research where haptic cues contributed negatively towards mental load and effort [74]. Over-tuning the controller was found to be more detrimental than providing no haptic support at all. This supports the notion that incorrect tuning can adversely impact user acceptance of HSC systems, and our formal tuning method provides a non-heuristic approach that prevents such incorrect tuning.

THE OPTIMAL TUNING RANGE IS RELATIVELY BROAD

For most dependent variables, no statistical differences were found between the admittance characteristics of the under- and relax-task tuned controllers; but both led to improved user acceptance relative to manual control.

The design space available for selecting an appropriate tuning profile is broader than expected and if either one should be preferred remains an open question. Selection between the two tunings might be task specific. For tasks where the operator should be actively involved, e.g., in car driving [34], under-tuning the haptic controller (up to half the strength of the relax task controller) might provide a preferred option, since the operator needs to *actively agree* and comply with the guidance to correctly follow a prescribed trajectory (withing a range of acceptable trajectories). However, if failing to follow the haptic guidance might lead to an accident, as with collision avoidance systems, relax task tuning presents a better alternative. Such tuning ensures a successful collision avoidance, unless the operator, by stiffening up, *actively disagrees*.

SAFETY AND PERFORMANCE ALONE ARE POOR TUNING METRICS

As formulated in the first hypothesis the number of collisions was lower for stronger tuning profile (TP). The observed decrease, Figure 2.10a, however, was not found to be statistically significant. The sample size used in this study ($n = 12$) was higher than the minimal $n_{\min} = 5$ for a sufficient statistical power $1 - \beta = 0.8$ estimated based on effects observed in some similar haptic collision avoidance experiments [27, 74]. However, total $n_{\text{collisions}}$ for all conditions and participants in this study was substantially lower than in those previous studies. Based on the observed effect sizes, a recommended sample size for a future study would be $n_{\min} = 20$. The low $n_{\text{collisions}}$ might be partially attributed to putting a strong emphasis on avoiding collisions during the task instructions and to the addition of the twenty second collision penalty.

Based on the results, and in accordance with the second hypothesis, TP had no measurable effect on performance. This may be due to subjects adapting their control strategies to ensure that task instructions are followed with similar performance for all TPs. This also suggests, that it would difficult to select an appropriate tuning setting using safety and performance metrics alone, whereas different tuning profiles do result in other differences.

2

THE NMS ADMITTANCE IDENTIFICATION STAGE CAN BE SHORTENED

In accordance with findings of a previous study [88], the measured admittance responses of all subjects over tested conditions, Figure 2.5, were similar. Moreover, the influence of bias force magnitude and direction followed a similar trend for all participants. This suggests, that to obtain a sufficient set of representative admittance measurements, for instance in a future practical application, a lower number of subjects and tested conditions could be used. The individual differences in the identified NMS setting fit within the UT/RT range, suggesting that there might be only little to gain in perusing an operator-individualized NMS tuning.

HAPTICS IS APPRECIATED WHEN NO VISUAL FEEDBACK IS AVAILABLE

Due to the limited lateral camera field of view supplied during the experiment, subjects had a greater appreciation for lateral haptic cues. It is interesting to note, that haptic activity decreased in the lateral direction, while control activity was found to be higher. Also the haptic controller agreement results show that agreement between the teleoperator and the haptic controller, both in terms of magnitude and direction of haptic moments, was better in the lateral direction. Due to the feedback architecture of the system, greater lateral stick motion combined with a decrease in lateral haptic activity implies that subjects were more willing to follow lateral haptic cues. This maybe due to insufficient lateral visual cues, forcing subjects to rely on lateral haptic moments: for obstacles with sharp turns (obstacles 1, 4, 5 and 6) or when visual cues from the camera were not in the direction of motion (obstacle 3).

In the longitudinal direction, however, differences between the provided haptic and visual cues apparently led to 'goal' related conflicts. These conflicts need to be addressed in the future to further improve user acceptance of HSC systems. Control activity was lower than in the lateral direction, which can be attributed to the continuous corrective

lateral stick inputs required to meet the secondary objective of flying through the center of waypoints.

2.6. CONCLUSION AND RECOMMENDATIONS

We experimentally verified the effectiveness of using a formal tuning method for haptic shared controllers, based on relax-task setting of the neuromuscular system. For the studied conditions, we conclude that:

- (1) Tuning based on safety and performance metrics alone would be difficult and the neuromuscular knowledge should be included.
- (2) Tuning based on the relax task NMS setting was appreciated by the operators, with both physical and mental workload reduced.
- (3) This above mentioned tuning optimum is, however, not sharp and both the under-tuned and the relax-task-tuned systems behaved equally well in the tested conditions and thus the requirements for the identification procedure could be reduced.
- (4) Haptic feedback is most effective in directions with limited visual feedback.
- (5) In contrast to the previous point, haptic feedback provided in the forward direction, where the operator had a good view, was more often opposed by the operators. Ways to minimize these conflicts should be investigated in future research.

3

ADAPTABLE HSC BASED ON OPERATOR GRIP FORCE

*The chapter explores haptic guidance systems beyond using only one fixed setting (as is the case in Chapter 2), namely by making the system adjustable based on the operator grip force. The problem is studied on a simple tracking task supported with **attractive guidance** type HSC. The chapter describes how this proposed system behaves in situations in which there is a disagreement between the human operator and the automatic system and make theoretical predictions how the operators could efficiently use this additional control input to the system. The proposed adaptable HSC system is evaluated in a human-in-the-loop experiment and compared with unassisted control and traditional 'fixed-setting' haptic guidance controller.*

This chapter is based on the following publication:

- Jan Smisek, Winfred Mugge, Jeroen B. J. Smeets, Marinus M. van Paassen and Andre Schiele, "Operator adaptable haptic guidance: A modeling approach to predict performance under external disturbances", IEEE Transactions on Haptics, 2017 (in revision)
- Jan Smisek, Winfred Mugge, Jeroen B. J. Smeets, Marinus M. van Paassen and Andre Schiele, "Adapting Haptic Guidance Authority based on User Grip", IEEE International Conference on Systems, Man, and Cybernetics, San Diego, 2014

CHAPTER SUMMARY

Scaling of guidance forces determines the level of control authority the haptic guidance system has over tasks. In real cases, tasks can change in reaction to external disturbances or to internal conflicts between the support system and the human operator, and thus one level of the guidance scaling will likely be insufficient. Adaptation of the control authority would better reflect this variability. In this chapter, we formalize the concepts of disturbances and conflicts and experimentally investigate ($n = 8$) an adaptable authority guidance scheme based on the operator's grip force. In a position tracking task we explore two opposite approaches to trade the control authority; increasing versus decreasing guidance strength with operator grip. These conditions were compared with unassisted control and two levels of fixed-gain haptic assistance. Results show that the grip-adaptable method allowed the operators to increase performance over manual control and over an under-tuned guidance system. At the same time, the method substantially reduced the operator physical control effort required to cope with conflicts and disturbances. Furthermore, predictions based on the formalized model of the system corresponded to results of the human-in-the-loop experiment, implying that such validated formalization can be used for model-based analysis and design of HSC systems.

3.1. INTRODUCTION

Haptic shared control (HSC) combines manual control inputs of an operator with haptic guidance support from an automatic control system [42]. Generally it is implemented as a ‘virtual spring’, guiding the operator to follow a prescribed reference trajectory using additional forces on the control input device. The stiffness of this spring needs to match the task and the desired level of the HSC system authority over the task while still allowing the operator sufficient control [37]. Methods to find the appropriate stiffness vary in literature, from iterative heuristic tuning [92], to performance based tuning [93] and tuning based on operator neuromuscular modeling and identification [53, 76]. It was found that operators adapt over time to the specific guidance system setting [70, 94].

However, it has been recognized [25, 95] that one fixed setting of the guidance stiffness is likely insufficient, especially in complex tasks, and a way to smoothly adapt the control authority during the task would be helpful. With an adaptable system, the operator would be able to rely on the guidance of the desired authority most of the time. Yet, when the task suddenly changes and becomes more difficult, or if an internal system malfunction causes the guidance to be incorrect, the possibility to quickly change the level of authority and resolve the situation is of great practical importance [96]. If we consider an example of a lane keeping HSC support system in a car, a change in the task difficulty could be caused by a wind gust pushing the car outside the lane or by the lane becoming more narrow [97]. In such a situation the driver would benefit from a higher level of haptic guidance support. On the other hand, the HSC system itself can be the source of the problem. For instance, the driver might have a different preference for the path to be taken than the HSC system, giving rise to a conflict. In such situation the driver would need to overrule the HSC system with increased effort and would actually benefit from a lower level of guidance support.

Traditionally, the research focus in the field has been on *adaptive* guidance systems, where the level of the HSC system control authority is decided internally, i.e., by the HSC system itself. Previously presented approaches adjusted the control authority based on: task performance [98], criticality [80, 95] and the level of agreement between guidance and operator [98–100], actively recognizing the control model [101, 102] or intended goal of the operator [103, 104]. It can be argued, that all these systems are making the final decision about *who is in control* internally, regardless of the operators in the control loop, leaving them no direct way to change the level of support.

However, we feel that the operators do envision what level of control authority they would like to hold and that this decision should be left to them. Our preliminary study proposed a *grip-adaptable* haptic shared control system, where the measured operator grip force was used as an additional input to the system [44]. The grip force provided the operator with a direct way to change the HSC system authority. We showed that such a system can reduce the physical workload of the operator as compared to HSC systems with fixed authority, while maintaining high tracking performance. In this chapter, the goal is to provide further insights in two directions. First, we aim to extend and formalize the theoretical understanding of the conflicts and disturbances impeding a system with HSC support. Second, in addition to tracking performance and physical workload, other system properties, such as the quantitative level of disagreement between the operator and the HSC system, are analyzed.

We first introduce a haptic shared control system with real-time adaptable authority, in Section 3.2, and we put the intuitively introduced system on a firmer, system-theoretical basis, in Section 3.2.1. We formulate predictions based on the theoretical understanding of the system on how the operators will react on the presence of conflicts and disturbances, and put them to the test in a human-in-the-loop experiment, in Sections 3.3 and 3.4. The chapter concludes with a comprehensive discussion of the results and summary of the main conclusions, in Sections 3.5 and 3.6.

3.2. HSC SYSTEM WITH GRIP-ADAPTABLE AUTHORITY

The underlying design goal of the presented grip-adaptable HSC is to make the system intuitive, so we built on the natural adaptation mechanism of the human neuromuscular system. In general, the operator adapts by stiffening up when keeping a precise position is required and by becoming more compliant when task natural constraints seems adequate [105]. As stiffening was found to be accompanied by increased grip force [106], one can capture these changes directly by measuring the force of the operator's grip on the master device handle. Based on this real-time grip force measurement, the stiffness of the guidance system, i.e., the level of control authority, is continuously adapted. This concept was explored by our preliminary study [44] and later by other authors [107, 108].

We aim to answer the following questions: 1) what are the reasons for the operator to increase the grip force during a task? 2) and how should the guidance system adapt once this is detected? With respect to the first question, from the previous literature we can distinguish two opposing effects:

- (a) *Task difficulty*. Increased grip force is a sign of task difficulty and therefore the operator desires to be more supported by the HSC system [33, 95, 106]. In this chapter, in order to increase task difficulty, sudden force disturbances were applied on the master device (effectively analogous to, e.g., wind pushing vehicle off the track), Figure 3.1(a). The operator needs to apply increased steering force to counteract the force disturbance, otherwise a tracking error would develop, see Figure 3.2.
- (b) *Conflict*. Increased grip force is a sign of conflict between the operator and the guidance and therefore the operator desires to have more control authority over the HSC system (i.e., less support to reduce the influence of the conflicting guidance system) [26, 98]. Here, to replicate a conflict between the operator and the HSC, a step change in the reference trajectory for the HSC system was introduced (for example corresponding to the vehicle sensor picking-up a parallel track), Figure 3.1(b). The operator needs to apply increased steering force to counteract the conflicting guidance force generated by the guidance system to maintain the same level of task performance, as shown in Figure 3.2.

These alternatives would lead to two competing control strategies: in (a) with increased grip force the level of support, i.e., guidance stiffness, should be increased; and in (b) with the increased grip force the level of support should be decreased.

In this chapter we explore both control strategies separately and compare their effect on operator's performance and operator control effort. As a basis for comparison we use

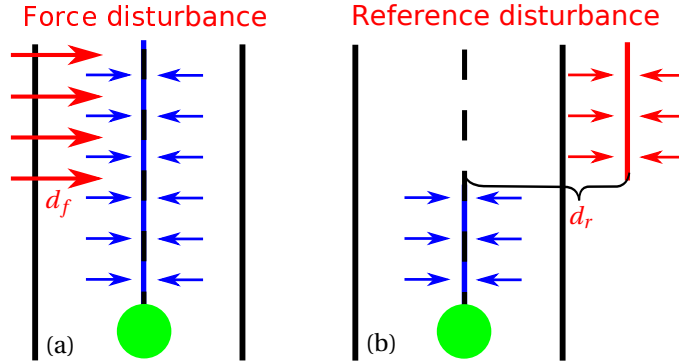


Figure 3.1: Disturbances used in the experiment. The operator's task is to keep the green dot on the center-line of the track with the help of guidance forces (in blue). The force disturbance (a) increases the task difficulty by addition of a force d_f 'pushing' the dot outside the track. The reference disturbance (b) creates a conflict by guiding the operator to a trajectory outside the track offset by d_r . Correct guidance (in blue) and disturbances (in red) are not seen by operators.

unassisted control and two levels of fixed guidance (with stiffness corresponding to the minimal and the maximal level of the adaptable-authority system).

3.2.1. FORMALIZING THE GRIP-ADAPTABLE HSC SYSTEM

This section proposes a control-theoretic formulation that allows assumptions to be made about the effects of the aforementioned disturbances and the corresponding control HSC strategies. A grip-adaptable HSC system is illustrated in Figure 3.3. The system comprises of an automatic *HSC system* part and a part representing a simplified model of an *Operator*. Both parts contribute to the task execution, namely in making the system output y follow the reference trajectory r (e.g., a road centerline detected by a sensor).

The system is modeled using transfer functions in Laplace domain, with a master input device (mass-damper):

$$G_m(s) = \frac{x_m(s)}{F_m(s)} = \frac{1}{m_m s^2 + b_m s}, \quad (3.1)$$

where x_m is the master device position, f_m is the sum of forces acting on it. The device has mass m_m and damping coefficient b_m . The master position, x_m , is tracked by a slave device position, x_s ; the slave device is for simplicity modeled as a closed-loop system perfectly following x_m , as:

$$G_s(s) = \frac{y(s)}{x_m(s)} \approx 1$$

We model operators by making simplifying assumptions about their cognitive control and their neuromuscular dynamics (i.e., by using simple linear models with neglected delays). The cognitive control loop of the operator is considered to react on the visual feedback of the task, based on the control error $r - y$, with a simple proportional controller $C_h(s) = k_h$. The operator's neuromuscular system is modeled as a mass-spring-damper:

$$H_{nms}(s) = m_{nms} s^2 + b_{nms} s + k_{nms}, \quad (3.2)$$

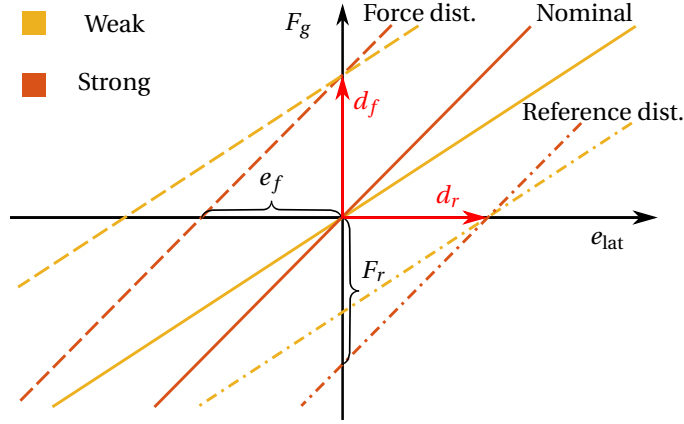


Figure 3.2: Guidance force as a function of lateral error e_{lat} . Two HSC stiffness levels compared in the nominal, force disturbance and reference disturbance situation. Under the disturbance force d_f the strong HSC stiffness results in a smaller tracking error e_f than the weak HSC. With reference disturbance offset of d_r , the strong HSC requires the operator to exert higher force F_r to mitigate its effect than the weak HSC.

3

with an assumed mass m_{nms} , damping coefficient b_{nms} , and stiffness k_{nms} . Finally, the grip adaptable haptic shared controller is introduced as a scalar function of the measured grip force $\mathbf{k}(f_{grip})$.

We describe the effects of two types of disturbance illustrated in Figure 3.1. In the proposed systematic description, disturbances are introduced at two locations: a) a force disturbance d_f is added as an additional input command to the master device, representing the category of disturbances that directly affect the controlled master-slave system; b) a reference disturbance d_r is added to the reference trajectory r before it enters the haptic guidance controller, and as such, it only influences the HSC system (note that a similar effect would be achieved if the visual feedback of the operator would be manipulated). It should be also noted that, in practice, the disturbances acting on the system are in general not known and can be only observed by their effects on the system.

The system outlined in Figure 3.3 is analyzed below. The response $y(s)$ to the reference trajectory $r(s)$, the force disturbance $d_f(s)$, and the reference disturbance $d_r(s)$, can be expressed as (Laplace s was left out for brevity):

$$\begin{aligned}
 y = & \underbrace{\frac{G_m G_s (C_h + \mathbf{k}(F_{grip}))}{1 + G_m (H_{nms} + G_s (C_h + \mathbf{k}(F_{grip})))}}_{\text{from reference trajectory}} r \\
 & + \underbrace{\frac{G_m G_s}{1 + G_m (H_{nms} + G_s (C_h + \mathbf{k}(F_{grip})))}}_{\text{from force disturbance}} d_f \\
 & + \underbrace{\frac{G_m G_s \mathbf{k}(F_{grip})}{1 + G_m (H_{nms} + G_s (C_h + \mathbf{k}(F_{grip})))}}_{\text{from reference disturbance}} d_r
 \end{aligned} \tag{3.3}$$

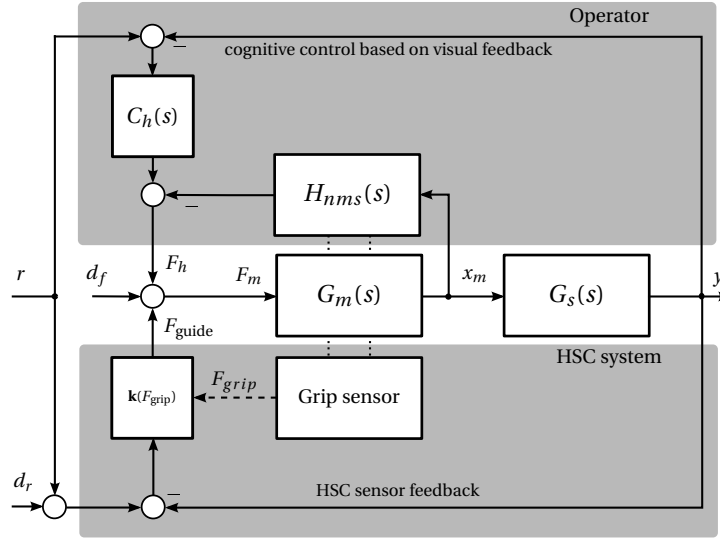


Figure 3.3: Grip-adaptable haptic shared control system. Control scheme containing a simplified human operator model that is supported in following the reference trajectory r by the proposed HSC system. The d_f and d_r are the force and reference disturbance, respectively.

3

To provide insight into functionality of the system and the effects of reference and force disturbances, Eq. (3.3) was combined with Eqs. (3.1,3.2), reformulated as a tracking error $e = r - y$ and evaluated for a steady-state:

$$e_{ss} = \frac{k_{nms}}{k_{nms} + k_h + \mathbf{k}(F_{grip})} r_{ss} \quad (3.4)$$

$$+ \frac{1}{k_{nms} + k_h + \mathbf{k}(F_{grip})} d_{fss} \quad (3.5)$$

$$+ \frac{\mathbf{k}(F_{grip})}{k_{nms} + k_h + \mathbf{k}(F_{grip})} d_{rss} \quad (3.6)$$

The goal of the complete human-in-the-loop system is to minimize this tracking error, as $e_{ss} \rightarrow 0$. The simplified system is influenced by three scalar system gains: the operator's hand neuromuscular stiffness k_{nms} , the operator's visual control proportional gain k_h , and finally the HSC system grip-force-adaptable gain $\mathbf{k}(F_{grip})$. We consider the three orthogonal inputs to the system, Eqs. (3.4,3.5,3.6), and argue the desirable setting of the system gains for the following cases:

- (1) *No disturbance.* Based on the Eq. (3.4), the HSC system system gains should: 1) the HSC gain $\mathbf{k}(F_{grip}) \rightarrow \infty$ and the operator visual gain $k_h \rightarrow \infty$ (or as high as practical) to provide maximal tracking performance; 2) and the operator needs to comply with the guidance force, $k_{nms} \rightarrow 0$.
- (2) *Force disturbance.* The complete human-in-the-loop system (both the HSC system and the operator) should contribute in resisting the force disturbance. In line with

Eq. (3.5), the HSC gain $\mathbf{k}(F_{grip})$, the operator's visual gain k_h , and the operator's stiffness k_{nms} should be as high as is practically achievable.

- (3) *Reference disturbance*. According to Eq. (3.6), the HSC gain $\mathbf{k}(F_{grip}) \rightarrow 0$ and to compensate the remaining effects of d_r the operator visual gain k_h and the operator's stiffness k_{nms} should be as high as is practically achievable.

In Section 3.3.7, these analytic observations are formulated into a set of hypotheses for the subsequent experiment.

3.3. METHOD

3.3.1. SUBJECTS

Eight subjects (one female), all employees of the European Space Agency, aged 28 to 41 years (with an average age of 32.6 years, $\sigma = 5.7$ years) participated in the experiment. All subjects had normal or corrected to normal vision. Seven subjects were right-handed and none reported recent injuries or any other disorder in the upper extremities. None of the subjects had any prior experience with haptic guidance. Subjects gave their informed consent prior to the experiment and no monetary compensation was offered.

3.3.2. PROCEDURE AND TASK INSTRUCTIONS

The control input position $x_m(t)$ was visualized on a black screen with a green dot and the subjects were instructed to stay inside a prescribed moving sinusoidal track (marked with thick white borders) on the screen, Figure 3.5, by actively moving the master device. To provide additional visual cues on (un-)satisfactory performance, the dot turned red when it got outside the track. During the experiment the subjects tracked a single sine reference trajectory, $r(t) = a \sin(2\pi f_r t)$, with amplitude of $a = 0.55$ rad (rotation required for the master device to follow the track), frequency of $f_r = 0.5$ Hz and the track half-width of $w_{track} = \pm 0.055$ rad (10 % of the peak amplitude).

At the beginning of the experiment the subjects were provided with written instructions and were allowed to familiarize themselves with the hardware setup and the experimental procedure. Before every condition, the subjects were explained how to use the specific HSC guidance scheme, which type of disturbance would be applied and then allowed to practice the condition for 60 sec. The complete experiment lasted approximately 90 minutes, including briefing, debriefing, practice runs, and breaks.

3.3.3. EXPERIMENTAL TRIAL

One experimental trial lasted 130 seconds (65 periods of the 0.5 Hz reference signal), see Figure 3.4. The first eight and the last two seconds of the measurement were removed from further analysis as run-in and run-out times.

For most of the trial, the subjects performed an undisturbed –nominal– task. However, one type of disturbance was applied on eight occasions, for details see Section 3.3.5. This way, during each trial, measurements for both the nominal task and for one disturbance type were obtained. During the disturbance, the subjects were ‘pushed’ outside the track while their task was still to follow the visual reference track, i.e., they needed to actively resist the disturbances and stay on the track. The disturbances each lasted

between two and four seconds, yielding between 16 and 32 seconds of disturbed signal per trial. After every disturbance, 2 seconds of data were removed to allow the subjects to recover. The remaining part of the trial resulted in between 74 and 90 seconds of undisturbed (nominal) task. The time between disturbances was randomized to be between 7 and 15 seconds long.

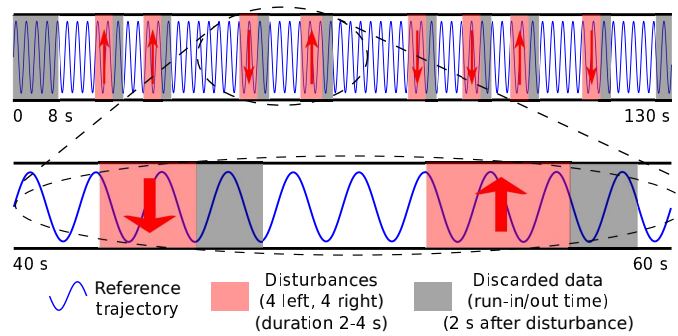


Figure 3.4: Example of an experimental trial. During every trial disturbances were introduced at eight random occasions, yielding at least 16 seconds of measurement with disturbance and at least 74 seconds of undisturbed measurement.

3.3.4. APPARATUS

The subjects were seated in an adjustable chair, such that the right forearm was parallel with the rotational axis of the joint, Figure 3.5. The subjects sat approximately 80 cm from a 19-inch LCD screen and were presented with the green dot as the actual position $x_m(t)$, the white center-line and the thick white boundaries of the track. To provide additional visual cues on (un-)satisfactory performance, the controlled dot turned red when it got outside the boundaries of the track.

The master position x_m was scaled to the horizontal position of the dot on the screen by 0.075 rad/cm, resulting in a side-to-side width of the track of approximately 16 cm. The track moved *downward* on the screen with a constant velocity, while the dot only moved sideways. At any time, the view contained 1.5 seconds of the future track and 2 seconds of the past track.

The study was conducted on a 1-DOF experimental setup, Figure 3.5, with one rotary joint additionally instrumented with foil force sensors to measure the operator's grip force. The control loop ran at a sampling frequency of 1 kHz. The unit composed of a brush-less DC motor, gearing stage (planetary gear and capstan) and an output handle. The motor was instrumented with an incremental encoder for velocity and position measurements.

The output shaft has a torque sensor that is used for the steering torque measurement. The handle of the device (with a length of $l_h = 70$ mm from the axis to the grip sensors) was equipped with a pair of foil force sensors (Tekscan FlexiForce A201 Sensors, with measuring range 0-110 N). The sensors were sampled at 100 Hz with a 10-bit A/D converter. The sensors were calibrated such that the effective linear range was between 0 and 15 N, with resolution of approximately 0.1 N. The reading from the sensors, $F_{\text{grip}_1}(t)$

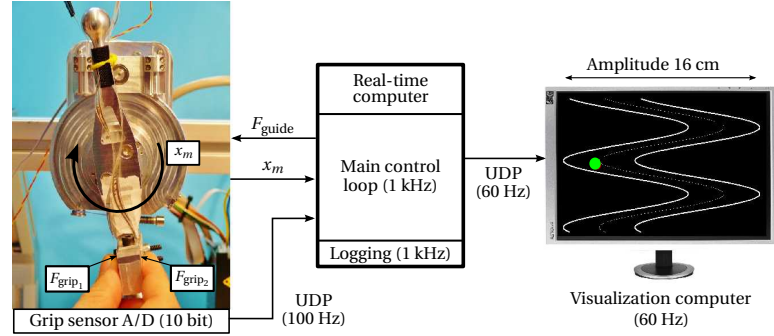


Figure 3.5: Experimental setup. Input device (left) instrumented with grip force sensors was used to control the green dot on the screen (right) to stay inside the track (adapted from [44]).

and $F_{grip_2}(t)$, is low-pass filtered with a cut-off frequency of 10 Hz to suppress noise and use only data on frequencies the operator is able to generate.

However, in this configuration the measured forces not only contained the grip force but also a portion of the force used by the operator to move the control device. To get a real-time estimate of the grip force separately, only the reading from the sensor that is on the opposite side as is the direction of motion is used (i.e., only the sensor that is on the other side than the operator is pushing toward), as:

$$F_{grip}(t) = \begin{cases} F_{grip_1}(t), & \text{for } \dot{x}_m(t) \geq 0 \\ F_{grip_2}(t), & \text{for } \dot{x}_m(t) < 0 \end{cases} \quad (3.7)$$

3.3.5. EXPERIMENT DESIGN AND INDEPENDENT VARIABLES

The experiment used a within-subjects repeated-measures design consisting of two independent variables: 3 (types of disturbance: nominal task, the force disturbance, and the reference disturbance) x 5 (types of haptic shared controller: unassisted control, two levels of fixed-gain haptic assistance, and two grip-adaptable controllers). In total, each subject performed 10 trials during the experiment, as listed in Table 3.3. Every trial consisted of the nominal task part and of one type of (force-reference) disturbance, for details see Section 3.3.3. The order of the trials was balanced to minimize the effects of learning and fatigue on the experiment.

HSC CONTROLLER IMPLEMENTATION

The subjects were supported to stay on the center-line of the track $r(t)$ by applying a guidance force proportional to the deviation between the reference trajectory $r(t)$ and the green dot position $y(t)$ as:

$$F_{guide}(t) = \mathbf{k}(F_{grip}(t)) [r(t) - y(t)], \quad (3.8)$$

where $\mathbf{k}(F_{grip})$ is the guidance stiffness (for generality expressed as function of momentary grip force $F_{grip}(t)$). For the fixed-gain controllers two stiffness levels were used, specifically the weak and the strong guidance. The weak guidance stiffness k_{WG} was

selected such that the HSC system provides noticeable guidance force, but the operator is required to supply most of the control effort. In contrast, the HSC system with strong guidance stiffness k_{SG} setting was designed such that the HSC system itself can fully facilitate the nominal task (i.e., task without any disturbances).

The grip-adaptable controllers calculate their stiffness as proportional with the gain c_{AG} to the momentary measured grip force $F_{grip}(t)$ (obtained by Eq. (3.7)), with a positive sign for increasing guidance stiffness with operator grip force, and a negative sign for decreasing stiffness with operator grip. To allow the operator to comfortably hold the master device handle without affecting the HSC system stiffness gain, the grip force measurement is first subjected to a dead-band nonlinearity $db(x)$, so that the stiffness gain is not adapted until a minimal grip force threshold F_{grip}^{\min} is applied by the operator (note that the grip force is non-negative), as:

$$db(x) = \begin{cases} 0, & \text{for } x \leq F_{grip}^{\min} \\ x - F_{grip}^{\min}, & \text{otherwise.} \end{cases} \quad (3.9)$$

The calculated stiffness gain is limited between the stiffness gains of the fixed controllers (k_{WG} and k_{SG}), as:

$$sat(x) = \begin{cases} x, & \text{for } k_{WG} \leq x \leq k_{SG} \\ k_{WG}, & \text{for } x < k_{WG} \\ k_{SG}, & \text{for } x > k_{SG} \end{cases} \quad (3.10)$$

Finally, by including Eqs. (3.9) and (3.10), the complete grip-adaptable controllers stiffness functions are defined such that with increased grip force $F_{grip}(t)$ the stiffness is:

$$\begin{aligned} \text{increased: } \mathbf{k}(F_{grip}(t)) &= sat(k_{WG} + c_{AG} db(F_{grip}(t))), \\ \text{decreased: } \mathbf{k}(F_{grip}(t)) &= sat(k_{SG} - c_{AG} db(F_{grip}(t))) \end{aligned}$$

For convenience, these stiffness functions are visualized in Figure 3.6, for grip forces F_{grip} between 0 and 13 N.

A summary of the guidance stiffness functions $\mathbf{k}(F_{grip})$, that were used as experimental conditions, is given in Table 3.1. The actual controller gains, provided in Table 3.2, were selected experimentally during a pilot experiment.

DISTURBANCES

As illustrated in Figure 3.1, the subjects were challenged in the task completion by two distinct types of disturbances:

- (a) *Force disturbance.* The operators benefited during the whole task from correctly working guidance. On occasion, the task difficulty was increased by additional force ($d_f(t) = \pm 0.1$ [Nm]) applied by the master device. The operators then need to exert increased steering force to compensate for the disturbance (e.g., a wind gust).
- (b) *Reference disturbance.* In the nominal situation, the visual task reference for the human operator and the haptic guidance reference are the same. However during some parts of the trial, a step disturbance is introduced to simulate a malfunction of the automatic system (e.g., the HSC picks-up a parallel lane). The operators

Table 3.1: HSC controllers used as experimental conditions






Color	HSC	HSC stiffness $k(F_{grip}(t))$	HSC description
	NG	0	Unassisted control
	WG	k_{WG}	Fixed, weak
	SG	k_{SG}	Fixed, strong
	AG ₊	$\text{sat}(k_{WG} + c_{AG} \text{db}(F_{grip}(t)))$	Adaptable, increase with increased grip
	AG ₋	$\text{sat}(k_{SG} - c_{AG} \text{db}(F_{grip}(t)))$	Adaptable, decrease with increased grip

Table 3.2: System parameters of the experimental setup and HSC system gains

Master inertia $m_m = 0.01$ [kg]	Fixed-weak stiffness $k_{WG} = 0.5$ [Nm/rad]	AG ₊ – tuning gain $c_{AG} = 0.5$ [/]
Master damping $b_m = 0.2$ [Nms/rad]	Fixed-strong stiffness $k_{SG} = 5$ [Nm/rad]	Minimal grip force $F_{grip}^{\min} = 1.75$ [N]

3

are still supposed to follow the reference trajectory $r(t)$ but the disturbed guidance ($d_r(t) = \pm 0.3$ [rad]) will essentially guide them to follow $r(t) + d_r(t)$, which they then need to compensate.

During every trial, a disturbance was introduced on 8 occasions (4 times to the left and 4 times to the right). The direction (left-right), time between disturbances and their duration were randomized to prevent anticipation.

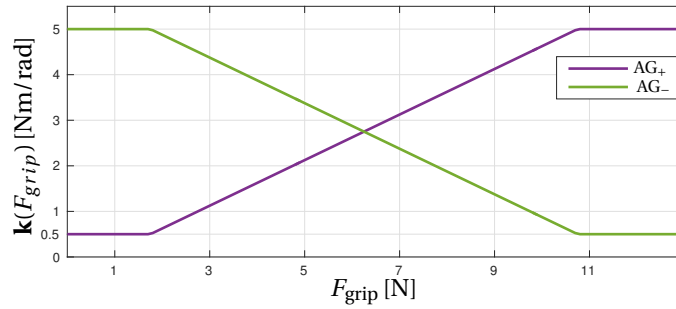


Figure 3.6: Grip-adaptable controllers stiffness. HSC controller stiffness as function of the momentary grip force, saturated at the stiffness of the fixed controllers (k_{WG} and k_{SG}).

Table 3.3: Combinations of experimental conditions completed by every subject during the experiment

Disturbance	HSC controller				
	NG	WG	SG	AG ₊	AG ₋
Nominal	• ¹	•	•	•	•
Force	•	•	•	•	•
Reference	o ²	•	•	•	•

¹ Each column represents a single experimental trial (the order was balanced between subjects).

² The reference disturbance only affects the HSC system, i.e., it has no effect on the unassisted control condition.

3.3.6. DEPENDENT MEASURES

The dependent measures used to compare the studied conditions can be divided into three categories: task performance, operator workload, and HSC effectiveness. The dependent measures are listed in Table 3.4.

Table 3.4: Experiment dependent measures.

Measure	Symbol	Description
Performance	\bar{E}_{off}	Mean off-track excursion [rad]
Operator control effort	\bar{F}_h \bar{F}_{grip}	Mean steering force [N] Mean grip force force [N]
HSC effectiveness	\bar{D} \bar{k}	Mean guidance disagreement [/] Mean HSC stiffness [Nm/rad]

The dependent measures were calculated for every trial, at discrete times n (with a time step of 1 ms). All metrics were averaged separately for the disturbance conditions (nominal and disturbed). In other words, the range of time steps $n \dots N$ signifies that based on the specific disturbance conditions, the metrics were averaged only over the corresponding parts of the trial.

MEAN OFF-TRACK EXCURSION

To assess how well the subjects managed to stay within the bounds of the prescribed trajectory (of half-width w_{track}), a mean off-track excursion was calculated as: $\bar{E}_{off} = \frac{1}{N} \sum_{n=1}^N e(n)$, where

$$e(n) = \begin{cases} |r(n) - y(n)| - w_{track}, & \text{for } |r(n) - y(n)| > w_{track} \\ 0, & \text{otherwise} \end{cases} \quad (3.11)$$

MEAN STEERING FORCE

The physical workload of the operator was calculated as the mean magnitude of the interaction force between the operator and the master device, recorded by the torque sensor in the handle output shaft, $\bar{F}_h = \frac{1}{l_h} \frac{1}{N} \sum_{n=1}^N |\tau_{\text{sensor}(n)}|$, where the handle length $l_h = 0.07$ m was used to scale the torques to forces at the contact point where the operators held the handle, see Figure 3.5.

MEAN GRIP FORCE

The mean magnitude of the grip force was calculated both as a means to study the different adaptable controllers and to assess the physical workload associated with maintaining increased grip force. The metric was calculated from a mean of the grip force sensor measurements, pre-processed according to Eq. (3.7), as $\bar{F}_{\text{grip}} = \frac{1}{N} \sum_{n=1}^N |F_{\text{grip}}(n)|$.

MEAN GUIDANCE DISAGREEMENT

The possible disagreement between the operator and the HSC system was evaluated using the haptic guidance disagreement metric [98]. The metric is based on calculating the internal forces $F_i(n)$, that occur if the forces generated by the operator, $F_h(n)$, and force by the HSC, $F_{\text{guide}}(n)$, are in opposite directions (the time-step n was omitted for brevity):

$$F_i = \begin{cases} F_h, & \text{if } \text{sign}(F_h) \neq \text{sign}(F_{\text{guide}}) \wedge |F_h| \leq |F_{\text{guide}}| \\ F_{\text{guide}}, & \text{if } \text{sign}(F_h) \neq \text{sign}(F_{\text{guide}}) \wedge |F_h| > |F_{\text{guide}}| \\ 0, & \text{if } \text{sign}(F_h) = \text{sign}(F_{\text{guide}}) \end{cases} \quad (3.12)$$

The disagreement is then calculated as the mean internal force $\bar{D} = \frac{1}{N} \sum_{n=1}^N |F_i(n)|$.

MEAN HSC STIFFNESS

The mean HSC system stiffness was calculated to study how the operators were able to use the two different adaptable controllers.

3.3.7. HYPOTHESES

Two hypotheses were formulated for the experiment. First, as H_1 , we hypothesize that, for the unassisted control and the fixed-gain controllers, a higher HSC gain (i.e., $\text{SG} > \text{WG} > \text{NG}$) will provide better task performance in the nominal task and in the force disturbance condition. In contrast, we hypothesize that a higher HSC gain would in the reference disturbance condition lead to lower task performance.

Second, as H_2 , we look beyond task performance and focus on the suitability of the two proposed grip-adaptable HSC controllers (AG_+ and AG_-) for the three disturbance conditions (no, force, and reference). The H_2 is presented as three sub-hypotheses, which are summarized in Table 3.5. In this table, the hypothesized desirable settings (column ‘Desired setting’) of the operator’s hand neuromuscular stiffness k_{nms} and of the HSC controller gain \mathbf{k} are based on the analysis discussed in Section 3.2.1. The decision which of the proposed grip-adaptable controllers constitutes a more suitable HSC method (column ‘Suitable HSC?’) is based on the assumption that stiffening-up of the operator’s k_{nms} is accompanied by increased operator’s grip force [106].

To illustrate this hypothesis, we consider the following example: in a nominal task, the desired low stiffness of the k_{nms} would correspond to low grip force of the operator F_{grip} . Now if we consider the two grip-adaptable strategies: using the AG₊ controller would result in low \bar{k} , which is not desirable (in Table 3.5, column ‘Suitable HSC?’ marked as a ‘No’). Whereas using the AG₋ controller would provide the desired high \bar{k} gain (marked as a ‘Yes’).

Assuming that the operators strive to keep high task performance with minimal control effort, following the same line of reasoning as in the previous example, we hypothesize that for the human-in-the-loop experiment: H_{2a}) in a nominal task, the controller AG₋ will constitute a more suitable HSC; H_{2b}) in presence of a force disturbance, the controller AG₊ will be more suitable; and H_{2c}) in presence of a reference disturbance, the controller AG₋ will be more suitable.

Table 3.5: Hypothesized suitability of the proposed adaptable HSC controllers (sub-hypotheses of H_2).

Hypothesis	Disturbance	Desired setting		Suitable HSC?	
		k_{nms}	$\mathbf{k}(F_{grip})$	AG ₊	AG ₋
H_{2a}	No (nominal)	Low	High	No	Yes
H_{2b}	Force	High	High	Yes	No
H_{2c}	Reference	High	Low	No	Yes

3.3.8. DATA ANALYSIS AND VISUALIZATION

To investigate H_1 and to provide general comparison of the studied HSC methods, the statistical analysis of the experimental results was first conducted using a two-way repeated measures ANOVA, with significance level of $\alpha < 0.05$. These results were further evaluated with post-hoc multiple comparison Tukey HSD tests. The assumption of sphericity was assessed using Mauchly’s test; for non-spherical data the Greenhouse-Geisser corrections were applied to the degrees of freedom [91]. The sub-hypotheses of H_2 were assessed using a paired t-test.

The results are first presented separately for the ‘Nominal’ and both ‘Disturbed’ parts of the task. Median, 25th and 75th percentiles and the maximal and minimal values for all subjects are shown in the following figures. The test HSC controller conditions are color coded according to Table 3.1. Statistic significance is visualized in the plots below with the following notation marking the significance levels: • for $p \leq 0.05$, •• for $p \leq 0.01$, and ••• for $p \leq 0.001$.

For the ANOVA test, the effect size η^2 (proportion of variance accounted for by each of the factors) is reported. In the pair-wise comparisons, the absolute effect sizes are reported for measures with intrinsic meaning (e.g., the difference of mean steering forces).

3.4. RESULTS

The results of the two-way repeated measures ANOVA tests for the respective dependent measures are summarized in Table 3.6. In following section, statistically significant re-

sults based on the post-hoc multiple comparisons are reported together with appropriate effect sizes. The *nominal* part of the trials is evaluated separately from the *disturbed* parts for both types of disturbance.

Table 3.6: Summary of the two-way ANOVA results.

Metric	Factors		
	HSC	HSC \times Dist.	Disturbance
\bar{E}_{off}	$F_{0.67,4.71} = 6.3$ $p = .004, \eta^2 = .06$	$F_{1.35,9.43} = 44.5$ $p < .001, \eta^2 = .58$	$F_{0.34,2.36} = 23.0$ $p < .001, \eta^2 = .14$
\bar{F}_h	$F_{0.67,4.72} = 10.5$ $p = .001, \eta^2 = .13$	$F_{1.35,9.44} = 61.3$ $p < .001, \eta^2 = .63$	$F_{0.34,2.36} = 14.7$ $p < .001, \eta^2 = .04$
\bar{F}_{grip}	$F_{0.77,5.36} = 7.9$ $p = .005, \eta^2 = .24$	$F_{1.53,10.71} = 7.5$ $p = .001, \eta^2 = .24$	$F_{0.38,2.68} = 8.9$ $p = .005, \eta^2 = .03$
\bar{D}	$F_{0.48,3.36} = 59.6$ $p < .001, \eta^2 = .36$	$F_{0.96,6.71} = 47.7$ $p < .001, \eta^2 = .27$	$F_{0.24,1.68} = 113.3$ $p < .001, \eta^2 = .26$
\bar{k}	$F_{0.41,2.84} = 131.8$ $p < .001, \eta^2 = .65$	$F_{0.81,5.68} = 25.5$ $p < .001, \eta^2 = .10$	$F_{0.20,1.42} = 193.4$ $p < .001, \eta^2 = .16$

3

3.4.1. TASK PERFORMANCE: MEAN OFF-TRACK EXCURSION

To investigate hypothesis H_1 , that relates task performance to HSC controller stiffness, the mean off-track excursion was compared in Figure 3.7. In the nominal part of the trial, Figure 3.7a, all haptic shared controllers provided better performance over the unassisted control condition NG ($p < 0.01$).

In the disturbed part of the trial, Figure 3.7b, when the force disturbance was applied, the fixed strong controller SG, and both adaptable controllers AG₊ and AG₋ performed better than the unassisted control condition NG and the fixed weak controller WG ($p < 0.01$). For the reference disturbance, both adaptable HSCs AG₊ and AG₋ performed worse than the WG ($p < 0.01$).

3.4.2. OPERATOR CONTROL EFFORT: STEERING FORCE

When the force disturbance was introduced, the SG, and both adaptable controllers AG₊ and AG₋ required the operator to apply lower mean steering force than the unassisted control condition NG and the fixed weak controller WG ($\Delta \bar{F}_h = 1.42\text{N}$, CI_{95%} [0.78, 2.06], $p < 0.001$). In the reference disturbance case, the strong fixed guidance SG required the operator to apply the highest steering force among the controllers (compared to AG₋: $\Delta \bar{F}_h = 4.79\text{N}$, CI_{95%} [3.55, 6.03], $p < 0.001$). When comparing the adaptable controllers, the AG₊ required higher steering force than AG₋ ($\Delta \bar{F}_h = 1.77\text{N}$, CI_{95%} [0.28, 3.26], $p = 0.022$).

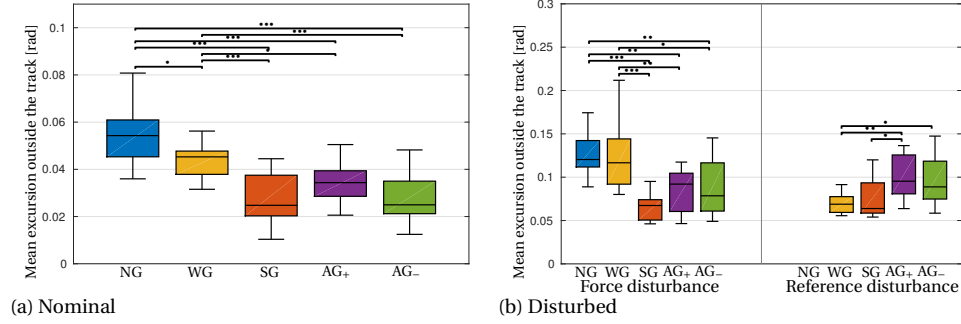


Figure 3.7: Mean off-track excursion showing the effect of disturbances on the tested HSC controllers, with higher values denoting lower task performance. Stronger guidance in general provided better task performance. Note that the y-axes are substantially different.

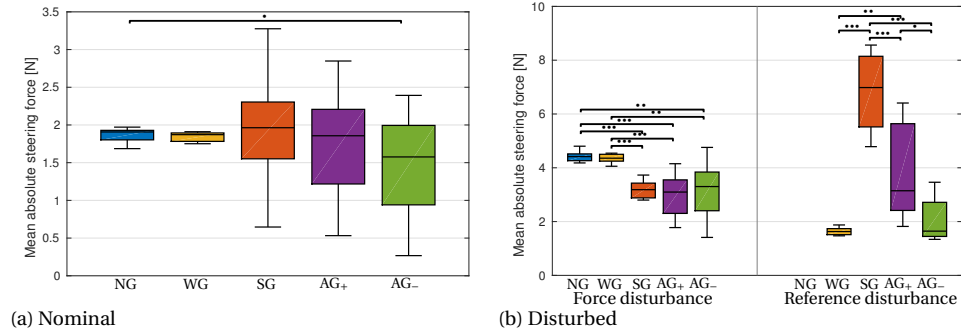


Figure 3.8: Mean steering force showing the effect of disturbances on the tested HSC controllers. Both adaptable controllers allowed to reduce the steering force necessary to compensate effect of the reference disturbance. Note that the y-axis are substantially different.

3.4.3. OPERATOR CONTROL EFFORT: GRIP FORCE

In Figure 3.9, mean grip force was compared. In the nominal part of the trial, Figure 3.9a, the adaptable controller AG_+ resulted in highest mean grip force among the controllers (compared to AG_- : $\Delta \bar{F}_{grip} = 5.06\text{N}$, $CI_{95\%} [2.69, 7.44]$, $p < 0.001$). When the force disturbance was present, Figure 3.9b, the AG_+ still required higher \bar{F}_{grip} than the other controllers (compared to AG_- : $\Delta \bar{F}_{grip} = 7.69\text{N}$, $CI_{95\%} [4.94, 10.45]$, $p < 0.001$). The adaptable controller AG_- resulted in lower mean grip force than WG ($\Delta \bar{F}_{grip} = 4.41\text{N}$, $CI_{95\%} [1.57, 7.25]$, $p = 0.004$). When the reference was disturbed, the fixed weak controller WG resulted in the lowest mean grip force among the controllers (compared to AG_- : $\Delta \bar{F}_{grip} = 6.04\text{N}$, $CI_{95\%} [2.23, 9.86]$, $p = 0.004$).

3.4.4. HSC EFFECTIVENESS: HAPTIC GUIDANCE DISAGREEMENT

Mean haptic guidance disagreement results are shown in Figure 3.10. In the nominal part of the trial, Figure 3.10a, the fixed weak controller WG was the least opposed by the subjects, i.e., resulted in the lowest disagreement ($p < 0.05$). When the force disturbance

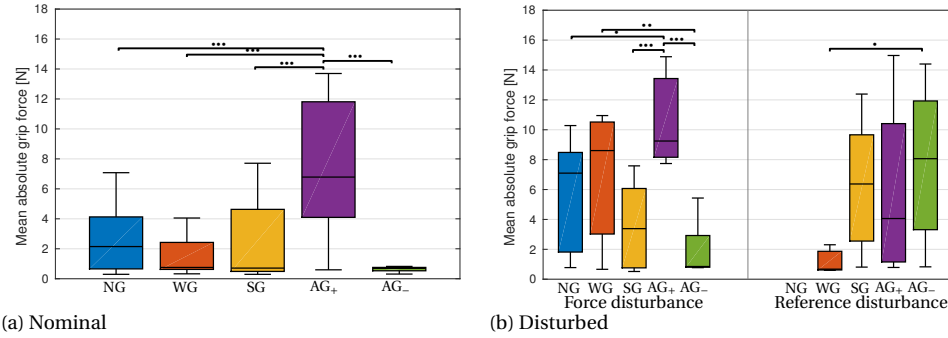


Figure 3.9: Mean grip force showing the effect of disturbances on the tested HSC controllers. The AG₊, in accordance with its design, requires higher grip force.

was present, Figure 3.9b, the WG still resulted in the lowest disagreement among the controllers ($p < 0.001$). When the reference was disturbed, the fixed weak controller WG resulted in lowest disagreement ($p < 0.05$), the adaptable AG₋ scored second ($p < 0.05$), with lower \bar{D} than AG₊ ($p < 0.05$). Finally, the fixed strong controller SG exhibited the highest level of disagreement ($p < 0.001$). It should be noted that the low haptic guidance disagreement values for the WG controller are not surprising and are due to the low scaling of the HSC guidance forces.

3

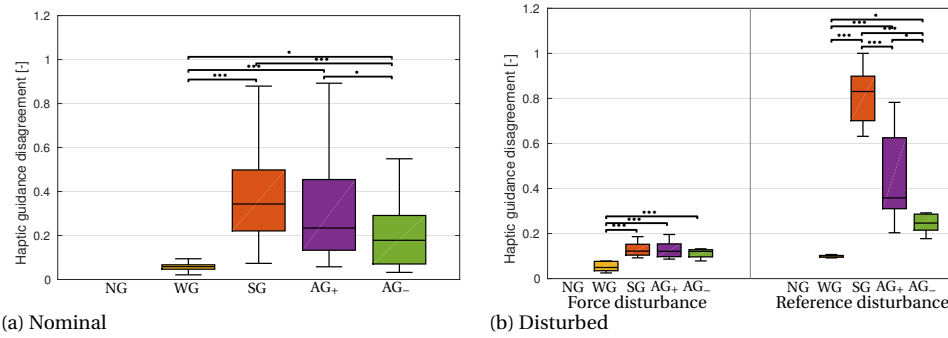


Figure 3.10: Mean haptic guidance disagreement showing the effect of disturbances on the tested HSC controllers, with higher values denoting lower agreement between the operator and the HSC system. The SG exhibited highest disagreement.

3.4.5. HSC EFFECTIVENESS: MEAN HSC STIFFNESS

To investigate the predicted usage of both adaptable controllers (hypothesis H_2), mean haptic guidance stiffness gains \bar{k} are analyzed in Figure 3.11. In the nominal case (sub-hypothesis H_{2a}), for both force and reference disturbance trials, a paired t-test did not reveal a statistically significant difference between the AG₊ and AG₋ controllers ($t_7 = -0.51$, $p = 0.63$). With both controllers the operators could on average maintain equally high \bar{k} gain settings.

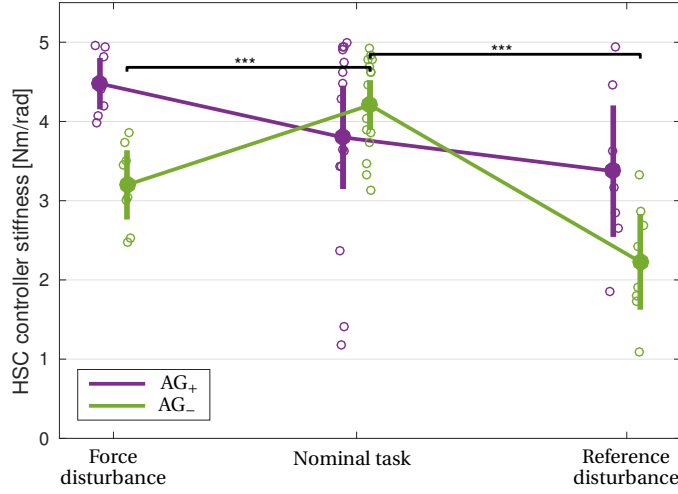


Figure 3.11: Subject means (open symbols) and mean over all subjects (filled symbols \pm 95% CI) of the mean HSC controller stiffness showing change in reaction on disturbance. For the force disturbance, the operators were able to maintain HSC stiffness with the AG₊ controller when the disturbance was introduced. When the reference was disturbed, the AG₋ controller allowed the operators to reduce the HSC stiffness.

The absolute effect sizes were calculated to evaluate the effect of the applied disturbance on \bar{k} . Comparing the nominal task in contrast to the force disturbance case, addressed by sub-hypothesis H_{2b} , while using the AG₊ controller, the operators maintained the level of \bar{k} between the Nominal and Disturbed situations ($\Delta\bar{k} = 0.62\text{Nm/rad}$, $\text{CI}_{95\%} [-0.21, 1.45]$, $p = 0.121$). In trials when the AG₋ controller was used, the HSC gain decreased in reaction to the disturbance ($\Delta\bar{k} = -0.97\text{Nm/rad}$, $\text{CI}_{95\%} [-1.14, -0.79]$, $p < 0.001$). The operators on average managed to maintain high \bar{k} gain setting with the AG₊ controller. In contrast, the average \bar{k} gain even decreased with the AG₋ condition.

Comparison of the nominal task to the reference disturbance case, addressed by sub-hypothesis H_{2c} , there was no adaptation of the \bar{k} between the Nominal and Disturbed situations with the AG₊ controller ($\Delta\bar{k} = -0.37\text{Nm/rad}$, $\text{CI}_{95\%} [-1.00, 0.26]$, $p = 0.210$). When the AG₋ controller was used, the HSC gain decreased in reaction to the reference disturbance ($\Delta\bar{k} = -2.02\text{Nm/rad}$, $\text{CI}_{95\%} [-2.58, -1.46]$, $p < 0.001$). Using the AG₋ controller, the operators were able to decrease the \bar{k} gain setting, when they were in conflict with the HSC system (reference disturbance). However, there was no decrease of the \bar{k} when the AG₊ was used.

3.5. DISCUSSION

This study provides a formalized and validated operator adaptable haptic shared control (HSC) system. We studied how the operator can take advantage of this system in three different situations: 1) we studied how operators can use the system in a nominal (undisturbed) task; 2) moreover, we investigate how the operators can cope with the effects of the force disturbances (that increased the task difficulty but the HSC system was still act-

ing on the same control goal as the operator); 3) and of the reference disturbance (which represented a conflict between the goals of the operator and the HSC system). Following effects were observed during the human-in-the-loop experiment:

STRONGER GUIDANCE IMPROVES PERFORMANCE BUT PROMOTES DIS-AGREEMENT

In accordance with the hypothesis H_1 , stronger HSC stiffness resulted in higher performance, with comparable steering force for all controllers, both in the nominal and force disturbance parts of the task. However, the fixed strong SG controller was also on average the most opposed by the operators (highest HSC disagreement \overline{D}). This can be caused by the operators having a different preference on how to follow the reference trajectory (e.g., by ‘cutting curves’ as observed in [37]). A promising method to alleviate this issue might be to adjust the HSC system reference trajectory (within task limits) to match more closely a operator-preferred trajectory [59].

Surprisingly, opposite to what was hypothesized in H_1 , when the reference was disturbed, the operators still managed to achieve high task performance, even with the strong fixed HSC controller (which presented the highest erroneous guidance force). The operators compensated for this by exerting substantially higher steering force \overline{F}_h , which would be exhausting if implemented in a real application.

3

THE MODELING FORMALIZATION ALLOWS ANALYSIS OF CONFLICTS AND DISTURBANCES IN HSC SYSTEMS

We performed and analyzed an experiment in which operators had to perform a task in the three aforementioned disturbance conditions. The results of the conducted experiment match the predictions based on the control-theoretic model of the system (formulated as hypothesis H_2).

Following the analysis presented in Section 3.2.1, we hypothesized (for summary of sub-hypotheses of H_2 see Table 3.5), that in the nominal situation it is desirable to provide high HSC system gain \overline{k} while the operator remains compliant with the haptic guidance forces. We predicted that the more suitable controller would be the AG₋. Based on the experimental results, Figure 3.11, both adaptable controllers exhibited comparably high \overline{k} in the nominal condition. The AG₋ controller allowed to achieve that with substantially lower HSC disagreement \overline{D} , i.e., the operators tended to comply more with the guidance. This finding is in agreement with the sub-hypothesis H_{2a} .

In case of the force disturbance, the AG₊ was predicted to be the more suitable controller. In accordance with this expectation, the AG₊ allowed the operators to maintain the high \overline{k} , whereas the AG₋ controller was accompanied with a decreased \overline{k} . This observation agrees with the assumption that high operator neuromuscular system stiffness corresponds to high grip force. When the force disturbance is present and the operators have to resist it (by stiffening up), the accompanied increased grip force causes an unwanted decrease in the AG₋ controller gain (and a desirable increase with AG₊), supporting sub-hypothesis H_{2b} .

For the reference disturbance, the AG₋ was expected to be the best controller. In agreement with the prediction, the operators were able to correctly utilize the AG₋ and decrease \overline{k} , effectively lowering the negative influence of the disturbed guidance and

substantially minimizing the necessary steering force \overline{F}_h to overcome it. In contrast, there was no measurable reduction while using the AG_+ controller gain \overline{k} , supporting sub-hypothesis H_{2c} , and the operators had to use higher \overline{F}_h to compensate for it.

We conclude that the average reaction of the operators match our theoretical predictions and it is thus possible to formalize the effects of aforementioned disturbance in HSC systems. In the future, such validated formalization can be used for model-based analysis and design of HSC systems in presence of disturbances.

PERFORMANCE INCREASED BY ADAPTABLE GUIDANCE WITH REDUCED STEERING FORCE

Results of both adaptable controllers, AG_+ and AG_- , in the nominal and force disturbance parts of the task, show that the operators were able to perform the task better than with the fixed weak guidance WG. In other words, the operators were able to take advantage of the flexibility provided by the adaptable guidance method and increase their task performance by opting for higher guidance stiffness setting, up to the level of strong fixed guidance SG. Moreover, the operators were able to use the adaptable controllers AG_+ and AG_- to minimize the necessary steering they had to apply (SG level).

IMPLICATIONS FOR APPLICATION DOMAINS

The proposed approach essentially adds an additional degree of freedom – without negatively affecting the performance. We observed that the operators did not significantly change their grip during the task with fixed-authority systems whereas they took advantage of the authority adaptation if provided with the option. The described system can serve as a fast and intuitive ‘manual-override’ function in case of automatic system malfunction when the operator needs to quickly take over [80, 96], possibly limiting negative effects of inaccuracies in guidance systems [45, 46]. Alternatively it might also prove useful in more complex tasks where easier departures from original goals might be a desirable property, for example in lane changing with car driving support systems [109] or to allow switching between several sub-goals in teleoperated assembly tasks [103, 110].

Furthermore, the method could be suitable for training of manual skills using haptic guidance. It was shown that progressively decreasing level of guidance force better facilitates learning and retention of tasks [63, 111]. From this point of view, the training would be at the beginning facilitated by strong guidance force, that could then diminish as the operator gets more confident and assumes higher authority of the task.

LIMITATIONS

The experimental conditions only exposed the operator to either increased task difficulty (force disturbances) or to conflicting goal of the guidance (reference disturbances), with the operator fully aware what to expect. In a practical application both types of disturbances could arise. How well the operators would be able to distinguish those and perform in such situations remains for further investigation.

3.6. CONCLUSIONS

This chapter provides an experimentally verified formalization of a haptic shared control guidance system operating in the presence of goal-related conflicts and task-difficulty-altering disturbances. To cope with these additional realistic challenges, a new method for adapting the authority of the guidance based on the operator's grip force was presented. For the studied experimental conditions we conclude that:

- (1) The proposed formalization provides a viable method to analyze goal-related conflicts for systems with haptic shared control.
- (2) Using the proposed adaptable-authority haptic shared controller the operator achieved increased performance over the weak (possibly 'under-tuned') fixed guidance, up to the level comparable with the strong fixed guidance setting.
- (3) Thanks to the adaptable-authority control method, the steering force necessary to overcome the incorrect guidance was significantly reduced over the fixed-authority strong guidance system for the 'decreasing guidance authority with increased grip' controller (while maintaining comparable performance).
- (4) The same controller also exhibited a reduced disagreement between the operator and the guidance, suggesting that the subjects were able to successfully adapt the HSC system setting closer to their preference.

II

TELEOPERATION SYSTEM RELATED UNCERTAINTY

4

GEOMETRICAL GOAL UNCERTAINTIES IN A TELEOPERATED CONTACT TASK

*The chapter describes the challenges associated with using a position reference based haptic guidance to provide support in a contact task, specifically to support peg-in-hole insertion with **attractive guidance** type HSC. Such an HSC system is used to support the operator to precisely align the peg prior and during the insertion into the hole. It is highlighted how the inevitable geometrical inaccuracies of the guidance reference models negatively interact with the natural force feedback in bilateral teleoperation. The chapter offers a system-theoretical analysis of the problem by extending the Lawrence framework [14]. The findings are confirmed by simulation and also experimentally on a 6-DOF master-slave teleoperation system.*

This chapter is based on the following publication:

- Jan Smisek, Marinus M. van Paassen and Andre Schiele, “Haptic guidance in bilateral teleoperation: Effects of guidance inaccuracy”, IEEE World Haptics Conference, Evanston, 2015

CHAPTER SUMMARY

The purpose of this chapter is to analyze the effects of inaccuracies of haptic guidance systems during execution of constrained tasks. The Lawrence teleoperation framework is extended in this chapter by addition of an impedance type, position-based attractive haptic guidance and analyzed from a control system perspective; the analysis is based on a linear, non-delayed, time-invariant model of the system.

Specifically, we focus on systems where haptic guidance is used together with position or force-based feedback from a slave robot to a master device. The forces due to the inaccuracy of the guidance partially counteract the feedback force, effectively masking this problematic inaccuracy from the operator. This effect is discussed by using the proposed framework and quantified. Theoretical results are supported with numerical simulation and experimentally verified on a real 6-DOF haptic teleoperation setup.

4.1. INTRODUCTION

Haptic guidance systems provide synthetic guidance forces on the master device that help the operator to follow a prescribed trajectory in a teleoperated task. Haptic guidance is considered a viable paradigm for combining human and machine capabilities in one system, that offers reduced workload and potentially higher performance, yet allows the operator to keep final authority over the task [68]. If haptic guidance is used to support a constrained task, its efficiency strongly depends on the quality of the reference trajectory that an operator is supposed to follow. For example, we can consider a haptically guided peg-in-hole insertion task, see Figure 4.1(a). The robot (by force input to the master device) is guided by appropriate trajectories to align itself perfectly with the hole's center-line prior to the insertion. If the operator now commands the slave robot to move into the hole, the interaction forces should be minimal.

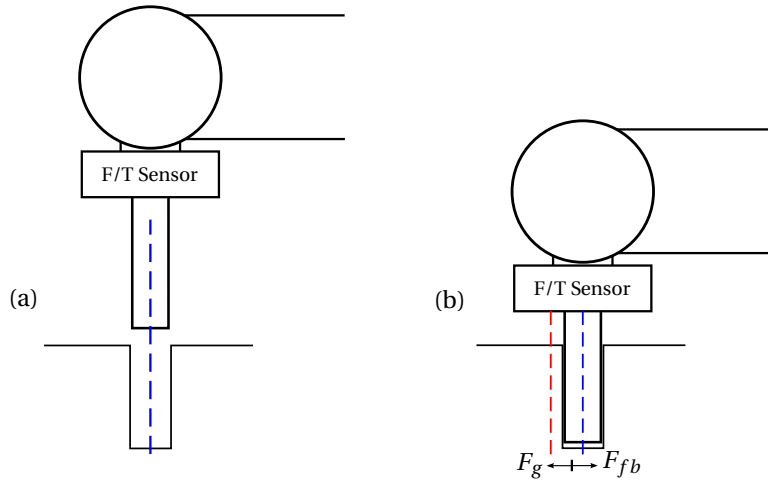


Figure 4.1: A slave robot performing a peg-in-hole insertion. In (a), the robot is guided in free air to perfectly align to the blue reference, which coincides with the hole centerline. Drawing (b) shows a situation where the peg is already inserted, but the red haptic guidance reference is inaccurate, i.e., erroneous and then ‘pushing’ the operator to command the slave to the walls of the hole. The feedback force from the force sensor is having an opposite direction and acts against the guidance.

However, the reference is not always sufficiently accurate, i.e., it does not always match the specific task and the expected model of the environment. If we consider operating in an unstructured environment, where we do not have perfect knowledge of the objects, a sensor has to be used to determine the optimal reference positions or trajectories to be used for haptic guidance (e.g., through computer vision in [112]). The reference position is then affected by the uncertainties of the sensor system.

Environments that are unstructured and hard to automatically analyze are challenges traditionally tackled by bi-lateral teleoperation. The physical interaction of the slave is fed back to the master device and the operator is able to feel how much force the slave robot is experiencing, increasing the performance of a teleoperated task [20]. Combining a virtual haptic guidance force and a real feedback force is the next natural step. We can see an example in Figure 4.1(b). Here the peg is already inserted, however;

the haptic guidance reference is inaccurate (in red), guiding the operator by the force F_g to command the slave off the hole's centerline. The feedback force F_{fb} coming from the force sensor has, however, an opposite direction and acts against the guidance.

Let's now consider the effect of adding these forces together on the master device. On the one hand, depending on the design of the guidance system, the real and virtual forces can be easily misinterpreted and such a system has indeed been shown to be confusing for the operator [113]. On the other hand, in a study that explicitly focused on haptic guidance system inaccuracies, test subjects were able to use force feedback to their benefit and complete a task despite the intentional guidance offsets [45]. A combination of haptic guidance with force feedback was also investigated earlier [22, 114, 115] and showed benefits mainly in non-constrained sub-tasks (i.e., in free air operations and contact transitions). The problem of inaccuracies creating conflicting information to the operators during constrained contact tasks, however, is especially troublesome, and is addressed in this chapter.

The goal of this chapter is to abstract this problem into a system perspective, to analyze the performance of the haptic guidance system and to quantify the effects of operator compliance with the guidance forces. For this purpose, the Lawrence teleoperation scheme [14], a convenient framework to study a range of different teleoperation architectures, together with effects of the environment and of the operator, is extended by adding an impedance type, position-based haptic guidance channel. We focus the analysis of this general guidance system on a sub-set of the three most elementary bilateral control architectures, where the haptic guidance is combined with: no slave feedback, slave position feedback and slave force feedback. The theoretical results are supported with a numerical simulation and with a simple peg-in-hole insertion experiment that is conducted on a real 6-DOF master and slave setup.

4

HAPTIC GUIDANCE: FUNCTION AND PERFORMANCE DEFINITION

The goal of the haptic guidance system is to support the operator in following a desired trajectory by providing additional *guidance* forces on the master device. The underlying design idea is that the operator feels the control inputs from the guidance system (the guidance forces) and is always able to overrule them if he/she considers it necessary [68]. The operator is able to do so by either deciding to follow the guidance by giving way to the haptic guidance forces, i.e., becoming more compliant, or by deciding to resist them, by stiffening up [76].

However, the operator can also assume a broad range of stiffness settings in-between these two extreme values [105], which makes tuning of the haptic guidance system (i.e., scaling of the guidance forces) challenging [50, 116, 117]. Current solutions proposed in literature span from a trial & error tuning [112], performance-based tuning [93], tuning based on operator's neuromuscular impedance modeling and identification [53, 76] to adaptive systems [44]. In this chapter we utilize the Lawrence teleoperation framework formalism, that takes the impedance of the operator's arm explicitly into account, to describe in detail the haptic guidance contribution and to quantify the effect of the operator's impedance on the teleoperated task.

The focus of the chapter is specifically on attractive impedance type haptic guidance, the main purpose of which is to guide the master device towards a defined reference

trajectory (or position). A natural way of how to assess performance of such a guidance system is to measure how well the system is able to track the reference. There is a range of metrics available that also takes the system dynamical response into account (e.g., settling time, overshoot, system norms) but to provide a first insight we focus here only on the steady-state tracking response.

Intuitively, the performance is then defined as the distance between the reference of the guidance and the position of the slave system. However, if the haptic guidance system is used to support a contact task, like in the peg-in-hole example (Figure 4.1), the environment can constrain the position of the slave. In such situation, we can assess the forces exerted on the environment, basically considering any force as a sign of misalignment between the real environment and its assumed model.

4.2. HSC IN COMMON TELEOPERATION ARCHITECTURES

The Lawrence teleoperation control diagram [14] is extended here by an impedance type position-based haptic guidance system in Figure 4.2. We limit our analysis to the three most elementary (and common) teleoperation architectures, namely:

- (a) Position control with No feedback with haptic guidance (PN) [22].
- (b) Position control with Position feedback with haptic guidance (PP) [22, 116].
- (c) Position control with Force feedback with haptic guidance (PF) [45, 114, 115].

The system equations are conventionally expressed in terms of velocities V_h, V_e [14] but here positions X_h, X_e are used instead to simplify the introduction of the position based haptic guidance.

The master and the slave devices are assumed to be mass-damper systems with local position proportional control as:

$$Z_m(s) := M_m s^2 + B_m s \quad C_m(s) := K_m \quad (4.1)$$

$$Z_s(s) := M_s s^2 + B_s s \quad C_s(s) := K_s \quad (4.2)$$

The controller C_1 constitutes the position command from the master to the slave and the controllers C_2 and C_4 provide the force and the position feedback from the slave to the master, respectively. The human operator is modelled as a mass-spring damper system:

$$Z_h(s) = M_h s^2 + B_h s + K_h,$$

and the environment is represented by a spring-damper:

$$Z_e(s) = B_e s + K_e,$$

where we assume that the environment is passive $F_e^* = 0$ and has its neutral point at the origin, i.e., $F_e = 0$ for $X_e = 0$.

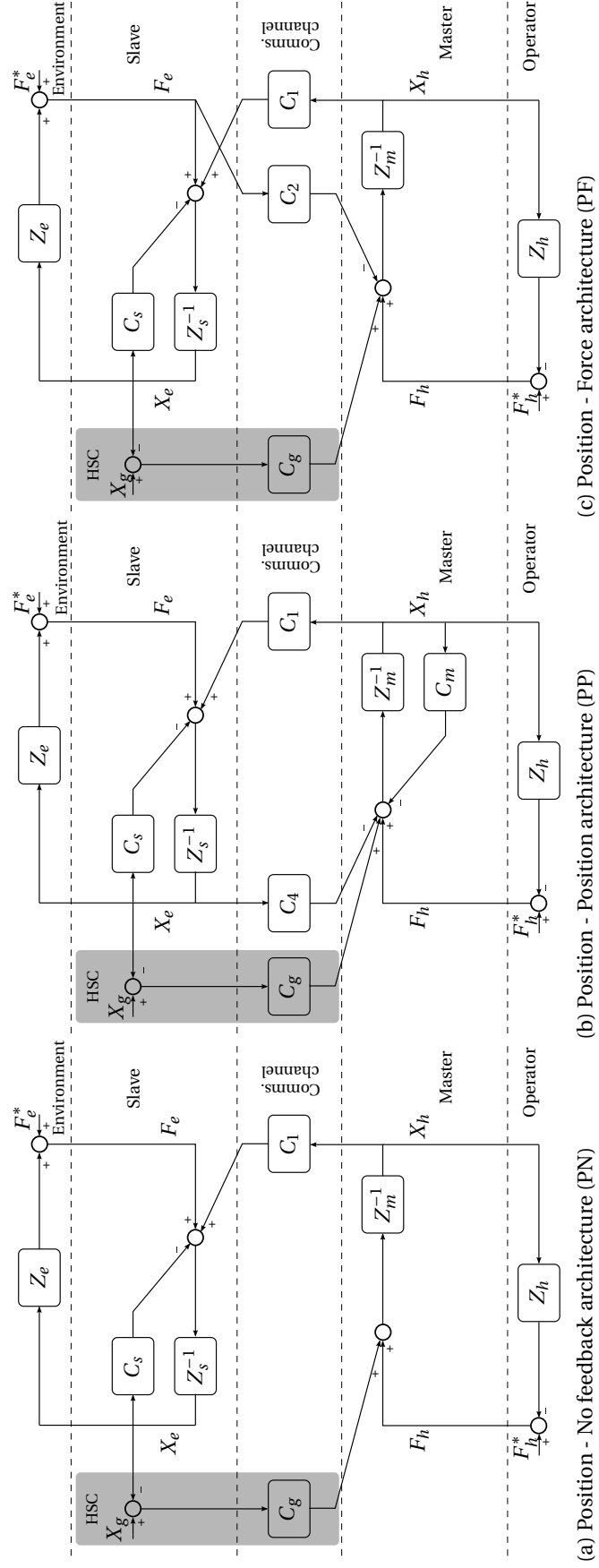


Figure 4.2: Control diagrams of the three teleoperation architectures studied in this chapter.

ADDITION OF HAPTIC GUIDANCE

Haptic guidance is implemented as a virtual spring (impedance $C_g(s)$) driving the master device by force F_g that is proportional to the deviation between the guidance reference $X_g(s)$ and the slave position $X_s(s)$ as:

$$F_g(s) = C_g(s) (X_g(s) - X_s(s))$$

4.3. THEORETICAL PERFORMANCE EVALUATION

In this section we aim to evaluate the steady-state performance of the haptic guidance system in two distinct situations: in a constrained task ($Z_e \rightarrow \infty$) and in free air ($Z_e = 0$).

4.3.1. EFFECTS OF GUIDANCE INACCURACY IN CONSTRAINED TASK

If the guidance reference would coincide with the origin of the environment ($X_g = 0$), the slave system would not be exerting any forces on the environment. In this section we quantify, by analyzing the transfer function from the offset guidance X_g to the force exerted on the environment F_e , what happens if the guidance is inaccurate ($X_g \neq 0$) and steers the system out of the origin, causing a non-zero F_e .

HAPTIC GUIDANCE WITHOUT DIRECT SLAVE FEEDBACK (FIGURE 4.2A)

The transfer function from the offset guidance $X_g(s)$ to the force exerted on the environment $F_e(s)$ can be expressed as:

$$\frac{F_e(s)}{X_g(s)} = \frac{Z_e(s)C_1(s)C_g(s)}{(Z_s(s) + C_s(s) + Z_e(s))(Z_m(s) + Z_h(s)) + C_1(s)C_g(s)}.$$

To provide further insight we can investigate the system after it reaches its steady state:

$$\lim_{s \rightarrow 0} \frac{F_e(s)}{X_g(s)} = \frac{K_e K_1 K_g}{(K_s + K_e) K_h + K_1 K_g}.$$

Assuming that the environment is much stiffer than the slave robot ($K_e \gg K_s$), and with controllers selected according [17] as $C_1 = K_s$, this further simplifies to:

$$\lim_{s \rightarrow 0} \frac{F_e(s)}{X_g(s)} = \frac{K_s K_g}{K_h}.$$

HAPTIC GUIDANCE WITH POSITION FEEDBACK (FIGURE 4.2B)

The transfer function, now also containing the position feedback from the slave robot, is:

$$\frac{F_e(s)}{X_g(s)} = \frac{Z_e(s)C_1(s)C_g(s)}{(Z_s(s) + C_s(s) + Z_e(s))(Z_m(s) + C_m(s) + Z_h(s)) + C_1(s)C_g(s) + C_1(s)C_4(s)},$$

and when evaluated in steady-state yields:

$$\lim_{s \rightarrow 0} \frac{F_e(s)}{X_g(s)} = \frac{K_e K_1 K_g}{(K_s + K_e)(K_m + K_h) + K_1 K_g + K_1 K_4},$$

and again assuming that the environment is much stiffer than the slave robot ($K_e \gg K_s$), and with $C_1 = K_s$ and $K_m = -K_4$, this equation further simplifies to:

$$\lim_{s \rightarrow 0} \frac{F_e(s)}{X_g(s)} = \frac{K_s K_g}{K_h + K_4}.$$

HAPTIC GUIDANCE WITH FORCE FEEDBACK (FIGURE 4.2B)

When we consider the direct feedback from the force exerted on the environment F_e , the transfer function takes form of:

$$\frac{F_e(s)}{X_g(s)} = \frac{Z_e(s)C_1(s)C_g(s)}{(Z_s(s) + C_s(s) + Z_e(s))(Z_m(s) + Z_h(s)) + C_1(s)C_g(s) + C_1(s)C_2(s)Z_e(s)},$$

and evaluated in steady-state as:

$$\lim_{s \rightarrow 0} \frac{F_e(s)}{X_g(s)} = \frac{K_e K_1 K_g}{(K_s + K_e)K_h + K_1 K_g + K_1 K_2 K_e}$$

Assuming that the environment is much stiffer than the slave robot ($K_e \gg K_s$), and with $C_1 = K_s$, this equation further simplifies to:

$$\lim_{s \rightarrow 0} \frac{F_e(s)}{X_g(s)} = \frac{K_s K_g}{K_h + K_s K_2}$$

4.3.2. EFFECTS OF OPERATOR'S ARM IMPEDANCE

Similarly to the previous section, effects of the operator's arm stiffness K_h can be studied when we calculate the transfer function from the guidance reference $X_g(s)$ to the slave robot position $X_e(s)$.

HAPTIC GUIDANCE WITHOUT DIRECT SLAVE FEEDBACK

In free-air, the system will follow the guidance reference according to:

$$\frac{X_e(s)}{X_g(s)} = \frac{C_1(s)C_g(s)}{(Z_s(s) + C_s(s))(Z_m(s) + Z_h(s)) + C_1(s)C_g(s)}.$$

When the system reaches the steady-state (and with $C_1 = K_s$) the transfer function becomes

$$\lim_{s \rightarrow 0} \frac{X_e(s)}{X_g(s)} = \frac{K_g}{K_h + K_g}.$$

HAPTIC GUIDANCE WITH POSITION FEEDBACK

The feedback from the slave robot position enters the dynamical equation as:

$$\frac{X_e(s)}{X_g(s)} = \frac{C_1(s)C_g(s)}{(Z_s(s) + C_s(s))(Z_m(s) + C_m(s) + Z_h(s)) + C_1(s)C_g(s) + C_1(s)C_4(s)},$$

and when evaluated in steady-state ($C_1 = K_s$ and $C_4 = -K_m$), it yields:

$$\lim_{s \rightarrow 0} \frac{X_e(s)}{X_g(s)} = \frac{K_g}{K_h + K_g}$$

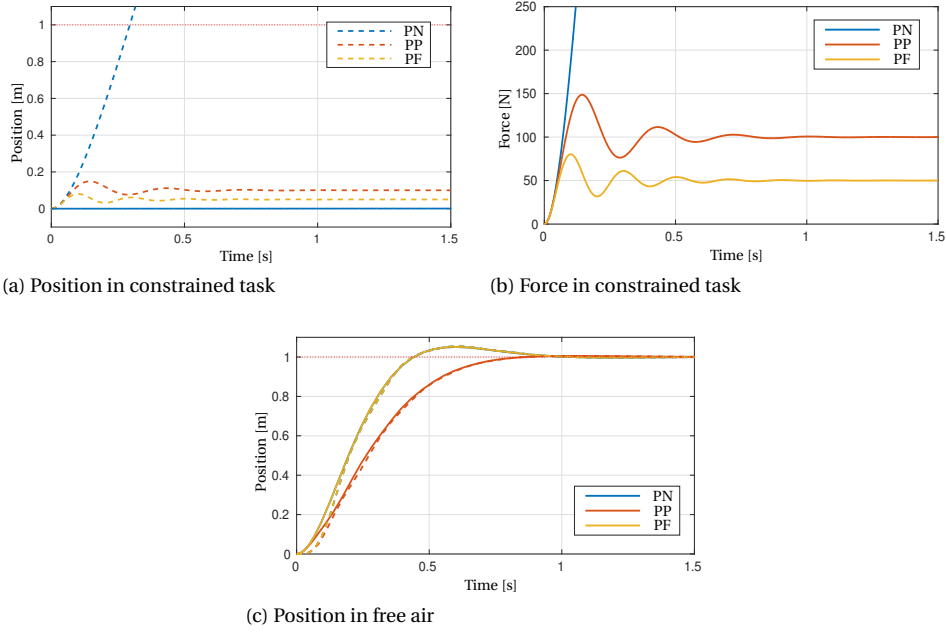


Figure 4.3: Performance in constrained and free air task, for a simulated teleoperation setup with compliant operator ($K_h = 0$); the guidance reference position X_g is driven with a unit step at $t = 0$. The slave robot readings are marked with a solid line and the master device's are shown with dashed lines. In (a) and (b), the PN architecture exhibits instability, whereas the PP and PF converge to a steady-state value. In free air (c), all three architectures provide perfect steady-state position tracking. Note that the PN trace is occluded by PF.

HAPTIC GUIDANCE WITH FORCE FEEDBACK

With no environment constraints to base the force feedback upon, the system effectively reduces to the PN architecture, with transfer function:

$$\frac{X_e(s)}{X_g(s)} = \frac{C_1(s)C_g(s)}{(Z_s(s) + C_s(s))(Z_m(s) + Z_h(s)) + C_1(s)C_g(s)},$$

and in steady-state ($C_1 = K_s$) as:

$$\lim_{s \rightarrow 0} \frac{X_e(s)}{X_g(s)} = \frac{K_g}{K_h + K_g}$$

4.4. SIMULATION RESULTS

In this section, a simulation study is carried out to demonstrate the properties of the three architectures analyzed above. The simulated teleoperation system consists of a master and a slave unit, with $Z_m(s) = s^2 + 10s$ with local proportional position control $C_m(s) = 500\text{N/m}$ and $Z_s(s) = s^2 + 10s$ with position controller $C_s(s) = 1000\text{N/m}$. The position command gain is set to $C_1(s) = C_s(s) = 1000\text{N/m}$ and the position and force feedback gains are selected as $C_4(s) = -C_m(s) = -500\text{N/m}$ and $C_2 = 1$, respectively. The environment is modelled as a stiff spring-damper system with $Z_e(s) = 100s + 10^7$. The

haptic guidance controller is programmed as a pure proportional gain with $C_g(s) = K_g = 50\text{N/m}$. The system parameters and controller gains were selected similarly to [15] and tuned to provide satisfactory response in free air, see Figure 4.3c.

In the following simulation, we focused on the particular situation when the operator is fully complying with the guidance force (i.e., he/she is actively reducing his/her arm stiffness to minimize the interaction force on the master device, $K_h \rightarrow 0$). At time $t = 0\text{sec}$, a unit step is applied as the guidance reference X_g . In free air, as seen from Figure 4.3c, all three architectures provided a very good step reference tracking with a satisfactory dynamical response.

If the slave manipulator is constrained by a stiff environment (e.g., the slave stays inside a hole at the origin $X_e = 0$), see Figure 4.3a, the haptic guidance force steers the master device in the direction of the guidance reference. As expected from the previous analysis, the position control (PN) architecture would require the operator to hold the master device in position ($K_h > 0$), otherwise it will quickly escape from its workspace, commanding the slave to exert an unacceptably large force on the environment (Figure 4.3b). Both the PP and PN architectures remained stable also without any contribution of the operator. The guidance force and the feedback force (from either the position or the force feedback) counteracted each other, reaching an equilibrium, and so the master moved to a position between the hole ($X_e = 0$) and the guidance reference ($X_g = 1$).

4.5. EXPERIMENTAL RESULTS

4.5.1. EXPERIMENTAL SETUP

For evaluation of the proposed method a KUKA LWR slave robot was teleoperated using a Force Dimensions Sigma 7 master device (see Figure 4.4). The slave robot is operated in actively compliant mode with programmed Cartesian stiffness of $K_s = 1000\text{N/m}$ for translations and $K_s = 50\text{Nm/rad}$ for rotations. A 150 mm long titanium peg is rigidly mounted on a 6-DOF force/torque sensor on the end-effector of the arm. The sensor was sampled at 1 kHz, low-pass filtered with $f_c = 100\text{ Hz}$ and corrected for the force due to the weight of the peg. The control software is implemented on a real-time operating system (Xenomai) with a 1 kHz sampling rate. The position command gains are set to $C_1(s) = C_s(s) = 1000\text{N/m}$ and the position and force feedback gains are selected as $C_4(s) = -C_m(s) = 200\text{N/m}$ and $C_2 = 0.3$, respectively. Higher feedback gains were attempted but the system then easily became oscillatory, especially in the situation when the master device was held very loosely. The relatively low values can be partially attributed to the different inertias of the master and the slave devices, as discussed in [17].

HAPTIC GUIDANCE CONTROLLER

The haptic guidance system is designed to be only effective in the directions perpendicular to the hole's principal axis, i.e., the system is not actively guiding the operator to insert the peg but rather it provides support with proper peg-hole alignment. The controller is programmed as a proportional-derivative controller:

$$C_g(s) = \text{diag}(B_g^t, B_g^t, 0, B_g^r, B_g^r, 0)s + \text{diag}(K_g^t, K_g^t, 0, K_g^r, K_g^r, 0),$$

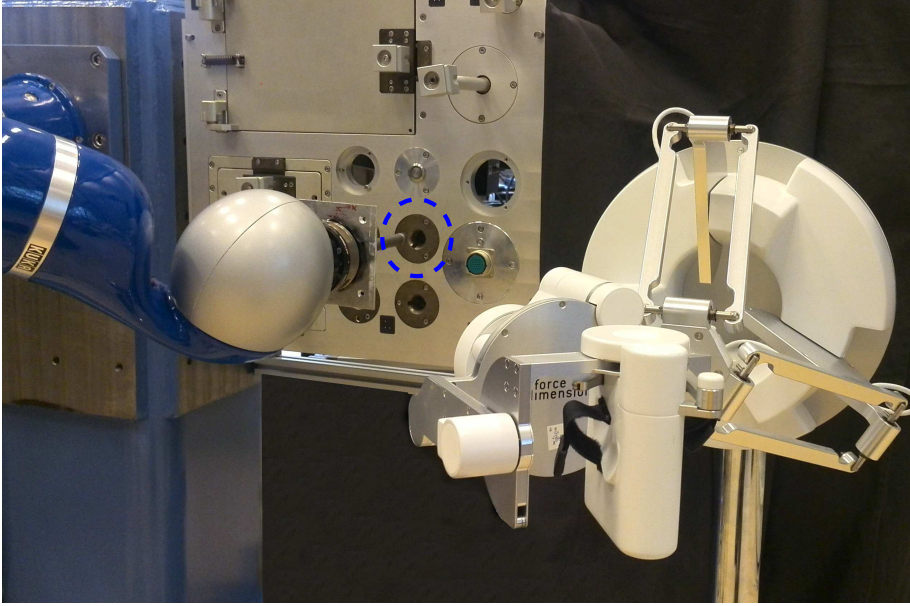


Figure 4.4: A 6-DOF force-feedback master device controlling a slave robot to insert a peg into a hole on the task-board. The haptic guidance system is programmed to provide support for peg insertion into the circular hole marked in dashed blue.

with the translational and rotational gains set to $B_g^t = 10 \text{Ns/m}$, $K_g^t = 180 \text{N/m}$ and $B_g^r = 0.1 \text{Ns/m}$, $K_g^r = 1.8 \text{N/m}$, respectively.

The guidance is provided for the upper right hole on the task-board (marked by a blue circle in Figure 4.4). The attractive guidance field is activated when the slave robot enters a cylinder with its center-line at X_g and with a diameter of 40 mm.

4

4.5.2. TASK AND RESULTS

The task was to insert the peg (diameter of 14 mm) into a tight brass hole (diameter of 14.75 mm), located at the origin $[0, 0, 0, 0, 0, 0]^T$. The guidance reference is intentionally made inaccurate by a constant -10 mm offset in the horizontal direction, $X_g = [-0.01, 0, 0, 0, 0, 0]^T$. The magnitude of the tested inaccuracy is adequate considering the dimensions of the slave robot workspace. Comparable reference offsets were also investigated in [45]. Beside that, the guidance still provides correct support with the peg angular orientation and thus is useful for the operator.

To illustrate the effects of inaccurate guidance reference, the experiment starts when the peg is already inserted in the hole and the operator has to stiffly hold the master device to counteract the effect of the off-centered guidance, then the operator releases the master device (to replicate a completely compliant behavior). It is worth noting that, based on our practical experiments, this absence of the operator hold of the master device was the most challenging behavior for the system stability and produced a practical upper limit on the guidance controller gains K_g .

The reactions of the master device and the force exerted by the slave robot on the environment in the next 1.5 seconds are shown in Fig. 4.5. As we can see from Figure 4.5a,

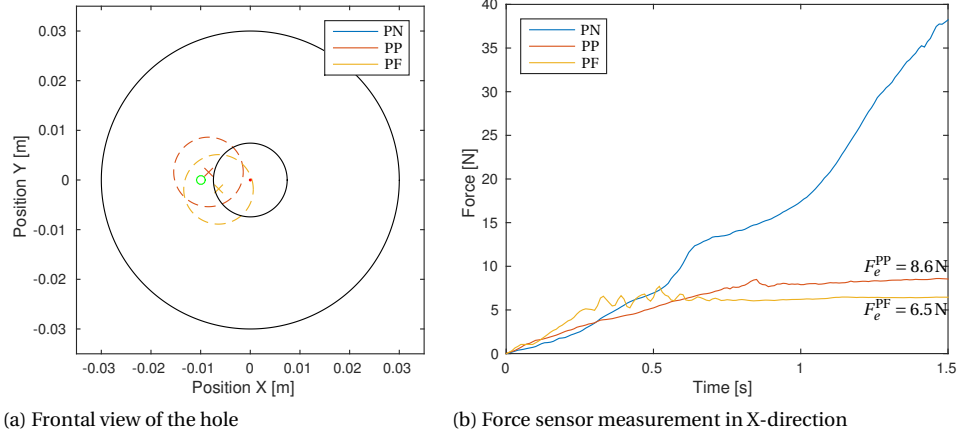


Figure 4.5: Position and force measurements from the peg-in-hole experiment. In (a), a planar view of the hole is overlaid with the position of the inaccurate guidance reference (green circle) and with the steady-state positions of the master device X_h . The PN architecture is not shown because it does not converge to a steady value and quickly causes high interaction forces at the slave robot end-effector, as can be seen from the measured force F_e in (b).

the haptic guidance system moves the master device towards the reference position and settles to a steady-state. The PN architecture (not shown) does not converge and quickly causes high interaction force at the slave robot, as can be seen from the measured force F_e in Figure 4.5b.

COMPARISON OF THEORETICAL AND EXPERIMENTAL RESULTS

The results obtained by the theoretical analysis (using expressions provided in Table 4.1) are in this section compared with the results of the experiment. The calculated steady-state forces (with $K_h = 0$) of the PP and PF architectures (as expected the PN does not settle to a steady-state) and $\hat{F}_e^{PP} = X_g(K_s K_g)/K_4 = 9\text{ N}$ are $\hat{F}_e^{PF} = X_g(K_s K_g)/(K_s K_2) = 6\text{ N}$, respectively.

The measurements obtained during the experiment are shown in Figure 4.5. After less than one second, both teleoperation architectures reached an equilibrium and settled approximately on $F_e^{PP} = 8.6\text{ N}$ for the PP system and on $F_e^{PF} = 6.5\text{ N}$ for the PF system, which we consider in good accordance with the calculated values.

4.6. DISCUSSION

The steady-state tracking results are summarized in Table 4.1. Despite its limitations, we find results provided by the steady-state analysis insightful. Moreover, performance of a teleoperated task greatly depends on the low-frequency part of the force-feedback information [20], the constant force offsets due to guidance inaccuracy can cause difficulties. In free air, for perfect reference tracking the ratio $\frac{K_h}{K_g}$ should be minimized (by either the

Table 4.1: Summary of the steady-state tracking performance of the analyzed teleoperation architectures.

Architecture	Steady-state performance	
	Constrained contact $\left. \frac{F_e(s)}{X_g(s)} \right _{s=0}$	Free air $\left. \frac{X_e(s)}{X_g(s)} \right _{s=0}$
Position - No	$\frac{K_s K_g}{K_h}$	$\frac{K_g}{K_h + K_g}$
Position - Position	$\frac{K_s K_g}{K_h + K_4}$	$\frac{K_g}{K_h + K_g}$
Position - Force	$\frac{K_s K_g}{K_h + K_s K_2}$	$\frac{K_g}{K_h + K_g}$

operator becoming compliant or by increased the guidance gain), which corresponds to what was intuitively established in the introduction.

The analysis of the PN architecture, in a constrained task, showed the importance of having an operator holding the master device – otherwise the master will be ‘pushed away’ by a constant force ($F_g = K_g X_g$), and the force exerted on the environment F_e , caused by the slave following the master, would become unacceptably high. Both the PP and PF architectures converge to a steady-state value. The main problem that is apparent in the previous sections is that the slave robot can be exerting significant forces on the environment (see Figure 4.3b), yet the operator could not ‘feel’ any force on the master device. The comparison of PP and PF architectures depends on the parameters of the actual system; however, if we focus on the tested experimental setup, the PF architecture exerted lower forces on the environment F_e .

4.7. CONCLUSIONS

In this chapter, we analyzed the effects of combining haptic guidance forces with feedback forces from the slave robot, especially in situations where the haptic guidance reference does not accurately coincide with the environment. Moreover, haptic guidance has been formulated as an extension to the generalized Lawrence teleoperation architecture, and analyzed on a sub-set of the three most simple architectures.

The main conclusions of the study are:

- (1) If the slave robot is fully constrained by the environment and the haptic guidance reference is inaccurate, the *Position control - No feedback* architecture requires the operator to hold the master device ($Z_h > 0$) to prevent it from quickly *escaping* its workspace.
- (2) If the slave robot is fully constrained by the environment, the *Position control - Position feedback* and *Position control - Force feedback* architectures remains stable even without the contribution of the operator. However, the guidance force and the feedback force, from both position or force feedback, counteract each other, effectively masking the inaccuracy of the guidance from the operator (i.e., the slave robot can still exert significant forces on the environment, without the operator being able to perceive it through haptic sense).
- (3) In free air, all three architectures facilitate perfect tracking of a (step) guidance reference if the operator is compliant to the guidance force ($Z_h \rightarrow 0$).

This study focused on the steady-state behavior of the teleoperation system; however, investigating the dynamic response of the system could provide further insights.

5

CONTACT TASK HSC SYSTEM ROBUST TO TIME DELAY

*The chapter introduces a haptic shared control method that offers support in contact tasks, by providing **mediated contact** HSC. Using a force sensor on the slave robot, the system continuously searches for contact with the remote environment and updates the environment model based on this measurement. The proposed method is also designed to be robust against guidance model geometrical inaccuracies that were described in Chapter 4. Moreover, by communicating the task model instead of the force measurements directly, the proposed method is inherently robust to delays in the communication channel.*

This chapter is based on the following publication:

- Jan Smisek, Marinus M. van Paassen and Andre Schiele, “Naturally-transitioning Rate-to-Force Controller Robust to Time Delay by Model-mediated Teleoperation”, IEEE International Conference on Systems, Man, and Cybernetics, Kowloon, 2015

CHAPTER SUMMARY

In this chapter a new model-mediated teleoperation framework based on rate-control input is presented. The system facilitates force feedback teleoperation and is inherently robust to severe time delays, yet still provides high quality representation of the feedback forces. Previously published methods on model-mediated teleoperation are here extended to accept rate commands and use the slave robot's programmed impedance as a contact model for force feedback generation. The system is designed to ensure decoupling of the control loops in case of environment changes, which also allows to cope with a severe and possibly variable time-delay in the communication channel. Stability and performance is analyzed and the system is shown to remain stable for finite delays. Tuning guidelines with design trade-offs are provided. The analysis is based on a linear, non-delayed, time-invariant model of the system. The presented method is demonstrated on an experimental 1-DOF master/slave setup in a teleoperation scenario, showing stability and reference rate and force tracking performance over 2 seconds of round-trip communication delay in bilateral control.

5.1. INTRODUCTION

In rate control teleoperation, the position of the master is interpreted as a velocity command to the slave. Rate control allows the comfortable use of master and slave devices with different workspaces [15] and is also instrumental in situations that require better-than-human slave movement precision [118]. However, how to best provide force feedback in the rate control mode is not obvious. Methods optimized for transparency (in the sense of environmental impedance transmitted to the operator), e.g., [15], use the derivative of the measured environment force in the feedback path, which is reported to be very sensitive to time delays, with respect to ensuring stability [119]. A different approach was proposed by Williams [120], that is by design not transparent, yet provides rate control behavior in free space and force control behavior once in contact.

In this chapter the latter method is conceptually followed and extended to provide robustness against time-delays. To overcome time delay-induced difficulties (instability and delayed force feedback), model-mediation [40], i.e., generating feedback forces based on a local non-delayed virtual model of the remote environment, has been suggested in a non-rate controlled context. Instead of a direct exchange of commands and sensed data between master and slave units, a model of the environment is continuously updated at the master side. The feedback information to the operator is based on this model and is, by its nature, not affected by the delay in the communication channel. Hence, if the remote environment remains static, the feedback control loop is not closed over the delayed communication channel and so stability of the system is only dependent on two decoupled control loops.

A challenge of model-mediated approaches is the difficulty of maintaining accurate slave environment models. Early methods of model-mediated telemanipulation relied on a precise a priori known model of the remote environment [121–123]. Later studies focused on the correction of geometrical and dynamical errors of the model for improved fidelity [124–128]. Mitra and Niemeyer [40] showed that model-mediated telemanipulation can be even performed, in a safe manner, in unstructured environments and over large communication delays. They described a position command based framework where contact force measurements are used for detecting unknown objects, presenting the operator with a ‘stiff object’ response. In a user study [129] they also compared several approaches on how the master side model could be updated. Stability of this framework was further investigated by Willaert et al. [130]. Recent works [131, 132] aimed at extensions of the model-mediation to more-DOF with ‘contacting tasks’.

However, up to this point, no model-mediated framework has been proposed to allow the use of rate control inputs in a stable manner, without relying on slave-environment a-priori models. The goal of the chapter is, building on previous works [40, 120], to design and evaluate a rate control teleoperation system with force feedback that is robust to (possibly variable) time delays and resembles a delay-free operation from the user perspective. Furthermore we aim to investigate how impedance-controlled slave robots can be used for an ‘open-loop force feedback’ allowing execution of force commands without estimation of the environment properties and without an explicit force-feedback control loop.

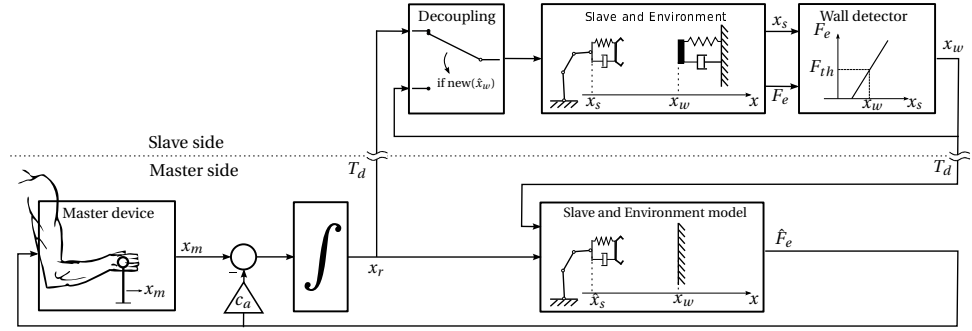


Figure 5.1: Conceptual diagram of the proposed teleoperation framework.

5.2. APPROACH

The main components of the proposed framework are shown in Figure 5.1 and described in detail in the following sections. The system is physically separated into a master side and a slave side. Both parts are connected through a communication channel (with time delay T_d). The operator moves the master device, whose position (deflection) x_m is interpreted as the velocity reference for the slave $v_r := \dot{x}_m$. It is integrated to create a position reference $x_r = \int v_r dt$ that is sent over the communication channel to the slave robot. The slave robot moves to track x_r and interacts with the surrounding environment. If an object is encountered (contact force at slave end-effector), the system updates the model of the environment on the master side with a new virtual wall at the position of contact x_w , after T_d . The slave robot is temporarily decoupled from the master side by the *Decoupling* block. After master and slave side environment models converge, the decoupling is disabled and the operator can proceed to contact the new local virtual model of the object. Thus interaction forces \hat{F}_e are fed back to him on the master device while the slave robot applies the same magnitude of force at the remote side. Since \hat{F}_e is computed from the robot programmed impedance setting, the behavior is exact and predictable.

5.2.1. DECOUPLING FOR INTERACTION WITH UNKNOWN ENVIRONMENT

When a newly discovered wall position is transmitted to the master side (and arrives after T_d), the commanded reference position x_r (can have) passed the wall position x_w already. If the slave followed the reference x_r and tried to move into the object, an unacceptable increase of forces exerted on the environment by the slave robot would occur.

Therefore, as a safety measure, when a new wall position x_w is discovered for the first time, the slave motion is temporarily stopped at that position. Only after the master side has been updated with the change, the operator starts to feel the feedback force from the contact. At this point, the slave robot still does not follow any commands in the direction of the wall. Once the operator is aware of the obstacle, he/she must stop commanding the forward motion to acknowledge the newly discovered object and to allow the environment model to adjust and to re-enable the slave robot motion. Once both the master and slave side environment models are updated, the wall becomes a proper part of the

updated model and the operator can engage/disengage in contact arbitrarily and exert forces on it without further constraints. When the operator approaches the wall again he/she is not any more restricted in the interaction. As indicated by an informal user test, this initial operation constraint at first contact was viewed as rather natural, and did not alter the teleoperation behavior of the human, especially for time delays below 1 second.

5.2.2. MASTER INPUT DEVICE AND OPERATOR MODEL

The control input device produces rate commands based on its deflection, $v_r := x_m$. It is programmed to resemble a mechanical, spring centred device, i.e., to keep the master in the central position by applying force proportional to its deflection (with m_m , b_m and k_m being its mass, damping, and stiffness, respectively). This behavior is desirable to support fine control and to prevent the slave robot from drifting [15]. The operator is, similarly to [15], represented by a voluntary human force input F_h^* and by a mass-spring-damper model of the arm holding the master device (m_h , b_h and k_h).

The master device, Figure 5.2, is moved by operator's exerted force F_h^* and by the feedback force \hat{F}_e arising from contact with the local environment model (with force feedback gain c_f),

$$G_m(s) = \frac{x_m(s)}{F_h^*(s) - c_f \hat{F}_e(s)} = \frac{1}{(m_m + m_h)s^2 + (b_m + b_h)s + (k_m + k_h)}. \quad (5.1)$$

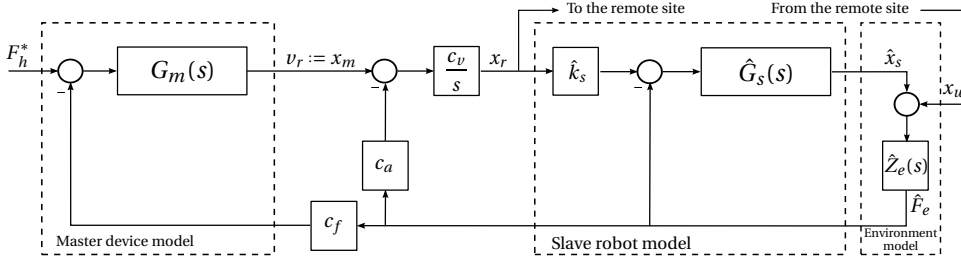


Figure 5.2: Linear model of the master side system.

5.2.3. SLAVE ROBOT

The slave robot is operated in active compliance mode (impedance control) [133]. The original robot system dynamics are modified using closed-loop control, to behave as a mass-spring damper system with constants m_s , b_s and k_s representing the desired slave robot mass, damping, and stiffness, respectively. The dynamic relation between the slave end-effector position and the interaction force with the environment is programmed to satisfy:

$$G_s(s) = \frac{x_s(s)}{k_s x_r(s) - F_e(s)} = \frac{1}{m_s s^2 + b_s s + k_s} \quad (5.2)$$

It should be noted that this programmed impedance cannot be selected arbitrarily, i.e., it cannot be significantly different from the real dynamics of the robot [134].

5.2.4. SLAVE ROBOT AND ENVIRONMENT MODELS

The environment model (implemented on the master side) contains only the position of the virtual wall x_w , that is continuously received through the communication channel from the *Wall detector*. The slave robot model is a master side representation of the slave robot. Conceptually, the dynamical model $\hat{G}_s(s)$ should be identical with the one of the real slave robot (5.2) as:

$$\hat{G}_s(s) = \frac{\hat{x}_s(s)}{\hat{k}_s x_r(s) - \hat{F}_e(s)} = \frac{1}{\hat{m}_s s^2 + \hat{b}_s s + \hat{k}_s}. \quad (5.3)$$

When the slave model engages into contact with the environment model, the interaction forces are based on the programmed impedance of the robot model. This virtual feedback force is only produced when the reference position x_r is inside the virtual wall. Because the slave motion in direction of the wall is stopped, from (5.3) the \hat{F}_e is according to:

$$\hat{F}_e = \begin{cases} \hat{k}_s(x_r - x_w) & \text{if } x_r > x_w \\ 0 & \text{otherwise} \end{cases}$$

5.2.5. WALL POSITION DETECTOR

The position of the wall is continuously monitored at the slave side and transmitted through the communication channel to the master side. As long as this wall position is known at the master, the operator can interact with the environment model, which essentially makes the communication delay T_d irrelevant. Estimation of the geometry and other physical properties of the environment can be based on different sensors or their combination, e.g., force sensors [40, 128, 130], cameras [131] or laser distance sensors [127]. Despite obvious shortcomings, in this chapter the model is only maintained through physical interaction of the slave robot with its surrounding environment, i.e., the slave robot has to be equipped with a force/torque sensor to detect contact with an environment.

Detection of a new contact. If the force reading F_e at the slave robot end-effector exceeds a predefined threshold F_{th} , the new wall position is recorded at the current manipulator position, as:

$$\text{if } F_e > F_{th} \quad \text{then} \quad x_w = x_s$$

Detection of wall removal. If the slave robot passes through the recorded position of the wall x_w , without measuring a corresponding force reading, i.e., if a physical object disappears from the real environment, the wall is removed from the model of the environment at the master side:

$$\text{if } (x_s > x_w \quad \& \quad F_e < F_{th}) \quad \text{then} \quad x_w = \infty$$

5.3. STABILITY AND REFERENCE TRACKING ANALYSIS

The slave side system is decoupled from the commanded reference if the environment model changes. In this section, we analyze how the master side system operates in free space, and how it reacts once it receives an updated wall position x_w .

5.3.1. MASTER-SIDE SYSTEM

A simplified scalar linear model of the master side system is shown in Figure 5.2. The master device and the slave robot model are operated in impedance control mode, as stable closed loop system with programmed mass-spring-damper behavior according Eqs. (5.1) and (5.2). The virtual environment is modelled as an impedance $\hat{Z}_e(s)$ and the human operator is represented by its intentional exogenous force input F_h^* . Remaining coefficients c_v , c_a and c_f are the tuning gains of the system. The stability and desired rate/force tracking of the system are examined in two distinct modes: in (a) free motion and in (b) constraint motion where the slave robot is placed in contact with a virtual wall.

- (a) *In free space* ($\hat{Z}_e = 0$). The desired master device position x_m^* is achieved by the operator by applying force $F_h^* = k_m x_m^*$ (assuming that the contributions of damping and mass are negligible). From Figure 5.2 we obtain the following transfer function, as:

$$\frac{\hat{x}_s(s)}{F_h^*(s)} = \frac{\hat{x}_s(s)}{k_m x_m^*(s)} \Big|_{\hat{Z}_e=0} = \frac{1}{s} c_v \hat{k}_s G_m(s) \hat{G}_s(s), \quad (5.4)$$

and by expressing the slave model velocity as $\hat{v}_s(s) = s \hat{x}_s(s)$ the system can be further investigated in steady-state as

$$\lim_{s \rightarrow 0} \frac{\hat{v}_s(s)}{x_m^*(s)} \Big|_{\hat{Z}_e=0} = c_v = \gamma_v, \quad (5.5)$$

where γ_v is defined as a velocity scaling gain.

- (b) *In contact* ($\hat{Z}_e \rightarrow \infty$). We assume that the slave robot model is initially placed in contact with a virtual wall. In that situation the loop closed over the gain c_a , Figure 5.2, essentially makes the system force controlled (similarly to [120]). The force exerted by the human operator F_h^* on the master device is related to the force exerted by the robot model on the virtual wall as:

$$\frac{\hat{F}_e(s)}{F_h^*(s)} \Big|_{\hat{Z}_e \rightarrow \infty} = \frac{c_v k_s G_m(s)}{s + c_v k_s (c_a + c_f G_m(s))}, \quad (5.6)$$

that in steady-state yields and assuming that $k_m \gg k_h$:

$$\lim_{s \rightarrow 0} \frac{\hat{F}_e(s)}{F_h^*(s)} \Big|_{\hat{Z}_e \rightarrow \infty} = \frac{1}{c_a k_m + c_f} = \gamma_f, \quad (5.7)$$

where γ_f is defined as a force scaling gain.

STEP MODEL UPDATE DUE TO COMMUNICATION DELAY

As described in Section 5.2.4 the remote environment is locally represented as a spring with the neutral position at \hat{x}_w . It is possible (for $T_d > 0$) that after the environment model update, the slave model position \hat{x}_s will be deep inside the environment, $\hat{x}_s > x_w$. This situation is analyzed below. In the block diagram of Figure 5.2, the model update is introduced as a step disturbance \hat{x}_w . A transfer function from $\hat{x}_w(s)$ to $\hat{F}_e(s)$, (for worst case $F_h^*(s) = 0$) is:

$$H_w(s) = \frac{\hat{F}_e(s)}{x_w(s)} = \frac{\hat{k}_s s}{s + c_v \hat{k}_s (c_a + c_f G_m(s))}, \quad (5.8)$$

which has the same characteristic equation as the other closed-loops, Eq. (5.6), that were tuned to be stable. We can investigate the initial and the final value \hat{F}_e of system (5.8) in reaction on a step input of size $R(s) = \frac{1}{s} |\Delta x_w|$ in time domain as:

$$\lim_{t \rightarrow 0} H_w(t) = \lim_{s \rightarrow \infty} s H_w(s) R(s) = \hat{k}_s |\Delta x_w| \quad (5.9)$$

$$\lim_{t \rightarrow \infty} H_w(t) = \lim_{s \rightarrow 0} s H_w(s) R(s) = 0. \quad (5.10)$$

To quantify the maximum size of the update step, we can compare the slave and slave model positions x_s , \hat{x}_s at the moment of the update t_u . The position reference in the time domain is generated as: $x_r(t) = \gamma_v \int x_m(t) dt$, and is tracked by the slave robot model and also, after the delay T_d , by the real slave robot, according to:

$$\begin{aligned} \hat{x}_s(t) &= \hat{G}_s(t) x_r(t), \\ x_s(t) &= G_s(t) x_r(t + T_d). \end{aligned}$$

In the worst case, when the maximum velocity was constantly commanded (using the maximum master deflection x_m^{\max}) and at a certain point the slave robot stopped on contact with a wall (at time t_u). At time t_u , the reference x_r becomes:

$$x_r(t_u) = \gamma_v \int_0^{t_u} x_m^{\max} dt \quad (5.11)$$

The difference between the actual slave robot position x_s and its simulated model \hat{x}_s is:

$$\begin{aligned} |\hat{x}_s(t_u) - x_s(t_u)| &= \hat{G}_s(t_u) x_r(t_u) - G_s(t_u) x_r(t_u + T_d) \\ &= \hat{G}_s(t_u) \gamma_v \int_0^{t_u} x_m^{\max} dt - G_s(t_u) \gamma_v \int_0^{t_u + T_d} x_m^{\max} dt, \end{aligned}$$

which, assuming that the slave dynamics (G_s , \hat{G}_s) can be neglected compared to T_d , simplifies to:

$$|\hat{x}_s(t_u) - x_s(t_u)| \approx 2\gamma_v x_m^{\max} T_d \quad (5.12)$$

We observe that $|\hat{x}_s(t_u) - x_s(t_u)|$ is proportional to the time delay T_d and has an upper bound for $T_d < \infty$.

The system will, after its initial response in the virtual force $\hat{F}_e = \hat{k}_s |\Delta x_w|$ Eq. (5.9), return to rest Eq. (5.10). This is a desirable behavior from the operator perspective. In previous studies by other authors on model-mediated teleoperation, model updates were identified as the moments requiring special attention from the system designer – both to preserve stability [40] and to be naturally presented to the user [129]. Here, the system was shown to remain stable during model updates. The operator is informed about a new wall position with a peak in feedback force. At the same time the reference position x_r is smoothly driven to the new wall which is, due to the rate-command nature of the framework, effectively masked from the operator (for an example see Figure 5.6b).

5.3.2. SLAVE-SIDE SYSTEM

In the presented framework the slave robot is only commanded with the reference position x_r . If the robot comes into contact with an environment, the interaction force will

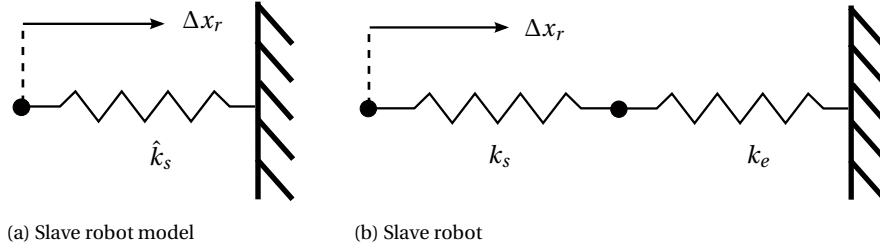


Figure 5.3: Environment and slave robot stiffness analysis.

be generated according to Eq. (5.2). After establishing contact, the robot-environment connection can be simplified, at least in steady-state, as two connected springs, see Figure 5.3b. This mechanical system can be expressed as one spring with equivalent stiffness k_{eq} as:

$$k_{eq} = \frac{k_e k_s}{k_e + k_s} \quad (5.13)$$

For stiff environments, where $k_e \gg k_s$, the equivalent stiffness equals $k_{eq} \approx k_s$. In effect, when the slave robot is constrained by the environment, the exerted force F_e is essentially proportional to the commanded position $F_e = k_s \Delta x_r$ (by the robot stiffness k_s).

At the master side, the virtual environment contact force is calculated based on a single virtual spring corresponding to the programmed slave stiffness, see Figure 5.3b, as $\hat{F}_e = \hat{k}_s \Delta x_r$. From that it follows that for matching the real and virtual environmental force, $F_e = \hat{F}_e$, the real and the model slave robots levels of stiffness have to be equal:

$$k_s = \hat{k}_s \quad (5.14)$$

SOFT ENVIRONMENTS

So far only stiff remote environments ($Z_e \gg Z_s$) were considered. However, we can extend our analysis to soft environments ($k_e \approx k_s$) where $k_{eq} < k_s$. Effectively, this means that the desired input force applied by the operator at the master side F_h^* will be smaller than the real contact force exerted by the slave robot F_e , which can be seen as a potentially unsafe behavior.

Quantitatively, the permitted force tracking error can be expressed as $pF_h^* < F_e$ where p [%] denotes the minimum acceptable relative force value. In steady-state this yields a lower bound on the acceptable environmental stiffness that can be still interacted with satisfactory force tracking performance:

$$k_e > \frac{p}{1-p} k_s \quad (5.15)$$

As an example, requiring minimal force magnitude fidelity of $p = 90\%$ yields the condition on environment: $k_e > 9k_s$. This is not too restrictive as some of the current actively compliant robots can have a very low stiffness [135] and considering for example remote assembly as a use case, we can assume to be mostly interacting with relatively stiff environments (metal, plastic, hard rubber) where this condition is easily met.

Table 5.1: System parameters of the 1-DOF setup experiment

m_s [kg]	b_s [Nms/rad]	k_s [Nm/rad]	γ_f	F_{th} [Nm]	c_f
10^{-2}	1.0	10.0	1.0	0.2	0.75
m_m [kg]	b_m [Nms/rad]	k_m [Nm/rad]	γ_v	c_v	c_a
10^{-2}	0.2	1.0	5.0	5.0	0.25

5.3.3. TUNING GUIDELINES

Firstly, the master and the slave systems should be tuned for stability and performance. Secondly, velocity and force scaling gains γ_v , γ_f should be selected according to the task requirements, e.g., downscaling commanded velocity and amplifying fed-back force for micro-manipulation. Thirdly, the tuning coefficients c_v , c_a and c_f are calculated using Equations (5.7) and (5.5).

We can now evaluate the limitations on the system tuning gains. Parameters of the desired closed-loop dynamics of the master and slave model systems should be positive, as Eq. (5.16), for asymptotic stability. However, the desired impedance can not be significantly different from the real hardware dynamics and so the actual constraints on the parameters are more strict, for details see [134].

To achieve an intuitive system behavior, where a positive master deflection $x_m > 0$ yields a positive slave movement $\hat{x}_s > 0$, and where the feedback force \hat{F}_e acts against the slave motion, parameters γ_v , γ_f should be positive as in Eq. (5.17).

The closed-loop system, Eq. (5.6), was further evaluated using the Routh-Hurwitz stability criterion that yielded additional bounds on the remaining tuning parameters, Eq. (5.18). Hence, the following bounds on system parameters should be observed:

$$m_m, b_m, k_m > 0 \quad \hat{m}_s, \hat{b}_s, \hat{k}_s > 0, \quad (5.16)$$

$$\gamma_v, c_v > 0 \quad \gamma_f, c_f > 0, \quad (5.17)$$

$$0 < c_a < \frac{1}{\gamma_f k_m}. \quad (5.18)$$

5.4. EXPERIMENTAL VALIDATION ON A 1-DOF SETUP

The proposed method was validated on a 1-DOF master/slave setup (Figure 5.4). The system consists of two identical brushless DC motor units. The output shaft has a potentiometer and torque sensor for absolute position and output torque measurement. The system parameters were according to Table 5.1. The control loop runs at a 1 kHz sampling rate.

FORCE CONTROL BANDWIDTH

To assess the bandwidth limitation imposed by the force control loop, a frequency sweep was manually performed by commanding the slave to push against the stiff environment, results are shown in Figure 5.5. The resulting transfer function from F_h^* to F_e was identified in frequency domain and compared to the theoretically calculated transfer function given in Eq. (5.7). The control bandwidth was identified to be approximately 2.7 Hz.

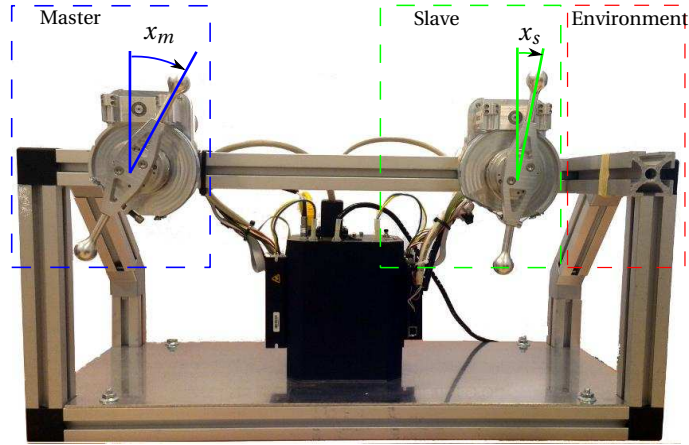


Figure 5.4: Experimental 1-DOF master/slave platform used for validation of the proposed method. The slave robot can interact with the remote environment (stiff aluminum bar).

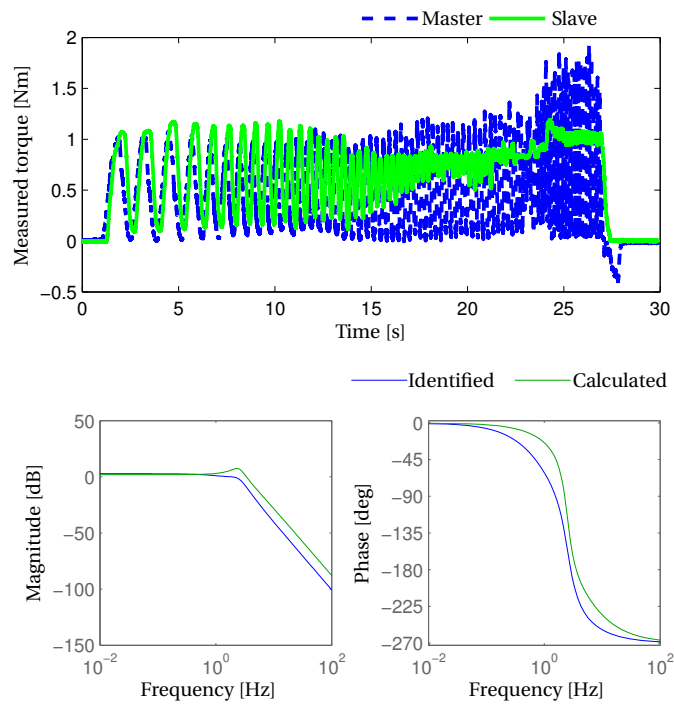


Figure 5.5: Frequency sweep to assess force tracking bandwidth of the tested system.

PRACTICAL FUNCTION DEMONSTRATION

A simple demonstration of the proposed system (with a simulated round-trip communication delay of 2s) is shown in Figure 5.6. In free air (a), the slave tracks the master reference commands with a communication time delay $T_d = 1$ s. At (b) the slave stops after touching an unexpected object. After the master wall model is updated, the operator is made aware of the new contact by increasing in feedback force ($t = 7$ s). As a safety measure, the slave position is still kept at the edge of the newly discovered wall until the operator stops commanding to “move forward”.

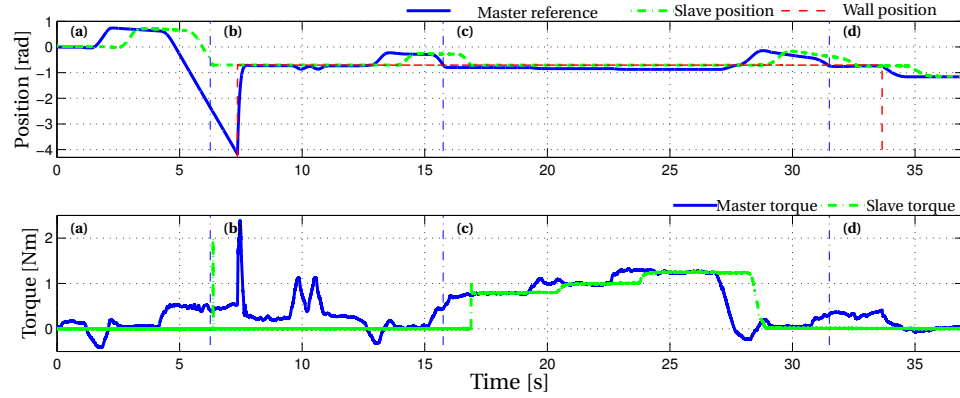


Figure 5.6: Function demonstration on a 1-DOF experiment with a round-trip communication delay of 2s. Contact torques are measured on the handles of both units. The slave robot follows the master position reference (a), until a physical wall is reached (b). The operator can exert forces on the wall, which have the same magnitude as the forces he applies on the control device (c).

Once the wall is a part of the model (c), the operator can exert a force on the remote environment ($t = 16 \sim 27$ s).

When a known wall was approached from free air ($t = 16$ s), the operator was instantly presented with an appropriate force feedback prediction, i.e., he/she can feel the contact and control the interaction force magnitude as if there would be no time delay present in the communication channel. It should be noted that this result is achieved without an explicit force control loop, but solely by using the same programmed impedance of the slave robot in its model at the master side. When the wall at the slave side is physically removed, (d), and the slave robot was commanded to approach it, no contact force is measured by the slave at the previous position of the wall. The wall location is then removed from the model. But at this point the master model still contains the old wall position and the operator can still feel the force feedback as he/she tries to exert force on it. After the delay T_d the master is updated again and the wall is removed from environment model ($t = 35$ s).

5.5. CONCLUSION

In this chapter we have presented a rate control teleoperation system that allows stable operation with force feedback over long time delays. The main conclusions are:

- (1) With a 1-DOF experiment it was demonstrated that the presented framework provides satisfactory reference position and force tracking performance even with 2 seconds of round-trip communication delay and remained stable in all phases, including model updates. The method is especially suitable for systems with delays in this range (i.e., below 2 seconds round-trip) because the model updates are sufficiently quick, and thus do not impose significant operational constraints.
- (2) The identified force control loop frequency response followed the theoretical prediction of a low-pass filter behavior (with an identified bandwidth of approximately 2.7 Hz). Since the operator is only provided with force feedback based on the local model (i.e., without any useful high-frequency information), this limitation in the *commanding direction* is not restrictive.
- (3) Robustness and tracking fidelity of the system were analyzed and shown to be asymptotically stable for $T_d < \infty$. If an unexpected object is encountered, the Decoupling block of the system ensures that the master and slave sides' control loops remain decoupled until the environment models on both sides converge.

The slave's programmed impedance-based force control has shown a satisfactory force tracking performance, however the provided analysis and the experiments so far focused on relatively stiff objects. In case of easily deformable materials the method was tested to still work through continuous wall position updates, but the exact properties require further investigation. We only analyzed the system in a simple 'contacting task' – although this is in line with the available literature on the topic, this limitation should be addressed in the future work.

III

FRAMEWORK

6

SYSTEMATIC FRAMEWORK FOR ANALYSIS OF HSC SYSTEMS

This chapter aims to connect the findings of previous chapters into one systematic framework. An extension of Lawrence's general teleoperation architecture [14] developed in Chapter 4 is in this chapter further extended by an additional haptic shared controller channel (conceptually based on the model-mediated teleoperation principles studied in Chapter 5). The theoretical findings are supported by numerical simulation and experimentally verified on a 6-DOF master-slave teleoperation system.

In principle, the newly developed generic model can be used to explore the effects of an operator's neuromuscular setting (Chapter 2), an operator's control authority in case of goal conflicts (Chapter 3), geometrical goal uncertainties (Chapter 4) and communication time-delays (Chapter 5), using one systematic description.

*However, the respective chapters dealt with a range of very different systems, which would make such unified description very complex. The presented framework allows analysis of **attractive guidance** HSC systems. In Section 7.2.4, we outline how this framework could be further extended to accommodate all system configurations studied in Chapters 2–5.*

This chapter is based on the following paper in preparation:

- Jan Smisek, Stefan Kimmer, Marinus M. van Paassen, Max Mulder and Andre Schiele, “Extending Lawrence teleoperation framework for haptic shared control”, 2017 (in preparation)

CHAPTER SUMMARY

Haptic shared control (HSC) is an emerging human-machine collaboration paradigm to principally combine problem-solving capabilities of a human operator with the precision offered by automation. This chapter provides a systematic method to analyze teleoperation systems with HSC, formalizing HSC as an extension of Lawrence's general teleoperation framework. The newly developed generic description is used to systematically analyze and compare performance differences and design trade-offs of two common attractive-force-field HSC implementations from the literature; here coined the slave- and master-based HSC types. Based on the new description, we derive theoretical steady-state responses and use them to formulate basic design guidelines for HSC in teleoperation. Results show that the master-based HSC type, that is so far used only sparsely, offers performance and robustness benefits for teleoperation systems with delayed communication or slow slave robot dynamics. Furthermore, it is shown that both types offer comparable levels of position and force tracking. Theoretical findings are supported by numerical simulations and experimentally verified on a 6-DOF haptic teleoperation setup, with a Sigma 7 haptic device controlling a KUKA LWR robot. In this experimental setup, the master-based HSC offered 4-times higher controller stiffness w.r.t. the slave-based HSC. The master-based HSC was tested to be operational up to 2 s of delay (theoretically with no upper limit), whereas the slave-based HSC was impractical beyond 80 ms of delay.

6.1. INTRODUCTION

Remote task execution principally offers two extremes for control of the teleoperated robot: *direct telemanipulation*, which provides flexible task execution, but requires continuous operator attention, and *automation*, which lacks flexibility but offers superior performance in predictable and repetitive tasks [1].

An emerging approach to improve the task performance of directly teleoperated tasks, by combining the robustness of a human operator with the repeatability of an automatic control system, is haptic shared control (HSC). In haptic shared control [67], the actions of the automatic system are presented to the operator as additional guidance forces on the master device, as is illustrated in Figure 6.1. This system configuration allows, in principle, for a continuous transfer of control authority between the human operator and the automation [34]. The operator remains fully embedded in the control loop; that is in contrast to the common interaction with automation, in which the operator acts rather as a supervisor of automation, instructing or permitting automated task execution [35, 69, 136].

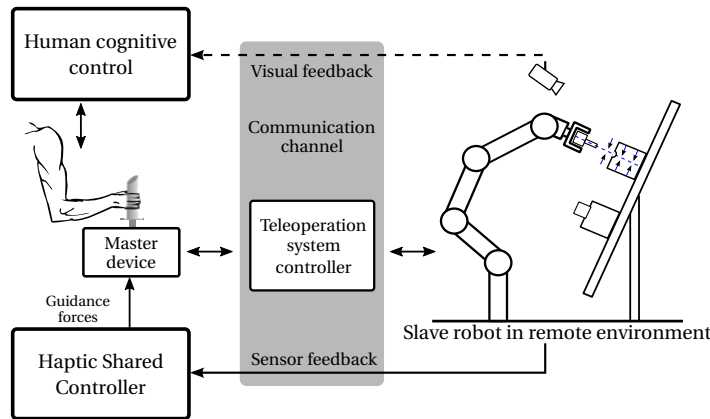


Figure 6.1: A teleoperation system (master device, slave robot, and teleoperation controller) is being supported by an attractive HSC (shown with blue arrows). The HSC guides the operator to accurately align a peg prior to its insertion into a hole.

Despite the growing interest in HSC systems, some significant problems are still open. Much of the research up to now has been based on empirical human studies. In this chapter, we aim to offer a system-theoretical view on the human-machine interaction with HSC. We propose a generic model of HSC systems applied in teleoperation and demonstrate its utility by systematically addressing the following three challenges that we have identified in our previous studies and encountered in literature.

First, it is currently unclear how practical implementation differences affect the overall properties of an HSC system. On the one hand, the behavior depends on the underlying teleoperation system, specifically, on what type of feedback information it offers (e.g., position or force feedback) [46]. On the other hand, there are several ways how the HSC guidance control laws are being implemented. Here we focus on the two most prevalent HSC types. Commonly, the HSC system determines the guidance force based on the dis-

tance of the slave robot from the desired reference position. For example, in Figure 6.1, the operator is provided with a guidance force that helps to minimize the slave misalignment before inserting a peg. In a second approach, advocated by studies [114, 137] on teleoperation with time delay, the guidance is based on the distance of the *master device* from the reference position. In the same example, the system would determine the necessary motion of the master device to steer the slave robot to an accurate alignment and provide a guidance force that would facilitate this motion locally (at the master device).

Second, so far there is no systematic way to analyze and quantify the level of control authority the operator is holding over a teleoperated task. Implementing the actions of the automatic system as additional forces on the master device allows the operator to decide how to react to the guidance. In a *nominal situation*, if the operator agrees with the provided automatic's support, he/she can become compliant and give way to the haptic forces. In contrast, if the operator disagrees, for example because of a *goal conflict* with the HSC, he/she can resist the haptic forces, effectively overruling the automation. In this manner, the operator can dynamically interact with the automation during the operation [68]. Improving our understanding of situations when the operator disagrees with the guidance (e.g., due to HSC system malfunction [44]) and wishes to assume a higher control authority has a large practical importance.

Third, little is known about how the addition of the guidance forces on the master device affects the force feedback from the remote environment provided to the operator by the teleoperation system. Teleoperation is often used in unstructured environments, where it is difficult to obtain an accurate model of the task that the HSC system can use to provide appropriate guidance. The operator is in many systems provided with force feedback aimed to resolve potential problems [22, 114, 115, 138], such as *geometrical inaccuracy* of the goal model [45]. However, since the measured feedback forces are being *combined* with the guidance forces, effectively masking potential inaccuracies of the guidance system from the operator, which can be unsafe [46]. It is thus unclear if, or to which extent, the operator can still rely on the force feedback.

The goal of this chapter is to address these challenges through providing a systematic method to study HSC systems used in teleoperation, compare different commonly used approaches and provide design guidelines on preferred system configuration. In Section 6.2, we present an extension of Lawrence's teleoperation framework, by adding two types of haptic shared control. In Section 6.3, we propose a new set of metrics to evaluate HSC systems, and use them to analyze several common teleoperation system implementations inspired by existing literature. These analytically obtained results are then verified in a numerical simulation study, in Section 6.5, and validated experimentally on a real teleoperation setup, in Section 6.6. The chapter concludes with a discussion of the results and summarizes the key findings, in Sections 6.7 and 6.8.

6

6.2. HSC IN A GENERAL TELEOPERATION ARCHITECTURE

In 1993, Lawrence [14] presented a formal framework to systematically study different configurations of teleoperation systems, to analyze and optimize their performance. In this chapter, we adopt this teleoperation system description (also called 4-channel architecture), and extend it through the addition of two haptic shared control channels, that we coined as the *slave-based* (SG) and *master-based* (MG) HSC guidance types, il-

lustrated schematically in Figure 6.2. The slave-based guidance (in Figure 6.2 shown in green) is calculated using the error between the actual slave position and the guidance reference, whereas the master-based guidance is based on the error of master device position with respect to the guidance reference (shown in blue).

The *4-channel* (4CH) architecture contains, as a subset, all other conventional teleoperation architectures, such as *position command - position feedback* (PP) and *position command - force feedback* (PF). We complement these two standard bilateral teleoperation architectures with a *position command - no feedback* (PN) architecture, where the haptic feedback provided to the operator is solely based on the HSC guidance force. This architecture can be used to model tasks where there is, in principle, no need for the direct force feedback from the environment, or such feedback would be counterproductive, e.g., due to severe communication delays. For instance, such systems are used for collision avoidance for UAV teleoperation [139], lane keeping during car driving [37], landing an aircraft using a haptic flight director [38], or providing predictive force feedback based purely on the task model [140]

The Lawrence framework allows for a broad range of different teleoperation architectures, which can be combined with these two HSC types mentioned previously (or their combination). However, in practice, to the best of our knowledge, only a subset of teleoperation architectures and haptic shared control types is commonly used. A summary based on a literature review is given in Table 6.1.

Table 6.1: Overview of teleoperation systems with HSC identified in literature.

Teleoperation architecture	HSC type	Symbol	Reference
Position command	Slave	PN-SG	[22]
Position-Position	Slave	PP-SG	[22, 116]
Position-Force	Slave	PF-SG	[45, 115]
Position-Force	Master	PF-MG	[114, 137]

6.2.1. TELEOPERATION SYSTEM MODEL

The general 4-channel architecture, Figure 6.2, is implemented through four separate controller channels C_i , with $i = \{1, 2, 3, 4\}$. The controllers C_1 and C_3 constitute the position command and force feed-forward from the master to the slave, respectively. For the feedback direction (from the slave to the master) the controllers C_2 and C_4 provide the force and the position feedback, respectively. Furthermore, controllers C_m and C_s implement the, respective, local master and slave position control loops. Further details on this controller configuration are given in Appendix 6.2.3.

For the Lawrence framework, the system equations are conventionally expressed in terms of velocities of the operator, V_h , and environment, V_e [14, 16]. In this chapter, similarly to Refs. [117, 141], the *positions* of the master device, X_m , and slave robot, X_s , are used instead. This modification toward using positions instead of velocities is purely

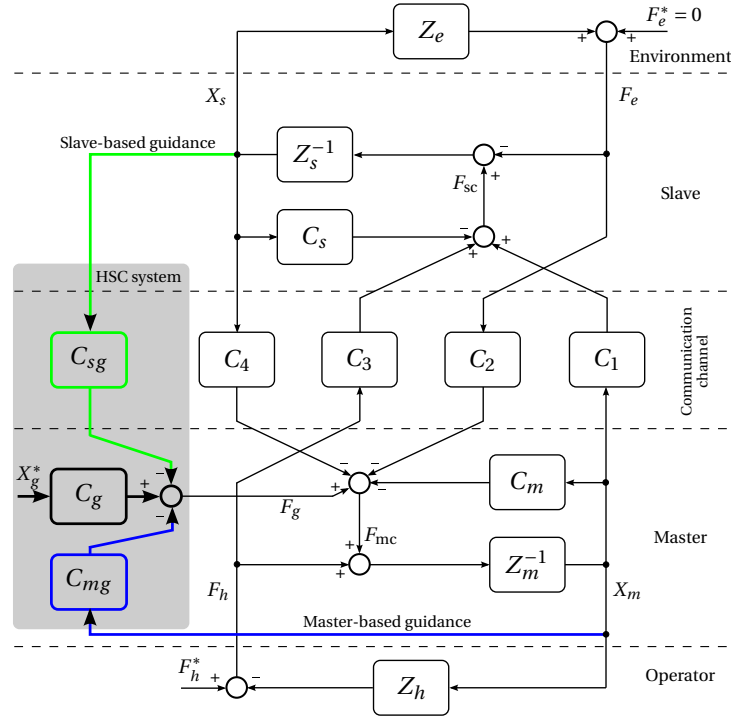


Figure 6.2: The general 4-channel teleoperation system [14]. We add two types of haptic shared control: *slave-based guidance* (in green, based on [46]), calculated using the error between the actual slave position and the guidance reference, and *master-based guidance* based on the master device position (in blue).

mathematical and is made to simplify the introduction of the haptic guidance reference, which is also defined as a position, X_g^* .

The master and slave are in this chapter modeled as impedance type devices $Z_{m/s}$, as:

$$\begin{aligned} Z_m X_m &= F_h + F_{mc} \\ Z_s X_s &= -F_e + F_{sc}, \end{aligned} \quad (6.1)$$

where F_h and F_e are the operator force on the master and the slave force on the environment, respectively. The master F_{mc} and slave F_{sc} motor control forces are force inputs that are commanded to a lower-level motor control system of the master and slave units.

We adopt a conventional continuous-time, linear time-invariant model and notation of the teleoperation system [14]. It should be noted, that real-life teleoperation systems are highly non-linear, digitally controlled systems with the dynamics depending on the actual kinematic configuration [3]. However, these systems are often made to behave like linear time-invariant system through closed-loop control.

The master and slave devices $Z_{m/s}$ are assumed to be pure masses:

$$\begin{aligned} Z_m(s) &:= M_m s^2 \\ Z_s(s) &:= M_s s^2 \end{aligned}$$

The neuromuscular admittance of human operator limb holding the master device Z_h is modeled as a mass-spring damper system:

$$Z_h(s) := M_h s^2 + B_h s + K_h,$$

together with an exogenous (voluntary cognitive control) operator force input F_h^* . The environment Z_e is represented by a spring-damper combination:

$$Z_e(s) := B_e s + K_e,$$

together with an exogenous environment force input F_e^* .

The actions of the controllers are implemented using the master F_{mc} and slave F_{sc} motor control forces:

$$F_{mc} = -C_m X_m - C_2 F_e - C_4 X_s \quad (6.2)$$

$$F_{sc} = C_3 F_h + C_1 X_m - C_s X_s \quad (6.3)$$

The controller gains C_i greatly influence the properties of the teleoperation system. It is assumed, that performing a teleoperated task would be easier if the system can represent the remote environment to the operator with a higher fidelity; with system ‘transparency’ being one of the widely accepted ways to assess it [14]. Ideal transparency is achieved when there exists equal operator and environment forces $F_h(s) = -F_e(s)$ (the negative sign originates from a customary direction definition) and also equal velocities of the hand and the end-effector on both sides $V_h(s) = V_e(s)$, where ‘ s ’ is the Laplace operator.

Lawrence, and later others, presented a design guidelines, sometimes referred to as a *practical transparency-optimized control law* [14, 15, 17], that recommends on how to select the controller gains C_i to maximize the transparency of the teleoperation system:

$$\left\{ \begin{array}{l} C_1 = C_s \\ C_2 = 1 \\ C_3 = 1 \\ C_4 = -C_m \end{array} \right. \quad (6.4)$$

In a realistic teleoperation system, perfect transparency is hard to achieve, however. Transparency is constrained by imperfections of the teleoperation system, such as hardware limitations [18], the control methods employed [17], sampling effects [142], and communication time delays [18, 19]. The aim of this chapter *is not* to discuss how to select these controller gains C_i , but rather how, for a given teleoperation system, one can analyze the additional haptic shared controller.

6.2.2. SLAVE-BASED AND MASTER-BASED TYPE HSCs

We extend the Lawrence teleoperation control architecture by an attractive position-based haptic shared control system, see Figure 6.2. The objective of an attractive HSC system is to make the slave robot position, X_s , follow a prescribed guidance reference position, X_g^* (the asterisk superscript is used here to denote an *exogenous* input signal, following Lawrence's notation of F_{hle}^*). A significant number of HSC systems described in the literature falls into this category.

Such an HSC system is commonly implemented directly as a virtual spring driving the master device, by the addition of a guidance force F_g that is proportional to the deviation between the guidance reference X_g^* and the slave robot position X_s . In this chapter, this method is referred to as *slave-based* guidance.

However, another approach can be found in literature, specifically in studies that consider applying HSC systems in the presence of time delays in the communication channel [114, 137]. This second method is here referred to as *master-based* guidance. Here, the guidance force F_g is based on the deviation between the guidance reference, X_g^* , and the master device position, X_m (after potential coordinate system conversion). In other words, the master-based guidance steers the position of the master device to follow the desired reference and relies on the teleoperation system to command the slave robot to move to the corresponding position. It is assumed that there is a good description of the geometry of the task available at the master side, for example based on a Computer-aided design (CAD) model of the remote environment.

It should be noted that both HSC types can be either applied simultaneously in one system, or separately, which is arguably more common, by setting the respective controller gains to zero (e.g., for a master-based HSC, as: $C_{sg} = 0$). The two guidance alternatives can be expressed as two components of the guidance forces $F_g = F_{sg} + F_{mg}$:

$$\text{slave-based guidance: } F_{sg} = C_{sg} (X_g^* - X_s) \quad (6.5)$$

$$\text{master-based guidance: } F_{mg} = C_{mg} (X_g^* - X_m), \quad (6.6)$$

where C_{sg} and C_{mg} are here PD type controllers (spring-dampers), defined as:

$$C_{sg}(s) = K_{sg} + B_{sg}s \quad C_{mg}(s) = K_{mg} + B_{mg}s \quad (6.7)$$

We adopt the typical controller structure of the Lawrence scheme (for details see 6.2.3), and so the joint guidance controller term C_g , in Figure 6.2, is set to:

$$C_g = C_{sg} + C_{mg} \quad (6.8)$$

The master motor command force F_{mc} , defined in Eq. (6.2), after including the guidance force F_g of the slave- and master-based HSC control loops Eqs. (6.5) and (6.6), now becomes:

$$F_{mc} = -(C_{mg} + C_m)X_m - C_2F_e - (C_{sg} + C_4)X_s + (C_{sg} + C_{mg})X_g^* \quad (6.9)$$

The slave motor command force F_{sc} remains as in Eq. (6.3).

We will use this generic system description in the following part of the chapter to make theoretical predictions on how the described HSC system would perform in different situations.

6.2.3. NOTE ON CONTROLLER STRUCTURE OF THE LAWRENCE SCHEME

In the Lawrence generalized teleoperation framework [14], and also for our proposed extension shown in Figure 6.2, the position controllers R are not connected around the plant P in the classical output error feedback structure, as is illustrated in Figure 6.3(a). We use R to denote the controller to avoid confusion with the controllers of the Lawrence framework C_i .

In contrast, the position controllers $C_{1,4}$ of Figure 6.2 are organized into two pairs, C_1 is paired with C_3 and C_4 is paired with C_m , as is illustrated in Figure 6.3(b). The transfer functions from the input U to the output Y for both configurations are:

$$(a) \quad \frac{Y}{U} = \frac{PR}{1 + PR} \quad (b) \quad \frac{Y}{U} = \frac{PR_1}{1 + PR_2} \quad (6.10)$$

Both configurations are equivalent for $R = R_1 = R_2$.

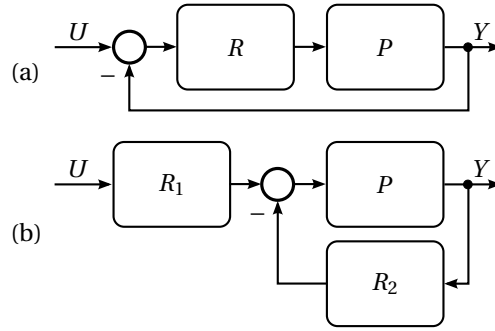


Figure 6.3: Simplified equivalent system interconnections of controller R and plant P . Configuration (a) depicts a common output error interconnection. In (b), a feedback configuration adopted in the Lawrence framework is shown. Both configurations are equivalent for $R = R_1 = R_2$.

6.3. PERFORMANCE METRICS FOR A HSC SYSTEM

In this section, three different situations in which an operator interacts with an HSC system are discussed and formalized. We then define a set of metrics to facilitate the analysis of HSC systems operating in these situations and derive these metrics from the framework presented in Section 6.2.

6.3.1. OPERATOR INTERACTION WITH THE HSC SYSTEM

In principle, the operators can interact with the teleoperation system in two opposing ways [34]: they can give way to the HSC forces, or oppose them. They can do so by either consciously generating a force (in the presented framework modeled as the exogenous operator force F_h^*) and/or by voluntarily changing the neuromuscular properties of the limb interacting with the master device (modeled as Z_h) [68, 139].

In this chapter, to explain and analyze the interaction of an operator with an HSC system, we make the simplifying assumption to only consider the operator's reaction on the guidance as an adaptation of the neuromuscular system (mainly of the spring

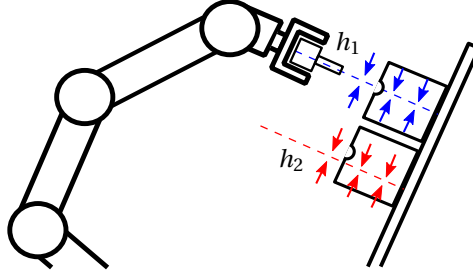


Figure 6.4: A teleoperated peg-in-hole insertion task with HSC guidance (shown with arrows). In a *nominal* situation, the robot is correctly guided to align with the hole h_1 to facilitate the insertion. However, if the operator's actual intention is to insert the peg in the hole h_2 , they would be in a *goal conflict*. Note that in this figure, the guidance to the hole h_2 is offset to illustrate a *geometrical inaccuracy*.

stiffness K_h). Later in Section 6.4, this intuitively established approach to model the reactions of the operator is put on a more systematic basis.

Next, a peg-in-hole insertion task is discussed to illustrate the operator's interaction with the HSC system in three different situations, see also Figure 6.4:

HSC SYSTEM OPERATING IN A NOMINAL SITUATION

First, we consider the performance of an HSC system in a nominal situation, where the goal of the operator and HSC are in agreement, and the guidance is providing support with a task. Since the operator agrees with the guidance, he/she can become compliant and give way to the haptic forces. For the example of an HSC system designed to support a teleoperated peg-in-hole insertion, see Figure 6.4, the HSC system can provide guidance to align the slave holding the peg accurately with the hole while still in free-air, before the actual insertion. The operator can take advantage of the support by yielding to the guidance force.

HSC SYSTEM IN A GOAL CONFLICT

One of the design philosophies behind HSC is to ensure that operators are kept in the control loop (while minimizing their workload, both physical and mental) [34, 67]. In contrast to the nominal situation example, if the operator intends to insert the peg into a different hole (i.e., in Figure 6.4, to h_2 instead of h_1), thus disagreeing with the actions of the HSC, he/she can 'stiffen up' to resist the guidance force and enforce the desired master device position, effectively overruling the automation.

HSC SYSTEM OPERATING WITH GEOMETRICAL INACCURACY

Once the peg is inserted into the hole, the slave robot holding it becomes physically constrained by the hole. If the guidance reference was not accurately programmed to be aligned with the hole, the HSC would guide the operator to exert undesired forces on the remote environment (through the slave robot). Such a situation is illustrated by an offset guidance reference of h_2 in Figure 6.4. This could complicate the insertion task or even lead to damage to the peg, hole, and/or the slave robot.

6.3.2. SYSTEM PERFORMANCE METRICS

The overall system performance can now be analyzed from two perspectives: 1) performance of the underlying teleoperation system, 2) performance of the HSC system.

The performance criterion for the underlying teleoperation system was previously formulated in the literature as a distortion of the environment transmitted impedance (transparency) [14], a dynamic range of the transmittable impedance (Z-width) [143], or a position and force tracking error over a range of frequencies [144]. Put plainly, the main idea behind the tracking error metric is that the master and slave positions $X_{m/s}$, and also the operator and environment forces $F_{h/e}$, should track each other perfectly, as:

POSITION TRACKING $|X_m - X_s|$

This metric expresses how well the master device X_m and slave robot X_s positions are coupled. In essence, it quantifies both the operator's ability to perceive the position of the slave robot, and also his/her influence on the slave robot position.

FORCE TRACKING $|F_h - F_e|$

Similarly, the force tracking metric quantifies the amount of feedback force the operator perceives, F_h , and also the amount of force he/she exerts through the slave robot on the remote environment F_e .

The performance of an attractive HSC system can be quantified by how well the slave robot X_s follows the guidance reference X_g^* , leading to the following metric:

GUIDANCE REFERENCE TRACKING $|X_g^* - X_s|$

In a nominal situation, the slave should track the guidance perfectly. However, as was described above, we also consider two situations in the reference tracking *cannot* be perfect: a) the operator decides to resolve a goal conflict and overrules the HSC system, enforcing a different slave robot position than the guidance reference X_g^* , or b) if a model of the remote environment is geometrically inaccurate (e.g., an offset in the hole location), upon insertion the slave robot becomes constrained by the environment at a different location than X_g^* .

6.4. THEORETICAL SYSTEM PERFORMANCE ANALYSIS

The HSC system's tracking performance is studied by analyzing the transfer functions from the guidance reference $X_g^*(s)$, to the respective master and slave positions $X_m(s)$ and $X_s(s)$, as:

$$\frac{X_s(s)}{X_g^*(s)} = \frac{(C_1(s) - C_3(s)Z_h(s))(C_{sg}(s) + C_{mg}(s))}{\text{den}(s)} \quad (6.11)$$

$$\frac{X_m(s)}{X_g^*(s)} = \frac{(Z_s(s) + Z_e(s) + C_s(s))(C_{sg}(s) + C_{mg}(s))}{\text{den}(s)}, \quad (6.12)$$

where the common denominator is:

$$\begin{aligned} \text{den}(s) = & (Z_s(s) + Z_e(s) + C_s(s))(Z_m(s) + C_m(s) + Z_h(s) + C_{mg}(s)) \\ & + (C_1(s) - C_3(s)Z_h(s))(C_4(s) + C_{sg}(s) + C_2(s)Z_e(s)) \end{aligned}$$

Table 6.2: Summary of the theoretical steady-state system performance in reaction to a ΔX_g^* step input.

Condition	Position tracking $ X_m - X_s $		Force tracking $ F_h - F_e $	
	$X_m / \Delta X_g^*$	$X_s / \Delta X_g^{*1}$	$F_h / \Delta X_g^*$	$F_e / \Delta X_g^*$
Free-air, nominal task $K_e = 0, K_h \rightarrow 0$	$\frac{K_{sg} + K_{mg}}{K_h + K_{sg} + K_{mg}}$	$\frac{K_{sg} + K_{mg}}{K_h + K_{sg} + K_{mg}}$	$\frac{K_h(K_{sg} + K_{mg})}{K_h + K_{sg} + K_{mg}}$	0
Free-air, goal conflict $K_e = 0, K_h \rightarrow \infty$	0	$-\frac{K_3(K_{sg} + K_{mg})}{K_s + K_3(K_m - K_{sg})}$	$-(K_{sg} + K_{mg})$	0
Constrained, geo-metrical inaccuracy $K_e \rightarrow \infty, K_h = 0$	$\frac{K_{sg} + K_{mg}}{K_{mg} + K_4 + K_s K_2}$	0	0	$-\frac{K_s(K_{sg} + K_{mg})}{K_{mg} + K_4 + K_s K_2}$

¹ $X_s / \Delta X_g^*$ is conveniently used to represent the guidance reference tracking metric $|X_g^* - X_s|$ (i.e.,

$$X_s / X_g^* = 1 \Leftrightarrow |X_g^* - X_s| = 0).$$

Based on these slave and master positions, $X_{s/m}$, the environment and operator forces, $F_{e/h}$, can be calculated as:

$$\begin{aligned} F_e &= Z_e X_s \\ F_h &= -Z_h X_m \end{aligned} \quad (6.13)$$

There is a large number of time-domain characteristics to evaluate the system dynamical response, e.g., settling time, overshoot, integrated error metrics [145]. However, in the following section we focus on the steady-state performance to illustrate how different design choices and trade-offs affect the behavior of the overall system.

6.4.1. STEADY-STATE THEORETICAL SYSTEM PERFORMANCE

To derive the HSC system steady-state performance, we combine the transfer functions Eqs. (6.11) and (6.12), substitute $C_s = C_1$ and $C_4 = -C_m$ (Eq. (6.4)), and evaluate them for a steady-state:

$$\frac{X_s}{X_g^*} = \frac{(K_s - K_3 K_h)(K_{sg} + K_{mg})}{\text{den}_{ss}} \quad (6.14)$$

$$\frac{X_m}{X_g^*} = \frac{(K_e + K_s)(K_{sg} + K_{mg})}{\text{den}_{ss}}, \quad (6.15)$$

where the steady-state common denominator is:

$$\text{den}_{ss} = (K_e + K_s)(K_m + K_h + K_{mg}) + (K_s - K_3 K_h)(-K_m + K_{sg} + K_2 K_e)$$

Furthermore, in a steady-state Eq. (6.13) reduces to:

$$\begin{aligned} F_e &= K_e X_s \\ F_h &= -K_h X_m \end{aligned} \quad (6.16)$$

The steady-state theoretical performance results, Eqs. (6.14) to (6.16), were then analyzed in the three distinct situations of Section 6.3.1: in a free-air nominal task ($K_e = 0$, to assess effects of the operator stiffness $K_h \geq 0$), in a free-air task with a goal conflict ($K_e = 0$, $K_h \rightarrow \infty$), and in a constrained task with geometrical inaccuracy ($K_e \rightarrow \infty$, $K_h = 0$). Results are summarized in Table 6.2.

6.4.2. DISCUSSION OF THE STEADY-STATE PERFORMANCE RESULTS

Our motivation to focus on the system performance in steady-state is twofold. First, we can gain an insight into the functionality of the system and derive a set of basic design recommendations. Although the simplified expressions in Table 6.2 are still relatively complicated, we obtained the following insights.

Nominal task:

- a) In free-air tasks, the slave position tracks the master ($|X_m - X_s| = 0$). The force tracking is evidently not perfect, since the operator perceives the guidance force, whereas the slave robot is in free air.
- b) Perfect slave robot position tracking of the guidance reference (i.e., $\frac{X_s}{X_g} = 1$) requires the operator to be fully compliant, as $K_h \rightarrow 0$.

Goal conflict:

- c) With the 4CH architecture, keeping the master device perfectly stationary to overrule the guidance (at $X_m = 0$), causes the slave position X_s to move in the *opposite direction* from the guidance reference position X_g^* .

Geometrical inaccuracy:

- e) The slave-based HSC using the PN architecture requires the operator to hold the master device ($K_h > 0$) in constrained tasks to maintain system stability.
- f) The slave- and master-based HSCs in most situations exhibit the same steady-state responses. However, in a constrained task with an inaccurate reference, the master-based HSC leads to smaller position and force tracking errors.

Second, the steady-state analysis requires only limited knowledge of the parameters of the studied system. The expressions presented in Table 6.2 only contain the system ‘gains’, i.e., only the proportional parameters of the system PD controllers ($K_{s/mg}$, $K_{s/m}$) and force feedback and feedforward gains ($K_{2/3}$). All these parameters are selected during the system design phase, and thus do not need to be experimentally identified (in contrast to some of the dynamical parameters of the system). Predictions based on these steady-state performance results are validated experimentally in Section 6.6 using a complex 6-DOF master-slave teleoperation system.

Besides the system parameters, an assumed stiffness of an operator’s limb (K_h) is also included in the steady-state expressions in Table 6.2. This is done to facilitate the discussion about the operator’s reaction to the HSC presented in Section 6.3.1 and this parameter does not need to be identified.

6.5. NUMERICAL SIMULATION

In this section, we use numerical simulations to study the dynamical performance differences and design trade-offs between the two studied HSC system types.

6.5.1. METHOD

The numerical study consists of five simulations, in which we illustrate different properties of the HSC system. The aims of the respective simulation parts are to show the effects of: 1) increasing HSC gain on identical master and slave units (equal dynamics); 2) the slave unit having significantly higher inertia (i.e., slower dynamics); 3) increasingly higher time-delay in the communication channel; 4) goal conflicts; and 5) geometrical inaccuracies in different underlying teleoperation architectures. The aims of the separate numerical studies are listed in Table 6.3, together with simulated system parameters (i.e., HSC controllers, underlying teleoperation systems, simulated operator/environment impedance).

Table 6.3: The focus, procedure, and system parameters for the individual simulation studies.

#	Simulation aim	Simulation parameters
1	Identical master and slave (varied gain $K_{s/mg}$) Procedures: S1 and S2	PN architecture, $M_s/M_m = 1$, $T_d = 0$, $K_{s/mg} \in \{100, 150, 200\}$ N/m, $Z_h, Z_e = 0$
2	Slow slave dynamics (varied slave mass M_s) Procedures: S1 and S2	PN architecture, $M_s/M_m \in \{1, 5, 10\}$, $T_d = 0$, $K_{s/mg} = 100$ N/m, $Z_h, Z_e = 0$
3	Communication delay (varied time-delay T_d) Procedures: S1 and S3	PN architecture, $M_s/M_m = 1$, $T_d \in \{0, 40, 80\}$ ms, $K_{s/mg} = 100$ N/m, $Z_h, Z_e = 0$
4	Goal conflict (varied architecture) Procedure: S1	PN, PP, PF, and 4CH architectures, $M_s/M_m = 1$, $T_d = 0$, $K_{s/mg} = 100$ N/m, $Z_h = 10^4 + 100s$, $Z_e = 0$
5	Geometrical inaccuracy (varied architecture) Procedure: S1	PN, PP, PF, and 4CH architectures, $M_s/M_m = 1$, $T_d = 0$, $K_{s/mg} = 100$ N/m, $Z_h = 0$, $Z_e = 10^7 + 10^3 s$

SIMULATION PROCEDURE

The respective simulations described in Table 6.3 are studied using the following procedures:

- (S1) The step response on guidance reference X_g^* . Step responses (a step of 0.1 m applied at $t = 0$ s) are compared to illustrate the effects of varying system parameters.
- (S2) Locations of the closed-loop system poles. The locations of closed-loop poles over a range of system parameters are calculated to explore the system stability limits.

- (S3) The highest acceptable HSC gain for a given communication delay, with the following tuning criterion: The step response settling time ($\pm 5\%$) is below 2 s, the guidance force F_g does not reach *both* positive and negative saturation limits (i.e., the system does not guide the operator with the *maximal* guidance force in one direction and immediately after that again with the maximal force in the opposite direction).

SIMULATED SYSTEM

The teleoperation system we simulate is configured as in Figure 6.2. It is composed of an impedance-type master device with a constant $M_m = 1$ kg mass. The mass of the slave robot M_s varies as specified in Table 6.3.

The slave position controller is of the PD-type: $C_1(s) = C_s(s) = K_s + B_s s$; the damping parameter B_s is calculated based on the slave mass M_s to yield a less-than-critically-damped system: $B_s = 0.5 \cdot 2\sqrt{M_s K_s}$. The teleoperation system tuning gains are listed in Table 6.4.

Table 6.4: System parameters used in the numerical simulation study ($C_{s/m}$ selected according to Eq. (6.4)).

Teleoperation architecture	Controller gains			
	C_1 [N/m]	C_2 [-]	C_3 [-]	C_4 [N/m]
PN	1000	0	0	0
PP	1000	0	0	500
PF	1000	1	0	0
4CH	1000	1	1	500

When a communication delay is simulated, the controllers located in the communication channel part of the diagram, in Figure 6.2, specifically controllers C_i where $i = \{1, 2, 3, 4, sg\}$, are extended by the addition of a continuous-time delay T_d :

$$C'_i = C_i e^{-sT_d} \quad (6.17)$$

The guidance force calculated by the HSC controller is in certain situations very high, e.g., immediately after a step change in guidance reference. This would be possibly unsafe for the operator. To mitigate this issue and make the system representative of practical implementations, the guidance force F_g is limited to ± 10 N.

Simulations are performed using a one degree-of-freedom model implemented in Matlab/Simulink.

6.5.2. SIMULATION RESULTS

SLAVE- AND MASTER-BASED HSC FOR IDENTICAL MASTER AND SLAVE UNITS

Figure 6.5a, shows that, for identical master and slave systems, both slave- and master-based HSC systems types exhibit similar step responses. The overshoot increases for higher $K_{s/mg}$ gains.

The slave-based HSC poles, shown in Figure 6.5b, approach the imaginary axes as K_{sg} increases, and the system becomes unstable for $K_{sg} > 401$ N/m. In contrast, the

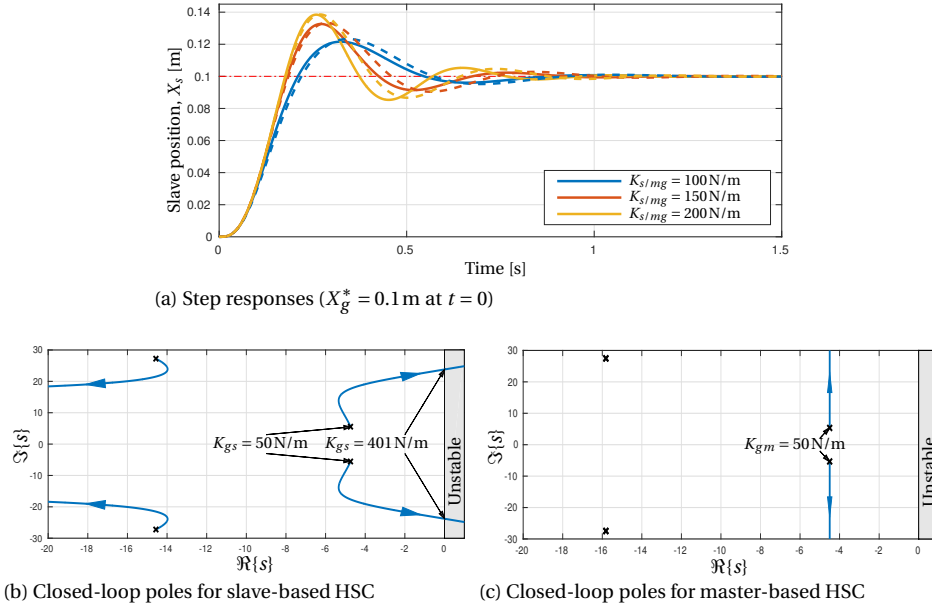


Figure 6.5: Effects of varying guidance gains for the PN architecture. (a) Step reference tracking for slave- (solid lines) and master-based (dashed lines) HSC types, showing that the overshoot increases for higher K_s/mg gains. The slave-based HSC system (b), is unstable for $K_g > 401 \text{ N/m}$, whereas the master-based HSC system poles (c), remain $\Re\{s\} < 0$.

master-based HSC system poles, in Figure 6.5c, theoretically remain in the left-half plane, indicating stability for any K_{mg} .

MASTER AND SLAVE SYSTEMS WITH SUBSTANTIALLY DIFFERENT DYNAMICS

To assess the effects of different dynamical parameters of the master and slave systems, three slave robot mass values M_s were compared (1-, 5-, and 10-times the master mass M_m). Figure 6.6a shows that for slave robots with higher mass relative to the master device, for the slave-based HSC, an 5-times slave mass increase already causes the system to oscillate (arguably to such an extent that the system would be impractical). In contrast, the master-based HSC type provides step responses with only minimal undershoot.

The poles of the slave-based HSC, shown in Figure 6.6b, approach the imaginary axes when M_s/M_m increases, and the system becomes unstable for $M_s/M_m > 12.2$. In contrast, the poles of the master-based HSC system, in Figure 6.6c, remain $\Re\{s\} < 0$, theoretically for any M_s/M_m .

EFFECTS OF TIME-DELAY IN THE COMMUNICATION CHANNEL

The influence of communication delay on an HSC system is evaluated in Figure 6.7. The step reference responses show, that when the communication is delayed, the slave-based guidance exhibits oscillatory behavior. The master-based HSC type response is not influenced by the delay.

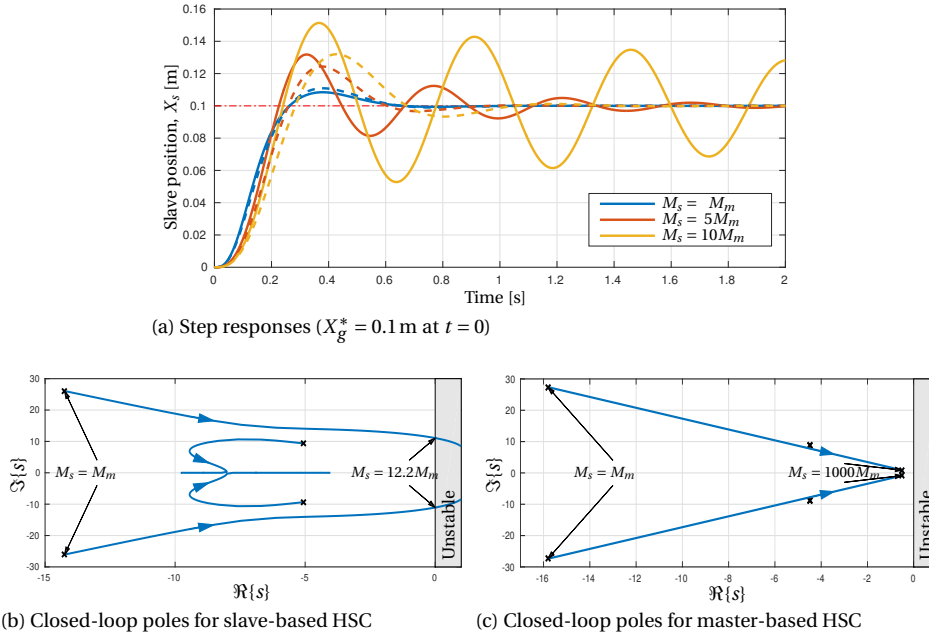


Figure 6.6: Effects of increasing slave robot inertia for the PN architecture. (a) Step reference tracking for slave- (solid lines) and master-based (dashed lines) HSC types. The slave-based HSC system (b), is unstable for $M_s > 12.2M_m$, whereas in (c), the master-based HSC system poles remain $\Re\{s\} < 0$ (plotted for $M_s/M_m \in \langle 1, 1000 \rangle$).

As shown in Figure 6.8, the maximal controller stiffness of the slave-based HSC type quickly decreases with longer delays, and for the simulated teleoperation system the slave-based HSC is not suitable for round-trip delays above 130 ms. The master-based HSC responses again remain unaffected by the delay.

GOAL CONFLICTS

The reaction of a simulated operator who rigidly holds the master device, effectively overruling the HSC to resolve a goal conflict, is shown in Figure 6.9. The slave- and master-based HSCs with the PN, PP, and PF architectures behave almost identically: the simulated operator exerts a force $F_h = -10$ N to overrule the guidance and manages to keep the slave at $X_s = 0$ mm. The 4CH architecture requires only approximately $F_h = -7$ N, but here the slave robot moves to $X_s = -7$ mm, i.e., in the *opposite* direction from the location of the reference ($X_g^* = 100$ mm).

GEOMETRICAL INACCURACY

The guidance reference step response while the slave is constrained by a stiff environment (i.e., $X_s = 0$) is shown in Figure 6.9. Note that the PN-SG HSC system is unstable and thus does not reach a steady-state.

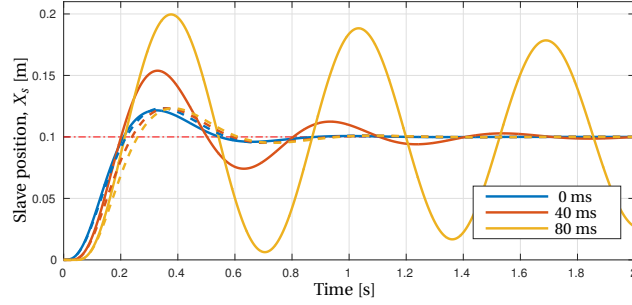


Figure 6.7: Simulation results of 0.1 m step reference tracking for slave- (solid lines) and master-based (dashed lines) HSC types, showing the effect of increasing round-trip time delays.

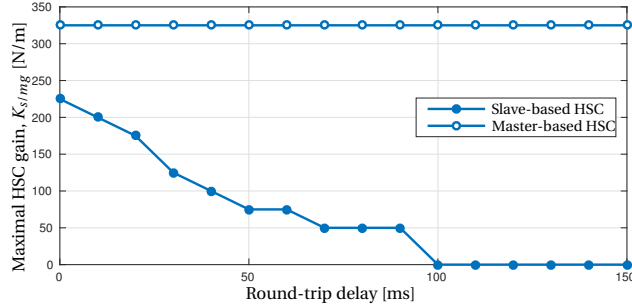


Figure 6.8: Simulation results showing the maximal practically stable HSC stiffness gains for varying round-trip communication delays for PN architecture.

COMPARISON WITH THEORETICAL STEADY-STATE RESPONSES

Table 6.5 shows the steady-state slave and master positions $X_{s/m}$, and the human and environment forces $F_{h/e}$, in reaction on a guidance step $X_g^* = 0.1$ m, for different teleoperation architectures. Results are based on the steady-state transfer functions presented in Table 6.2. The theoretical results match the simulated system responses at the steady-state very well, see Figures 6.9 and 6.10.

6

6.6. EXPERIMENTAL VALIDATION

The aim of the experimental study is to validate the findings of the theoretical analysis and numerical study. The experiment was conducted on a real teleoperation setup in 6-DOF to test whether the theoretical results obtained in the previous sections can be used to predict the behavior of a complex master-slave system.

The validation consisted of three separate experiments, with following goals: 1) to evaluate the force necessary to resolve a goal conflict; 2) to investigate the effects of geometrical uncertainties; 3) to find the highest stable HSC gain for a range of communication delays.

As a baseline for the experiment, the controller parameters of the teleoperation system with the slave-based HSC were taken from our previous studies performed on the

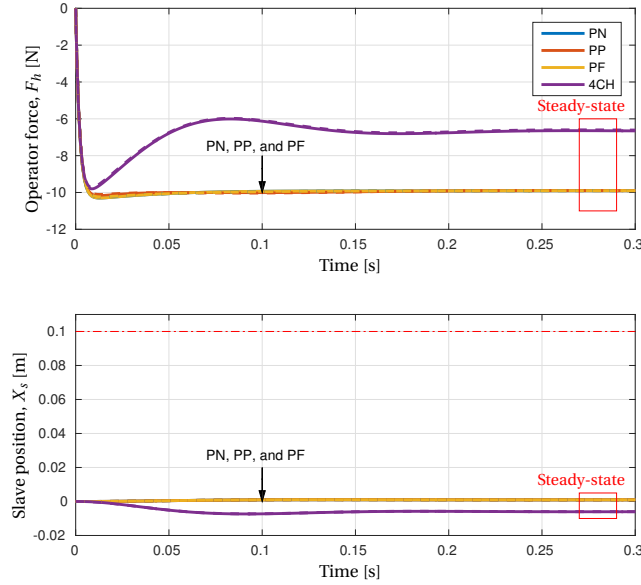


Figure 6.9: Simulation results for the goal conflicts for slave- (solid lines) and master-based (dashed lines) HSC types, showing the effect of different underlying teleoperation architectures.

same hardware setup [46, 55]. For the sake of comparison, these parameters were also used in the master-based HSC system.

6.6.1. METHOD

To keep the focus on the experimental validation mainly on the teleoperation system itself, we have chosen to imitate the behavior of human operators by mechanical means. In principle, we study two extreme ways how operators interact with the guidance forces: either they fully resist those, or they fully comply.

In our experiment, we imitate an operator completely resisting the guidance, effectively enforcing his/her commands to the system, by keeping the master device rigidly attached to an external force/torque sensor (allowing to measure the necessary force to keep the system stationary), that was fixed at the starting location. In contrast, to imitate an ideally compliant operator, the master device was not held by any operator and was left free to move in any direction.

EXPERIMENTAL SETUP

A KUKA Lightweight robot (slave) was teleoperated using a Force Dimensions Sigma 7 haptic device (master), see Figure 6.11a. The slave robot is operated in an impedance control mode, with programmed Cartesian stiffness of $K_s = 1000 \text{ N/m}$ for translations and $K_s = 50 \text{ Nm/rad}$ for rotations, respectively. A 150 mm long titanium peg is rigidly mounted on a 6-DOF force/torque sensor (ATI Gamma) on the end-effector of the slave

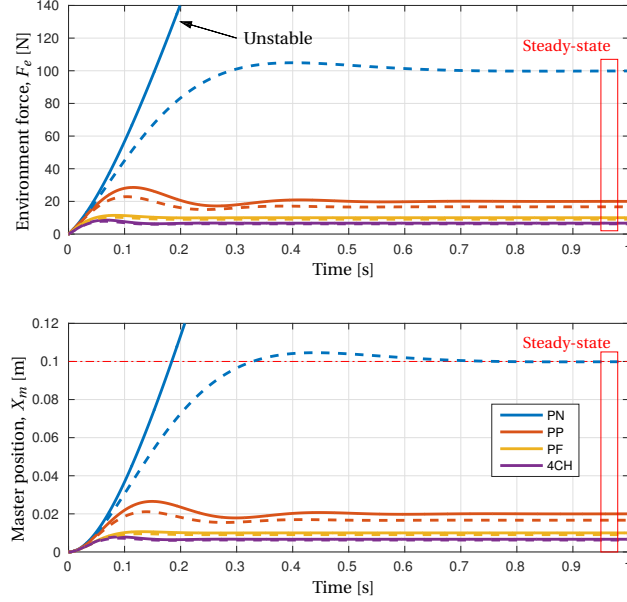


Figure 6.10: Simulation results for the geometrical inaccuracy for slave- (solid lines) and master-based (dashed lines) HSC types, showing the effect of different underlying teleoperation architectures.

robot arm. The peg (diameter of 14.5 mm) could be inserted into a tight brass hole (diameter of 14.75 mm), located at the origin $[0, 0, 0, 0, 0]^T$ of the used coordinate system. The force/torque sensor was sampled at 1 kHz, low-pass filtered with a 100 Hz cut-off frequency and corrected for the force due to the weight of the peg. The control software was implemented on a real-time operating system (Xenomai) with a 1 kHz sampling rate.

6

EXPERIMENTAL PROCEDURE

The three experiments were carried out with the following procedures:

- (E1) Goal conflicts in free-air. Ten step responses (step of $X_g^* = 0.02\text{m}$ in the x-direction) were recorded with the master device rigidly attached to an additional force/torque sensor, that was used to record the operator's force, F_h , necessary to resolve the goal conflict (i.e., keep the master device stationary), see Figure 6.11b. The additional force/torque sensor (also ATI Gamma) was not a part of the control loop and was used only to record the force measurements.
- (E2) Geometrical inaccuracy in a constrained task. Ten step responses (step of $X_g^* = -0.01\text{ m}$ in the x-direction) were performed while the slave robot was fully inserted into a tight hole (see Figure 6.11c). The force exerted by the slave on the hole, F_e , and the position of the master, X_m , were recorded.

Table 6.5: Steady-state analysis results for slave- (SG) and master-based (MG) HSC types, for $\Delta X_g = 100\text{mm}$.

Architecture	Goal conflict ¹		Geometrical inaccuracy ²	
	X_s [mm]	F_h [N]	X_m [mm]	F_e [N]
PN-SG	0.0	-10.0	No steady-state	
PN-MG	0.0	-10.0	100.0	-100.0
PP-SG	0.0	-10.0	20.0	-20.0
PP-MG	0.0	-10.0	16.7	-16.7
PF-SG	0.0	-10.0	10.0	-10.0
PF-MG	0.0	-10.0	9.1	-9.1
4CH-SG	-7.1	-7.1	6.7	-6.7
4CH-MG	-6.7	-6.7	6.2	-6.2

¹ Ideally, X_s should stay 0, requiring the least F_h .

² Ideally, X_m should stay 0, exerting the least F_e .

- (E3) Maximum stable HSC gain for a system with increasing communication delay. The guidance controller gains $K_{s/mg}$ for both slave- and master-based HSC types were varied, to find the highest gains that still provide stable operation for a given delay. To assess system stability, a step of $X_g^* = 0.05\text{m}$ was repeated multiple times to confirm that the current guidance gain setting provides a stable system response. The slave robot and the master device were both located in free-air. Notably, based on our practical experiments, this lack of the operator hold of the master device is the most challenging configuration for the system stability. A simulated communication delay between the master and slave sides was added to the control software implemented on the real-time computer.

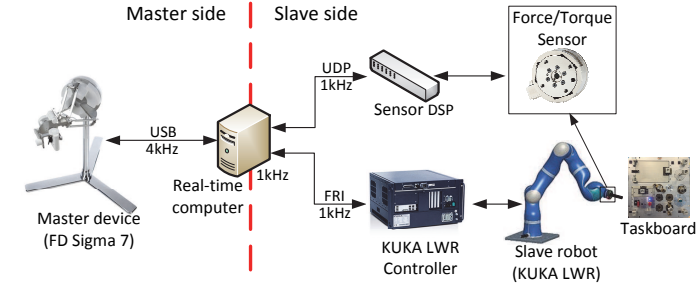
EVALUATED TELEOPERATION ARCHITECTURES

The teleoperation architectures that were evaluated are summarized, together with the respective system parameters, in Table 6.6. These values were based on our previous studies on this experimental setup [46, 55]. Less conservative (higher) tuning gains were attempted, but the system was then prone to oscillations upon contact with a stiff remote environment, especially in the situation when the master device was held loosely. The relatively low values can be partially attributed to the different values of inertia of the master and the slave devices, as discussed in [17]. The 4CH architecture was not tested in the experiment because the available setup was not equipped with the necessary force/torque sensor on the master device.

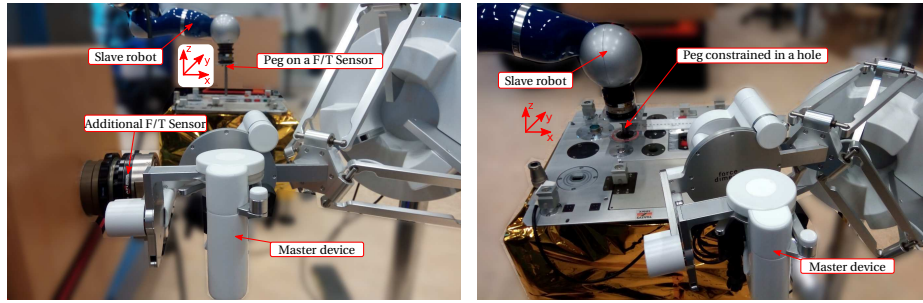
HSC SYSTEM

The HSC system was designed to support the operator in keeping a predefined reference position, for example to achieve fine alignment prior to the peg-in-hole insertion task. The HSC was implemented as an PD controller:

$$C_{sg}(s) = C_{mg}(s) = \text{diag}(K_g^t, K_g^t, 0, K_g^r, K_g^r, 0) + \text{diag}(B_g^t, B_g^t, 0, B_g^r, B_g^r, 0)s,$$



(a) Experimental system architecture overview



(b) Goal conflicts (slave robot in free-air)

(c) Geometrical inaccuracy (constrained slave)

Figure 6.11: Experimental setup with a force-feedback master device controlling a slave robot in a 6-DOF task. In (b), the master device is rigidly connected to the additional F/T sensor.

with the translational and the rotational gains set to $K_g^t = 180 \text{ N/m}$, $B_g^t = 10 \text{ Ns/m}$ and $K_g^r = 1.8 \text{ N/m}$, $B_g^r = 0.1 \text{ Ns/m}$, respectively. The guidance forces applied on the master device were limited to $\pm 5 \text{ N}$ for translations and $\pm 0.5 \text{ Nm}$ for rotations, respectively.

The guidance reference X_g^* coincided with the hole axis and was located at the origin of the coordinate system, as: $X_g^* = [0, 0, 0, 0, 0, 0]^T$.

For the procedure E1, to imitate a goal conflict, the guidance reference was commanded to 20 mm direction offset from the 'zero position', as: $X_g = [0.02, 0, 0, 0, 0, 0]^T$.

During procedure E2, the guidance reference was intentionally made inaccurate by a -10 mm x-offset, as: $X_g = [-0.01, 0, 0, 0, 0, 0]^T$. The magnitude of this inaccuracy is adequate considering the dimensions of the slave robot workspace. Guidance inaccuracies of a comparable size have also been investigated in [45].

VISUALIZATION OF RESULTS

The experimental results are presented as their steady-state values in the x-direction, in Figures 6.11b and 6.11c. The predicted theoretical values are calculated using the steady-state equations in Table 6.2.

6.6.2. EXPERIMENTAL RESULTS

E1) Goal conflict: Boxplots of the measured operator force F_h required to overrule the conflicting guidance (i.e., to keep the master device stationary despite the guidance

Table 6.6: System parameters used in the experiment.

Teleoperation architecture	Controller parameters			
	C_1 [N/m]	C_2 [-]	C_3 [-]	C_4 [N/m]
PN	1000	0	0	0
PP	1000	0	0	200
PF	1000	0.3	0	0

force) are shown in Figure 6.12. There is no influence of the architecture, and the differences with the theoretical values are less than 0.2 N, showing a good correspondence with the theoretical values. Note that the slave robot was in free air (i.e., $F_e = 0$).

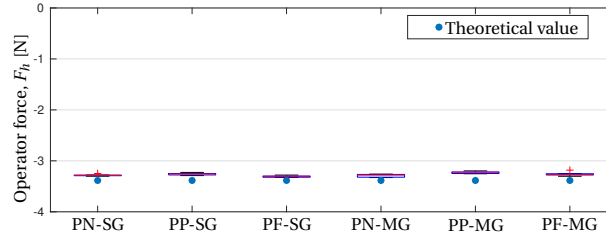


Figure 6.12: Measured steady-state force F_h necessary to compensate for a guidance goal conflict ($\Delta X_g = 20\text{mm}$).

E2) Geometrical inaccuracy: Boxplots of the master device deflection X_m and measured environment force F_e , caused by an inaccurate guidance reference during a peg-in-hole insertion task, are shown in Figure 6.13, showing again a good correspondence with the theoretical predictions. The variability of the measurement results is higher for the PP-SG and PF-SG conditions; possible causes for that are discussed in Section 6.7.3. The PF-MG method is the least sensitive to the guidance inaccuracy. Note that the master device was in free air (i.e., $F_h = 0$).

E3) Maximum stable HSC gain: The influence of communication delays on the stability of the HSC systems is shown in Figure 6.14. Without the additional delay, the master-based HSC type (highest stable gain $K_{mg} = 750\text{N/m}$) allowed for a 4-times higher controller gain than the slave-based HSC (highest stable gain $K_{sg} = 180\text{N/m}$). The highest slave-based HSC stable gain K_{sg} decreased with longer delay. At a round-trip delay of 80ms, the highest stable gain was $K_{sg} = 60\text{N/m}$, which was subjectively difficult to perceive clearly.

The highest stable gain of the master-based HSC was unaffected by the delay, which was experimentally tested for delay levels for up to 2 s (not shown in the figure).

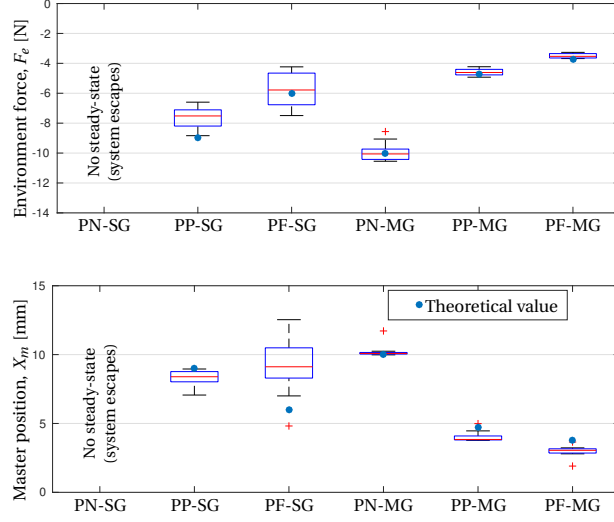


Figure 6.13: Steady-state experimental results showing the effects of guidance inaccuracy ($\Delta X_g = 10\text{mm}$) in a constrained peg-in-hole insertion task.

6.7. DISCUSSION

The overall goal of this chapter was to develop a systematic framework to study Haptic Shared Control (HSC) systems employed in teleoperation and validate its utility. Specifically, we aimed at: 1) discussing the differences and design trade-offs between the two most common HSC types, 2) quantifying the level of control authority an operator holds over a task, and 3) analyzing the effects of geometrical uncertainties on the fidelity of the feedback provided to the human operator. The following was observed:

6

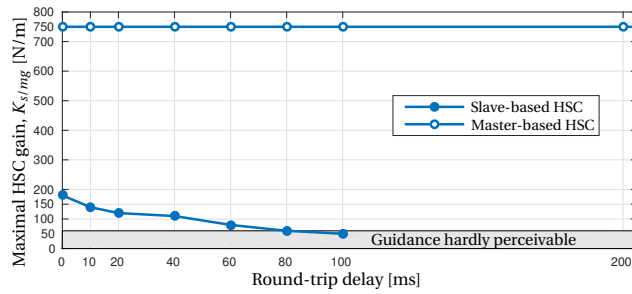


Figure 6.14: Influence of round-trip delay on maximal stable HSC gain, for the PN architecture.

6.7.1. USING THE MASTER-BASED GUIDANCE INCREASES PERFORMANCE, ESPECIALLY FOR ‘SLOW’ AND/OR DISTANT SLAVE ROBOTS

We studied two types of HSC systems employed in teleoperation: the slave- and master-based guidance. Currently, the slave-based guidance type is the more common configuration among HSC systems presented in literature.

However, throughout this chapter, as indicated by the theoretical analysis, numerical study, and experimental results, it became apparent that the master-based guidance has many benefits. It increases task performance in situations when the slave feedback is ‘slower’ compared to the master device. For instance, this can be the case when the slave robot mass is significantly higher than of the master device. In the presented experiment, the KUKA Lightweight robot has an approximately ten times higher mass than the Sigma 7 master device. Using the master-based guidance for this system allowed more than an 4-fold increase in the HSC system gain without any other modification to the system parameters.

The master-based guidance also appears to be a promising method to alleviate some difficulties caused by time delays in the communication channel. The slave-based HSC required reduction of its gain to maintain stable operation. In our experiment, approximately 80 ms was the maximum delay at which the slave-based HSC can be of practical use. The master-based HSC remains completely unaffected by delay.

The assumption for using the master-based HSC is that the guidance reference is known in advance on the master side, e.g., by using a CAD model of the task. If, on the other hand, the reference would be generated in real-time, for example by a contact-less sensor mounted on the slave robot [112], the guidance reference would also need to be communicated to the master side over the delayed channel. This reference should only change infrequently, on a time scale slower than the length of the delay, otherwise some of the benefits of the master-based guidance mentioned above might be lost.

6.7.2. TELEOPERATION ARCHITECTURE AFFECTS THE HSC SYSTEM

The results indicate that the underlying teleoperation architecture plays a major role in the overall system functionality. The teleoperation system interacts with the haptic shared control in a non-trivial fashion. In accordance with our previous study [46], we found that the combination of the guidance forces generated by the HSC system and feedback forces provided by the force sensor located at the slave end-effector alters the feedback given to the operator, which creates a potentially unsafe situation. For example, due to this interaction, the slave robot can be exerting significant forces on the remote environment, without the operator being able to perceive that through force feedback.

One of the system properties studied in this chapter is the amount of force the operators need to exert on the master device to overrule the HSC system and enforce their control commands. On the one hand, it is desirable to keep the control authority with the operator [34]. From this viewpoint, based on the experimental results, it would be recommendable to use the 4CH architecture.

On the other hand, this property can also be counterproductive. Some situations would benefit from a stiffer setting of the guidance system, for example, in assembly tasks with very tight tolerances [92, 93]. To address that, the stiffness setting of the HSC system should be increased, or the teleoperation system architecture should be changed.

Another way to accommodate these conflicting requirements in one system, would be to adjust the HSC stiffness setting based on the momentary situation, for example, by providing the operator with a direct way to self-adjust the stiffness [44].

However, if the HSC system is used to support tasks involving contact with the remote environment, such as peg-in-hole insertion, the lack of feedback from the task environment makes the system sensitive to inaccuracies of the task model, and it can even result in system instabilities [46]. From this point of view, using the master-based HSC type with any architecture, or, for the slave-based HSC, using an architecture with some form of environment feedback (i.e., PP, PF, or 4CH architectures) is preferred.

6.7.3. COMPARISON OF THEORETICAL VS. EXPERIMENTAL VALUES

The system-theoretic framework presented in Section 6.2 described the master-slave teleoperation system using a continuous-time, linear time-invariant model. However, real-life teleoperation systems are digitally controlled (i.e., sampled discrete-time systems), and contain many nonlinearities which are only partially compensated for by the underlying control system [135].

In the experimental validation, we compared the measured results with our linear model steady-state predictions. The master-based HSC results corresponded very well to the theoretical predictions. The slave-based HSC exhibited some offsets from the predicted values during the experiment investigating the effects of guidance inaccuracies. Upon closer inspection, these offsets can be attributed to the unmodeled (nonlinear) dynamics of the real master - slave system, mainly to Coulomb friction. The impedance controller of the robot and also the position and force feedback loops back to the master device are essentially P and PD type controllers, with a relatively weak P gain. In effect, the calculated control action is at times not high enough to overcome the friction. So in practice, after an initial transient both the master and slave devices converge off their 'ideal' positions. This effect is also responsible for the variability in the measurement data between the repetitions.

Despite certain (small) discrepancies, we can conclude that the presented framework applies even to complex master-slave robotic systems that have some difference in the system dynamics to the considered linear model. As a future step, the framework should also be extended to account for nonlinear effects.

6

6.7.4. IMPLICATIONS FOR OTHER APPLICATION DOMAINS

The method presented in this chapter was developed as an extension of the Lawrence framework for analyzing teleoperation systems with attractive HSC systems. However, the same principles and methods can be extended to other application domains beyond teleoperation, such as car driving or aircraft flight director-based pilot support systems.

The first difference to be addressed is that the teleoperation systems described in this chapter are position-based. Car steering, as just one example, is essentially based on rate commands, i.e., the system works such that a constant deflection of the steering wheel from its central position results in a lateral velocity of the vehicle. The slave-based guidance type is in principle compatible with this configuration, however, the master-based type would need to be reformulated. The necessary modification to accommodate this difference would be in creating and maintaining a model of the slave system at the

master side controller, instead of using the master position directly. The master-based guidance can be then directly calculated using this slave model.

6.8. CONCLUSIONS

The chapter formalizes haptic shared control as an extension of Lawrence's general teleoperation framework. Our primary focus has been to systematically study the slave- and master-based HSC types, compare their performance differences and design trade-offs with different teleoperation architectures, and investigate how those affect the position and force tracking offered by the teleoperation system. We conclude that:

- (1) The presented formalization can be used to make accurate predictions about the performance of the studied teleoperator systems with the addition of haptic guidance.
- (2) The master-based haptic guidance system provides robustness against communication delays, whereas, on the presented experimental system, the slave-based HSC became impractical for round-trip delays over 80 ms.
- (3) The master-based HSC type could be operated in a stable fashion for up to 4-times higher guidance stiffness gain than the slave-based HSC type (in a no delay case).
- (4) The underlying teleoperation architecture has a strong effect on the overall system properties and should be taken into account during the HSC design.

7

DISCUSSION AND CONCLUSIONS

7.1. RECAPITULATION OF RESEARCH GOALS

The goal of this dissertation was to develop methods to more systematically design and model haptic shared control systems applied in teleoperation, taking in account uncertainties in the human operator, in the environment and the communication channel. This goal was addressed by considering the following four objectives. First, we aimed to gain further insight into the uncertainties associated with the settings of operator **neuromuscular system** (NMS), and to investigate how we can use this insight to design a haptic shared controller. Our second objective was to analyze the possible **goal conflicts** between the operator and the automatic part of the shared control system. A system architecture was sought that would allow the operator to resolve these conflicts efficiently. Third, the objective was to develop a systematic description that allows analyzing **geometrical goal uncertainties** hindering haptic shared control in bilateral teleoperation, and develop a shared control system that would be robust to these geometrical uncertainties. Our fourth and final objective was to design a shared control system that would support operators in the execution of a teleoperated contact task, even in the presence of severe **time delays** in the communication channel.

7.2. DISCUSSION

The goal of the dissertation was achieved by providing greater insight in how to systematically model and analyze haptic shared control systems employed in teleoperation. The presented work supports the development of haptic shared control systems that are more robust to realistic uncertainties in the operator, in the environment and the communication channels. All presented methods and principles were investigated and validated through experiments on real teleoperation hardware and, in several chapters, also by extensive human-in-the-loop evaluations.

7.2.1. SCALING OF THE GUIDANCE FORCES

Throughout the dissertation, the reaction of operators to the haptic guidance forces was found to be of great significance. The operator and the automatic system share control over the task on a common control interface. Consequently, the effects of the haptic forces applied on the master device strongly depend on the *neuromuscular setting* of the operator's limb holding the interface. To give a specific example, if the operator agrees with the provided haptic guidance, he/she can become more compliant and give way to the haptic forces. In contrast, if the operator disagrees, he/she can stiffen up to resist the haptic force, effectively overruling the automation. In this manner, the operator can dynamically interact with the automation during the operation [68]. Operators can achieve a broad range of neuromuscular admittance settings [43]. Some of these settings are of special significance and offer advantages, such as ensuring that the operator is always actively involved in the task execution, by designing the system to provide only relatively weak support [34].

Hence, **Chapter 2** focused on finding a systematic method to select an optimal scaling of the guidance forces (i.e., tuning of the haptic shared controller) based on the knowledge of the operator's neuromuscular system. The design goal was to minimize the required physical workload of the operator, by making the system function optimally when the operator limb is relaxed. To this end, a formal methodology to identify the relaxed neuromuscular admittance setting of an operator is presented, and a way of how to include this knowledge in the HSC system architecture was proposed and validated successfully in a human-in-the-loop experiment.

This experiment showed the feasibility and benefits of using neuromuscular-analysis-based tuning for haptic shared control systems. Results indicate that the tuning procedure produces tuning values that indeed reduce workload and also improve situation awareness compared to traditional haptic settings that ignore the neuromuscular system. In fact, it is shown that over-tuning (i.e., using a too strong guidance force scaling), which we think frequently occurs for heuristically-tuned systems, leads to even lower user acceptance scores than interfaces without any haptic support at all.

To put these findings into a broader perspective, we still found that a strong guidance force based on a correctly working automatic system provides the best task performance. However, such designs are often uncomfortable for operators, giving rise to conflicts, and resulting in lower user acceptance. This dissertation advocates that an NMS-based tuning constitutes a better trade-off between performance and user acceptance.

In the following, we will discuss how allowing the operator to adapt the guidance scaling during the task may help to reduce conflicts while still reaching high task performance offered by strong guidance scaling.

GOAL CONFLICTS AND OPERATOR ADAPTABLE HSC SYSTEM DESIGN

During task execution, the communication of goals between the operator and the automation is often implicit. For example, in HSC systems designed to support lane keeping while driving a car, the automatic system's goal might be to help the driver to follow the centerline of the road [37]. How would such a driver-car system react, if the automation sensor would suddenly malfunction and 'pick-up' a parallel lane? **Chapter 3** was related to addressing this possible disagreement between the operator and the haptic shared control system using a system-theoretical approach.

Moreover, the aim was also to provide a way for the operator to resolve the conflict and allow for a smooth shift of control authority over the HSC system. Scaling of guidance forces determines the level of control authority a support system assumes over a task. As described in the previous example, task complexity can change in reaction on external disturbances or internal conflicts between the support system and the human operator. As a consequence, one level of the guidance scaling might be insufficient, and adaptation of the control authority would be helpful.

To this end, an architecture based on the operator's grip force was proposed in this dissertation and validated in a human-in-loop study. In a simple tracking task, two opposite approaches to trade the control authority were explored: increasing versus decreasing guidance strength scaling for higher operator grip force. These conditions were compared with unassisted manual control and a fixed-gain haptic shared control assistance. At random moments during the experiment, task difficulty was deliberately increased through the addition of force disturbances. To investigate operator–guidance conflicts, at other times also an intentionally incorrect guidance reference was used. In both cases, the task of the operators was to mitigate the negative effects and continue tracking a visual reference.

It was found that both grip-adaptable approaches allowed the operators to increase their performance over manual control and the under-tuned guidance system. Contrary to using a system with one fixed 'optimal' setting (**Chapter 2**), operators were able to directly adapt the level of support in real time during the task to their benefit. At the same time, both grip-adaptable approaches helped the operators to substantially reduce the physical control effort required to cope with conflicts and disturbances with respect to a fixed-setting HSC.

It should be noted that each of the newly proposed grip-adaptable approaches mainly offers an advantage in one type of disturbance, i.e., based on our results, there is no clearly superior method and each is more suited to cope with a given situation.

Furthermore, predictions based on the formalized models of the system corresponded to results of the human-in-the-loop experiment. This finding supports the notion that (validated) formalizations can indeed be used to study HSC systems in the presence of goal-related conflicts and disturbances. Such formalized models can then be used, for example, in a model-based design workflow while designing complex HSC system in industrial practice.

7.2.2. GEOMETRICAL GOAL UNCERTAINTIES

Contact tasks are naturally constrained by the task environment. Haptic shared control systems base their provided support on the available model of the task at hand. However, in practice there are often inaccuracies in the task models. The effects of these inaccuracies were analyzed in **Chapter 4**. So far, only a few empirical studies investigated these inaccuracies using human-in-the-loop experiments [45, 146]. In this dissertation, a system-theoretical approach was used to investigate the effects of these inaccuracies on the teleoperation system itself. An innovative system description (extending the framework proposed Lawrence [14]) was used to quantify the consequences of inaccuracies on task safety and performance. Interaction of the natural force feedback (e.g.,

the feedback force based on the slave robot end-effector force sensor) with the haptic guidance force was analyzed.

It was found that this interaction can have a large effect on the teleoperation system performance. The presented theoretical analysis showed that if the teleoperation system implements only haptic guidance forces, and no form of natural force feedback, the system can become unstable in constrained contact tasks if the master device is not held in place by an operator. Implementing any common form of natural force feedback, for example by using the ‘position-position’ or ‘position-force’ architectures [14], stabilizes the system even without any contribution of the operator. However, the guidance force and the natural feedback force counteract each other, effectively masking the inaccuracy of the guidance from the operator. In other words, the slave robot can still exert significant forces on the environment, without the operator being able to haptically perceive it, which can potentially create an unsafe situation. This result also suggests that the ability of the operator to compensate for inaccuracies of the HSC system would be rather limited. The theoretical predictions corresponded very well with the measurements taken in a 6-DOF assembly task on a real master-slave teleoperation setup, bringing confidence in the proposed systematical modeling approach.

The practically unavoidable uncertainties in the knowledge of the remote environment model reduce task performance and increase operator workload [45]. **Chapter 5** outlined a method that would provide more robustness against the aforementioned geometrical goal uncertainties. The approach to achieve robustness to model inaccuracies lies in continuously updating the model of the environment to more closely match the real environment. The accuracy of the environment model is assessed internally by the HSC system against real-time force sensor measurements from the slave robot end-effector force sensor. This way, the geometrical inaccuracies of the environment model can be continuously minimized to provide correct support to the operator.

In parallel with this dissertation, we have investigated two different approaches that aimed to actively reduce geometrical goal uncertainties. First, a method was developed, coined *nested compliant admittance control* [147], to use the slave robot end-effector force/torque sensor measurements to change the commands of the operator directly and minimize the geometrical uncertainties in real-time. It was found to be very effective in reducing misalignments (both rotational and translational) in a peg-in-hole insertion task. However, this approach does not belong to the haptic shared control paradigm since it directly adjusts the commands of the operator to the controlled system (i.e., it does not act through a guidance force).

Second, a method based on *Learning from Demonstration* was developed to generate real-time guidance for a peg-in-hole insertion task [148]. Traditionally, HSC systems rely on a position reference that facilitates a specific task (e.g., an a priori known location of a hole). The novelty of the approach lies in using the momentary slave robot end-effector force/torque sensor measurements to generate haptic guidance forces that are applied to the master device. In this way, the contact forces are used directly, and there is no position reference involved (that could be affected by the geometrical goal uncertainty).

Both approaches were successfully validated in a 6-DOF peg-in-hole insertion task. However, the exact trade-offs of either adjusting the guidance position, or directly the operator position commands, or their combination, remains to be investigated.

7.2.3. ROBUSTNESS TO COMMUNICATION TIME DELAY

The negative effects of a time delay for bilateral teleoperation are twofold: 1) to ensure system stability, the achievable system performance needs to be limited (e.g., by selecting more conservative control gains or injecting additional damping [65, 66]); 2) the operator needs to anticipate the delayed slave reaction to prevent unintended interaction with the remote environment [1, 49]. Two principally similar systems providing robustness to delay in the communication channel (especially for long delays, 0.1-2 sec) were studied in **Chapters 5 and 6**.

The first approach, developed in **Chapter 5**, addressed both challenges mentioned above by following the concept of model-mediated teleoperation [40]. Instead of directly exchanging the commands and feedback between master and slave, a *model* of the remote environment is first created and then continuously updated on the master side. The force feedback information to the operator is based on this local model and is not delayed. The system is designed to ensure decoupling of the control loops in case of environment changes, which allows coping with severe and possibly even variable time-delays in the communication channel. Stability and performance of the complete teleoperation system were analyzed, and the system was shown to theoretically remain stable for arbitrarily large time delays. The presented method was demonstrated on an experimental master-slave setup in a teleoperation scenario, showing stability and reference rate and force tracking performance over 2 seconds of round-trip communication delay in bilateral control. In the case of easily deformable materials, the method was tested to still work, with a somewhat reduced feeling of realism, via continuous wall position updates.

A major factor limiting a wider adoption of the model-mediated teleoperation approach is the practical complexity of the environment model. In other words, it is rather straightforward to model an environment that consists of a simple plane (and generate force feedback based on this model). However, practical environments with more complex geometries are still considered to be beyond the capabilities of current model-mediated research systems [149]. In line with the majority of available literature [40, 149], the system in **Chapter 5** was only implemented in 1-Degree-Of-Freedom. Nevertheless, such a 1-DOF system still proved beneficial in aiding practical teleoperated tasks. In a flight demonstration experiment called *Interact* [54], conducted by the European Space Agency, the presented system was used to support a peg-in-hole insertion task over a geostationary satellite relay network with 850 ms of round-trip communication delay. The operator was able to safely interact with the remote environment and recognized and corrected the insertion when the peg became ‘jammed’.

The second approach, studied in **Chapter 6**, provided an attractive guidance HSC system. It builds on the concept of a *master-based* guidance, where the HSC system steers the master device (by an addition of a guidance force) such that the slave robot will consequently be commanded to the desired position. The master-based guidance was found to be a promising method to suppress the aforementioned negative effects associated with a delay in the communication channel. The master-based guidance method was experimentally verified with a real 6-DOF haptic teleoperation setup. On the used experimental setup, the master-based HSC was tested to be operational up to 2 s of de-

lay (theoretically there is no upper limit), whereas the slave-based HSC was impractical beyond 80 ms of delay.

Notably, the master-based attractive guidance HSC system was easily extended to 6-DOF. The reason for this difference is obvious from Figure 1.5. Whereas a 6-DOF mediated contact HSC would potentially need to model an environment with complex geometry, attractive guidance can facilitate its tasks using a simple, attractive field. Using as an example the HSC system developed to support a peg-in-hole insertion task in **Chapter 6**, the HSC was programmed by recording the position and orientation of the centerline of the hole in 6-DOF, needing just six parameters to sufficiently describe the task.

7.2.4. TOWARDS A UNIFYING SYSTEMATIC APPROACH

The overall goal of this dissertation was to formalize the analysis and design of haptic shared control systems applied in teleoperation. For this purpose, a novel system-theoretical framework to study *attractive guidance* HSC systems was developed. The extension of Lawrence's general teleoperation architecture [14] presented in **Chapter 4** (slave-based HSC) was further extended by an additional haptic shared controller channel, in **Chapter 6** (master-based HSC). The control diagram of the resulting systematic framework is shown in Figure 7.1 (for details see Section 6.2).

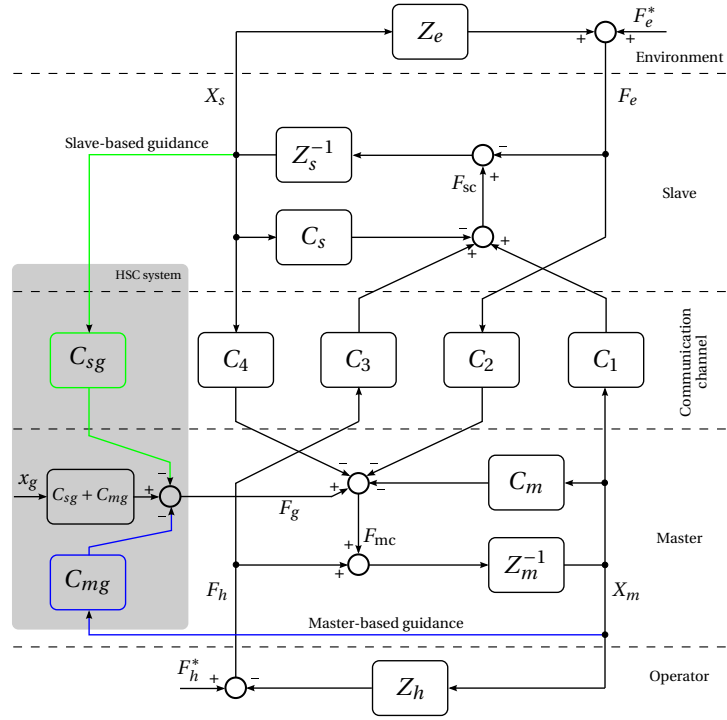


Figure 7.1: Systematic framework to study attractive guidance HSC systems applied in teleoperation (developed in Chapter 6).

In principle, the newly developed framework can be used to address the research

goals uniformly. Namely, it should allow to study the effects of operator's neuromuscular setting, **Chapter 2**, operator's authority in case of goal conflicts, **Chapter 3**, geometrical goal uncertainties, **Chapter 4**, and communication time-delays, **Chapter 5**, using one unified, systematic description. However, the respective chapters dealt with a range of very different systems, which would make such unified description very complex. For the reader's convenience, a summary of the different systems and HSC configurations studied in this dissertation is therefore provided in Table 7.1.

In spite of that, in the following text, we outline how the framework presented in **Chapter 6** can be further developed to accommodate all system configurations studied in **Chapters 2-5**.

Table 7.1: Overview of the HSC systems studied within this dissertation

Chapter	Architecture ¹	Commands	HSC type	HSC category
CH 2	PN	rate	slave	protected region
CH 3	PN	position	slave	attractive guidance ²
CH 4	PN, PP, and PF	position	slave	attractive guidance
CH 5	PN	rate	master ³	mediated contact
CH 6	PN, PP, PF, and 4CH	position	slave and master	attractive guidance

¹ Teleoperation architectures: 4-channel (4CH), position command - position feedback (PP), position command - force feedback (PF), and position command - no feedback (PN).

² Adaptable guidance stiffness gain based on operator's grip force.

³ Model-mediated teleoperation approach is here considered to be a special case of a master-based HSC.

Underlying teleoperation architecture:

The presented framework is already relatively general with respect to the underlying teleoperation architecture, as it builds on Lawrence's generalized, 4-channel, teleoperation architecture [14]. In its current state, it can be used to analyze all common teleoperation architectures, which are in principle a subset of the 4-channel architecture (4CH). By setting some of the controller gains C_i ($i = \{1, 2, 3, 4\}$) to zero, the other conventional teleoperation architectures can be modeled [15]. This dissertation focused on the *position command - position feedback* (PP) and *position command - force feedback* (PF) architectures. These two standard bilateral teleoperation architectures were complemented by a *position command - no feedback* (PN) architecture, where the haptic feedback provided to the operator is solely based on the HSC guidance force. This last architecture can be used to model tasks where there is, in principle, no need for the direct force feedback from the environment. For instance, such systems are used for collision avoidance for UAV teleoperation [87] (**Chapter 2**), lane keeping during car driving [37], or following a aircraft trajectory using a haptic flight director [38].

Type of commands:

Systems with *position* control commands, i.e., a configuration where the slave position is made to follow the position of the master, were the focus of **Chapters 3, 4, and 6**. This configuration is arguably the more common for teleoperation systems [15].

On the other hand, in **Chapters 2 and 5** systems using *rate* control commands, where the position of the master is interpreted as a velocity command to the slave, were inves-

tigated. Rate control allows to use master and slave devices with substantially different workspaces comfortably and is also instrumental in situations that require better-than-human slave movement precision [118, 150].

To allow analysis of both position and rate commands, the underlying teleoperation system controller gains C_i , with $i = \{1, 2, 3, 4\}$, that were given in Eq. (6.4), need to be modified. Following the approach described in [15], the new set of controllers is defined as (with s being the Laplace operator):

$$\begin{cases} C_1 = C_s / G \\ C_2 = G \\ C_3 = 1 / G \\ C_4 = -C_m G \end{cases}, \text{ where } G = \begin{cases} 1, & \text{for position commands} \\ s, & \text{for rate commands} \end{cases} \quad (7.1)$$

HSC type:

The two studied HSC implementations, namely the *slave-* and *master-based* HSC types, are directly treated as two separate controller paths of the systematic framework, where they are expressed as two components forming the guidance force: $F_g = F_{sg} + F_{mg}$. Notably, both HSC types can be either applied simultaneously in one system, or separately by setting the respective controller gains to zero (e.g., for slave-based HSC, we would set $C_{mg} = 0$).

Adaptable guidance stiffness gain: **Chapters 3** proposed a HSC system that allows the operators to adapt the guidance controller gain during the task execution, by changing how strongly they hold the master device, i.e., the HSC controller gain was adapted based on the change of operator grip force Eq. (3.8). Also other HSC systems described in the literature adapted the guidance controller on-line, for example based on: momentary task performance [98], criticality [80, 95], level of (dis-)agreement between guidance and operator [98–100], actively recognizing the control model [101, 102] or intended goal of the operator [103, 104].

These adaptable systems can be introduced into the current framework by modifying the fixed-gain HSC controllers $C_{s/mg}$ to become functions of some external input u_{ext} , as $C_{s/mg}(u_{\text{ext}})$. In **Chapters 3**, the momentary gripping force applied by the operator on the master device was utilized as this external input signal: $u_{\text{ext}} = F_{\text{grip}}(t)$.

HSC category:

In the individual dissertation chapters, haptic shared control (automation acting through the guidance force F_g) was used to facilitate conceptually very different tasks, see Figure 7.2. In **Chapters 3, 4, and 6** an *attractive guidance* was supporting the slave to follow a prescribed reference. On the other hand, in **Chapter 2**, the repulsive force created a *protected region* around obstacles where the controlled UAV was not allowed to enter. Later and with a different purpose, in **Chapter 5**, the repulsive force was positioned on the very edge of the remote environment, essentially providing a *mediated contact*, as an alternative for a regular force feedback.

The systematic framework presented in **Chapter 6** was created for analyzing attractive guidance HSC systems, see Figure 7.2(a). The guidance force is simply proportional by the gain K_g to the distance of the slave robot x_s from the the guidance reference x_g . To

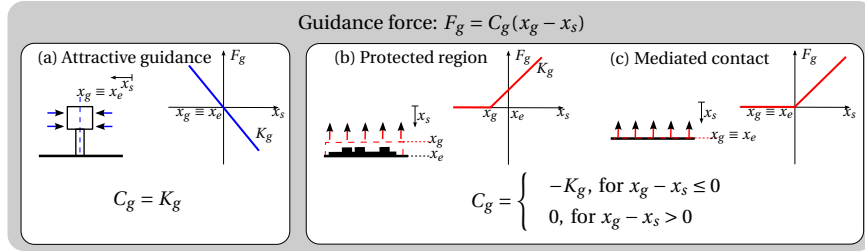


Figure 7.2: HSC facilitating three conceptually different tasks. The guidance force F_g is calculated based on the slave robot position x_s with respect to the guidance reference x_g (for the slave-based guidance type). For further details on the HSC tasks see Section 1.1.3.

accommodate also for the repulsive guidance (i.e., protected region, Figure 7.2(b), and mediated contact, Figure 7.2(c)) the guidance controllers $C_{s/mg}$, in Figure 7.1 need to be modified. If the slave robot is located outside the guidance field, $F_g = 0$. Within the field, the repulsive force (hence the minus sign) is $F_g = -K_g(x_g - x_s)$.

Such modified system is, alas, no longer linear, a property which needs to be taken into account for further analysis. In **Chapter 5**, the non-linearity was studied using traditional linear analysis tools as two separate cases (i.e., outside and inside of the field).

Model-mediated teleoperation approach as an HSC system:

The model-mediated teleoperation approach, investigated in **Chapter 5**, is in this dissertation considered as a special case of a master-based HSC. The task of such an HSC system is to provide virtual force feedback to the operator, using forces based on a pre-programmed model (i.e., instead of natural feedback forces). The virtual force field is made to coincide with the environment, Figure 7.2(c), essentially mediating the contact through this model.

A conceptual extension of the systematic framework to allow for an analysis of a model-mediated system is shown in Figure 7.3. In principle, the guidance reference X_g^* is continuously adjusted by the ‘Wall detector’ block to match the slave robot position X_s once it contacts a remote environment (by measuring the contact force F_e).

The behavior of such a system depends on its current situation during a teleoperated task. To give a specific example, the system will behave differently when the slave robot is in free air than when the slave establishes a contact with the remote environment. These different situations need to be accommodated by the analytical method. An approach to analyze these two situations separately as specific operation modes is discussed in **Chapter 5**.

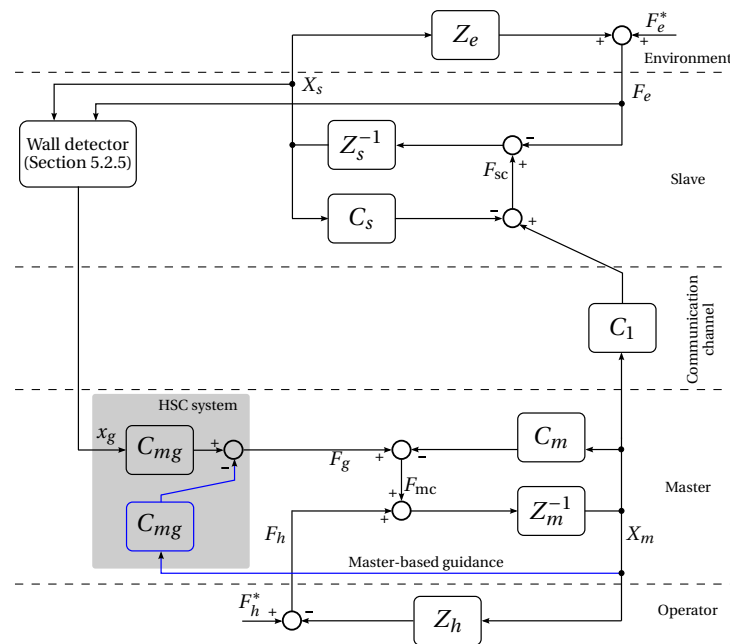


Figure 7.3: Systematic framework (Chapter 6) modified to accommodate the model-mediated teleoperation approach (Chapter 5).

7.3. CONCLUSIONS

In this dissertation, experimentally-verified systematic methodologies have been developed to study haptic shared control systems applied in teleoperation.

The main conclusions are:

Neuromuscular system uncertainty

- (1) Haptic shared control systems should not be tuned based on performance metrics alone. A strong tuning setting, that would yield the highest system performance, is often the least accepted by operators, invoking the highest workload (Chapter 2).
- (2) The approach of tuning the strength of the haptic feedback on the basis of the ‘relax task’ setting of the neuromuscular system, led to tuning settings that were appreciated by the operators, and maintained satisfactory task performance, with both physical and mental workload reduction (Chapter 2).
- (3) The optimal tuning setting of an HSC system with a human-in-the-loop is not crisp and clear. A wide range of controller tunings led to comparable behaviors in the tested conditions (Chapter 2).

Goal conflicts

- (4) Haptic guidance is the most effective when the visual feedback provided to the operators is limited; moreover, operators then tend to agree more with the guidance.

In contrast, haptic guidance applied in situations when the operator has a good visual feedback of task was more prone to conflicts and was more often opposed by operators (Chapter 2).

- (5) Goal-related conflicts and task-difficulty-altering disturbances of an HSC can be systematically modeled. Predictions based on these models match the behavior observed in human-in-the-loop experiments well (Chapter 3).
- (6) An operator grip force-based, adaptable-authority haptic shared controller can increase task performance over an ‘under-tuned’ fixed-authority guidance system. Moreover, the effort of the operator necessary to overcome an incorrect guidance can be significantly reduced with respect to the fixed-authority systems (Chapter 3).

Geometrical goal uncertainties

- (7) If an *attractive* haptic guidance system is supporting a contact task, some form of natural feedback (e.g., the measured force at slave end-effector) should be included to ensure system stability (Chapter 4).
- (8) The HSC system guidance forces and the natural feedback forces interact with each other in a nontrivial way, effectively masking potential inaccuracies of the guidance system from the operator, which can be unsafe (Chapter 4).

Time delays

- (9) Using a model-mediated approach to interact with the remote environment theoretically ensures teleoperation system stability for any practical value of the communication time delay (Chapter 5).

Systematic framework

- (10) The presented systematic framework can indeed be used to make accurate predictions about the performance of the studied teleoperator systems with the addition of haptic guidance, as the predictions were confirmed by both numerical simulations and experimental trials (Chapter 6).

7.4. RECOMMENDATIONS

Based on the results presented in this dissertation, the following recommendations can be made for future research:

EXTENSION TOWARDS A GENERAL SHARED CONTROL FRAMEWORK

In this dissertation, we concentrated on *haptic* shared control, i.e., on systems where the automation is acting solely through guidance forces added to the master device. However, another approach described in the literature is to let the automation directly alter the inputs to the controlled system. This approach to sharing control is sometimes referred to as the input-mixing shared control [34], in which the inputs to the controlled system are calculated as a weighted average of the inputs of the operator and the automation. Extending the currently presented methods towards such an even more general shared control framework remains as a future step.

APPLICABILITY OF PRESENTED FINDINGS IN REAL-LIFE TASKS

The set of tasks considered in this dissertation was mostly constrained to controlled, laboratory-based environments. We studied different aspects of HSC using relatively abstract tasks, such as the peg-in-hole insertion (Chapters 5 and 6) or signal tracking tasks (Chapters 2). We studied these abstract tasks with the hope that our findings would extend to a wider variety of real-life tasks (e.g., connector mating, car steering). In future research, the applicability of the presented methods should therefore also be investigated in these non-ideal, more realistic and uncertain conditions.

APPLY THE PRESENTED FINDINGS IN THE DESIGN STAGE

The aim of the dissertation was to develop analytic methods to provide a better understanding of haptic shared control systems employed in bilateral teleoperation. A logical next step would be to move from the systematic analysis towards ‘systematic design’, i.e., to apply the insights obtained using the presented methods directly into the design stage, and systemically tune the haptic shared controllers.

STUDY HSC ON THE FRINGE OF THEIR DESIGN SCOPE

As a next step, haptic shared control systems should be studied on the fringe of their design scope, operating in non-ideal situations. This dissertation already provided methods to analyze HSC systems that were intentionally brought into a goal conflict with the operator, or that were programmed to operate with a geometrically inaccurate task model. Future research efforts should be directed towards more complex, yet preferably still generalizable, potential failure modes of HSC systems.

BIBLIOGRAPHY

- [1] T. B. Sheridan, *Telerobotics, Automation, and Human Supervisory Control*. Cambridge: MIT Press, Aug. 1992.
- [2] E. A. a. E. Guizzo, "DARPA Robotics Challenge: Amazing Moments, Lessons Learned, and What's Next," Jun. 2015. [Online]. Available: <http://spectrum.ieee.org/automaton/robotics/humanoids/darpa-robotics-challenge-amazing-moments-lessons-learned-whats-next>
- [3] G. A. V. Christiansson, *Hard master, soft slave haptic teleoperation*. TU Delft: PhD dissertation, 2007.
- [4] M. J. Massimino and T. B. Sheridan, "Teleoperator Performance with Varying Force and Visual Feedback," *Human Factors: The Journal of the Human Factors and Ergonomics Society*, vol. 36, no. 1, pp. 145–157, Mar. 1994.
- [5] E. Samur, *Performance Metrics for Haptic Interfaces*, ser. Springer Series on Touch and Haptic Systems. London: Springer London, 2012.
- [6] A. Schiele, "Performance difference of Bowden Cable relocated and non-relocated master actuators in virtual environment applications," in *Intelligent Robots and Systems, 2008. IROS 2008. IEEE/RSJ International Conference on*, 2008, pp. 3507–3512.
- [7] N. Chopra, P. Berestesky, and M. Spong, "Bilateral Teleoperation Over Unreliable Communication Networks," *IEEE Transactions on Control Systems Technology*, vol. 16, no. 2, pp. 304–313, Mar. 2008.
- [8] A. Schiele, T. Kruger, S. Kimmer, M. Aiple, J. Rebelo, J. Smisek, E. den Exter, E. Matheson, A. Hernandez, and F. van der Hulst, "Haptics-2 - A system for bilateral control experiments from space to ground via geosynchronous satellites," in *IEEE International Conference on Systems, Man, and Cybernetics*, Budapest, Oct. 2016.
- [9] A. M. Okamura, "Haptic feedback in robot-assisted minimally invasive surgery:," *Current Opinion in Urology*, vol. 19, no. 1, pp. 102–107, Jan. 2009.
- [10] K. Kruckel, F. Nolden, A. Ferrein, and I. Scholl, "Intuitive visual teleoperation for UGVs using free-look augmented reality displays," in *Robotics and Automation (ICRA), 2015 IEEE International Conference on*. IEEE, 2015, pp. 4412–4417.
- [11] L. Fritsche, F. Unverzag, J. Peters, and R. Calandra, "First-person tele-operation of a humanoid robot," in *Humanoid Robots (Humanoids), 2015 IEEE-RAS 15th International Conference on*. IEEE, 2015, pp. 997–1002.

- [12] R. C. Goertz, "Fundamentals of General-Purpose Remote Manipulators," *Nuclearonics (U.S.) Ceased publication*, vol. Vol: 10, No. 11, Nov. 1952.
- [13] C. Passenberg, A. Peer, and M. Buss, "A survey of environment-, operator-, and task-adapted controllers for teleoperation systems," *Mechatronics*, vol. 20, no. 7, pp. 787–801, Oct. 2010.
- [14] D. Lawrence, "Stability and transparency in bilateral teleoperation," *IEEE Transactions on Robotics and Automation*, vol. 9, no. 5, pp. 624–637, 1993.
- [15] S. E. Salcudean, M. Zhu, W.-H. Zhu, and K. Hashtrudi-Zaad, "Transparent bilateral teleoperation under position and rate control," *The International Journal of Robotics Research*, vol. 19, no. 12, pp. 1185–1202, 2000.
- [16] K. Hashtrudi-Zaad and S. E. Salcudean, "Transparency in time-delayed systems and the effect of local force feedback for transparent teleoperation," *Robotics and Automation, IEEE Transactions on*, vol. 18, no. 1, pp. 108–114, 2002.
- [17] —, "Analysis of control architectures for teleoperation systems with impedance/admittance master and slave manipulators," *The International Journal of Robotics Research*, vol. 20, no. 6, pp. 419–445, 2001.
- [18] B. Hannaford and J.-H. Ryu, "Time-domain passivity control of haptic interfaces," *IEEE Transactions on Robotics and Automation*, vol. 18, no. 1, pp. 1–10, 2002.
- [19] G. Niemeyer and J.-J. Slotine, "Stable adaptive teleoperation," *IEEE Journal of Oceanic Engineering*, vol. 16, no. 1, pp. 152–162, 1991.
- [20] J. G. Wildenbeest, D. A. Abbink, C. J. Heemskerk, F. C. T. van der Helm, and H. Boessenkool, "The Impact of Haptic Feedback Quality on the Performance of Teleoperated Assembly Tasks," *IEEE Transactions on Haptics*, vol. 6, no. 2, pp. 242–252, Apr. 2013.
- [21] G. Christiansson, R. Q. van der Linde, and F. C. T. van der Helm, "The Influence of Teleoperator Stiffness and Damping on Object Discrimination," *IEEE Transactions on Robotics*, vol. 24, no. 5, pp. 1252–1256, Oct. 2008.
- [22] H. Boessenkool, D. A. Abbink, C. J. Heemskerk, F. C. T. van der Helm, and J. G. Wildenbeest, "A Task-Specific Analysis of the Benefit of Haptic Shared Control During Telemanipulation," *IEEE Transactions on Haptics*, vol. 6, no. 1, pp. 2–12, 2013.
- [23] M. K. O'Malley, A. Gupta, M. Gen, and Y. Li, "Shared Control in Haptic Systems for Performance Enhancement and Training," *Journal of Dynamic Systems, Measurement, and Control*, vol. 128, no. 1, p. 75, 2006.
- [24] L. B. Rosenberg, "Virtual fixtures: Perceptual tools for telerobotic manipulation," in *Virtual Reality Annual International Symposium, 1993., 1993 IEEE*. IEEE, 1993, pp. 76–82.

- [25] F. Flemisch, J. Kelsch, C. Löper, A. Schieben, and J. Schindler, "Automation spectrum, inner/outer compatibility and other potentially useful human factors concepts for assistance and automation," *2008, Human Factors for assistance and automation*, pp. 1–16, 2008.
- [26] L. Bainbridge, "Ironies of automation," *Automatica*, vol. 19, no. 6, pp. 775–779, 1983.
- [27] T. M. Lam, "Haptic interface for UAV Teleoperation," Ph.D. dissertation, Delft University of Technology, 2009.
- [28] T. M. Lam, M. Mulder, M. M. van Paassen, and F. C. T. van der Helm, "Teleoperating a UAV using Haptics - Modeling the Neuromuscular System," in *Proceedings IEEE Systems, Man and Cybernetics Society*, Hawaii, Oct. 2005, pp. 2695–2700.
- [29] A. Franchi, C. Secchi, M. Ryll, H. H. Bühlhoff, and P. Giordano, "Shared Control: Balancing Autonomy and Human Assistance with a Group of Quadrotor UAVs," *IEEE Robotics & Automation Magazine*, vol. 19, no. 3, pp. 57–68, Sep. 2012.
- [30] A. M. Brandt and M. B. Colton, "Haptic collision avoidance for a remotely operated quadrotor uav in indoor environments," in *IEEE International Conference on Systems Man and Cybernetics*, Istanbul, 2010, pp. 2724–2731.
- [31] H. I. Son, J. Kim, L. Chuang, A. Franchi, P. Giordano, D. Lee, and H. H. Bühlhoff, "An evaluation of haptic cues on the tele-operator's perceptual awareness of multiple UAVs' environments," in *IEEE World Haptics Conference*, Istanbul, 2011, pp. 149–154.
- [32] M. Mulder, D. Abbink, M. Van Paassen, and M. Mulder, "Design of a Haptic Gas Pedal for Active Car-Following Support," *IEEE Transactions on Intelligent Transportation Systems*, vol. 12, no. 1, pp. 268–279, 2011.
- [33] M. M. T. M. Lam, "Haptic interface in UAV tele-operation using force-stiffness feedback," pp. 835 – 840, 2009.
- [34] D. A. Abbink and M. Mulder, "Exploring the Dimensions of Haptic Feedback Support in Manual Control," *Journal of Computing and Information Science in Engineering*, vol. 9, no. 1, pp. 11 006–11 015, 2009.
- [35] R. Parasuraman and V. Riley, "Humans and Automation: Use, Misuse, Disuse, Abuse," *Human Factors: The Journal of the Human Factors and Ergonomics Society*, vol. 39, no. 2, pp. 230–253, Jun. 1997.
- [36] D. A. Abbink, M. Mulder, and E. R. Boer, "Haptic shared control: smoothly shifting control authority?" *Cognition, Technology & Work*, vol. 14, no. 1, pp. 19–28, 2012.
- [37] M. Mulder, D. A. Abbink, and E. R. Boer, "Sharing Control With Haptics: Seamless Driver Support From Manual to Automatic Control," *Human Factors: The Journal of the Human Factors and Ergonomics Society*, vol. 54, no. 5, pp. 786–798, Oct. 2012.

- [38] S. de Stigter, M. Mulder, and M. M. Van Paassen, "Design and Evaluation of a Haptic Flight Director," *Journal of Guidance, Navigation and Control*, vol. 30, no. 1, pp. 35–46, Jan. 2007.
- [39] B. H. Krogh, "A generalized potential field approach to obstacle avoidance control," Society of Manufacturing Engineers, Tech. Rep., 1984.
- [40] P. Mitra and G. Niemeyer, "Model-mediated Telemanipulation," *The International Journal of Robotics Research*, vol. 27, no. 2, pp. 253–262, Feb. 2008.
- [41] B. Willaert, D. Reynaerts, E. B. Vander Poorten, H. Van Brussel, and P. Goethals, *Transparent and shaped stiffness reflection for telesurgery*, ser. Advances in Haptics. INTECH Open Access Publisher, 2010.
- [42] P. Griffiths and R. Gillespie, "Shared control between human and machine: haptic display of automation during manual control of vehicle heading," in *12th International Symposium on Haptic Interfaces for Virtual Environment and Teleoperator Systems, 2004. HAPTICS '04. Proceedings*, Mar. 2004, pp. 358 – 366.
- [43] E. De Vlugt, "Identification of Spinal Reflexes," Ph.D. dissertation, Delft University of Technology, Delft, 2004.
- [44] J. Smisek, W. Mugge, J. B. J. Smeets, M. M. van Paassen, and A. Schiele, "Adapting haptic guidance authority based on user grip," in *IEEE International Conference on Systems, Man and Cybernetics (SMC)*, San Diego, 2014, pp. 1516–1521.
- [45] J. van Oosterhout, J. G. W. Wildenbeest, H. Boessenkool, C. J. M. Heemskerk, M. R. de Baar, F. C. T. Van Der Helm, and D. A. Abbink, "Haptic Shared Control in Tele-Manipulation: Effects of Inaccuracies in Guidance on Task Execution," *IEEE Transactions on Haptics*, vol. 8, no. 2, pp. 164–175, Apr. 2015.
- [46] J. Smisek, M. M. van Paassen, and A. Schiele, "Haptic guidance in bilateral teleoperation: Effects of guidance inaccuracy," in *IEEE World Haptics Conference*, Evanston, 2015, pp. 500–505.
- [47] R. Goyal, S. Kota, R. Jain, S. Fahmy, B. Vandalore, and J. Kallaus, "Analysis and simulation of delay and buffer requirements of satellite-atm networks for tcp/ip traffic," 1998. [Online]. Available: <http://arxiv.org/abs/cs/9809052>
- [48] J. Marescaux, J. Leroy, F. Rubino, M. Smith, M. Vix, M. Simone, and D. Mutter, "Transcontinental robot-assisted remote telesurgery: feasibility and potential applications," *Annals of surgery*, vol. 235, no. 4, pp. 487–492, 2002.
- [49] W. R. Ferrell, "Delayed force feedback," *Human Factors: The Journal of the Human Factors and Ergonomics Society*, vol. 8, no. 5, pp. 449–455, 1966.
- [50] D. A. Abbink, D. Cleij, M. Mulder, and M. M. van Paassen, "The importance of including knowledge of neuromuscular behaviour in haptic shared control," in *Systems, Man, and Cybernetics (SMC), 2012 IEEE International Conference on*. IEEE, 2012, pp. 3350–3355.

- [51] D. A. Abbink and M. Mulder, "Neuromuscular analysis as a guideline in designing shared control," *Advances in haptics*, vol. 109, pp. 499–516, 2010.
- [52] E. Sunil, J. Smisek, M. M. van Paassen, and M. Mulder, "Validation of a tuning method for haptic shared control using neuromuscular system analysis," in *IEEE International Conference on Systems, Man and Cybernetics*, San Diego, 2014, pp. 1499–1504.
- [53] J. Smisek, M. M. van Paassen, M. Mulder, and D. A. Abbink, "Neuromuscular Analysis based Tuning of Haptic Shared Control Assistant for UAV Collision Avoidance," in *IEEE World Haptics Confrence*, Daejeon, 2013, pp. 389–394.
- [54] A. Schiele, "ESA Telerobotics - Telerobotics, Haptics & Human-Robot Interfaces." [Online]. Available: <http://www.esa-telerobotics.net/>
- [55] S. Kimmer, J. Smisek, and A. Schiele, "Effects of Haptic Guidance and Force Feedback on Mental Rotation Abilities in a 6-DOF Teleoperated Task," in *IEEE International Conference on Systems, Man, and Cybernetics*, Kowloon, 2015, pp. 3092–3097.
- [56] N. Y. Lii, Z. Chen, B. Pleintinger, C. H. Borst, G. Hirzinger, and A. Schiele, "Toward understanding the effects of visual- and force-feedback on robotic hand grasping performance for space teleoperation," in *2010 IEEE/RSJ International Conference on Intelligent Robots and Systems (IROS)*, Oct. 2010, pp. 3745–3752.
- [57] J. Rasmussen, "Skills, rules, and knowledge; signals, signs, and symbols, and other distinctions in human performance models," *IEEE Transactions on Systems, Man, and Cybernetics*, vol. SMC-13, no. 3, pp. 257–266, May 1983.
- [58] M. M. Van Paassen, R. P. Boink, D. A. Abbink, M. Mulder, and M. Mulder, "Haptic Guidance, Interaction between the Guidance Model and Tuning," in *18th International Symposium on Aviation Psychology*, Dayton, May 2015, pp. 410 – 415.
- [59] A. de Jonge, J. Wildenbeest, H. Boessenkool, and D. Abbink, "The Effect of Trial-by-trial Adaptation on Conflicts in Haptic Shared Control for Free-Air Teleoperation Tasks," *IEEE Transactions on Haptics*, pp. 1–1, 2015.
- [60] R. J. Adams, D. Klowden, and B. Hannaford, "Virtual training for a manual assembly task," *Haptics-e*, vol. 2, no. 2, pp. 1–7, 2001.
- [61] S. Payandeh and Z. Stanisic, "On application of virtual fixtures as an aid for telemanipulation and training," in *Haptic Interfaces for Virtual Environment and Teleoperator Systems, 2002. HAPTICS 2002. Proceedings. 10th Symposium on*, 2002, pp. 18–23.
- [62] H. Nishino, K. Murayama, T. Kagawa, and K. Utsumiya, "A Japanese Calligraphy Trainer Based on Skill Acquisition Through Haptization," in *Advanced Information Networking and Applications (AINA), 2010 24th IEEE International Conference on*. IEEE, 2010, pp. 1225–1232.

- [63] T. Gibo and D. A. Abbink, "Movement Strategy Discovery During Training via Haptic Guidance," *IEEE Transactions on Haptics*, vol. 9, no. 2, pp. 243 – 254, 2016.
- [64] X. Xu, B. Cizmeci, A. Al-Nuaimi, and E. Steinbach, "Point Cloud-Based Model-Mediated Teleoperation With Dynamic and Perception-Based Model Updating," *IEEE Transactions on Instrumentation and Measurement*, vol. 63, no. 11, pp. 2558–2569, Nov. 2014.
- [65] J. L. Pinto Rebelo, "Robust and Transparent Multi-Degree-of-Freedom Bilateral Teleoperation with Time-Delay," Ph.D. dissertation, TU Delft, 2015.
- [66] D. J. F. Heck, "Delayed bilateral teleoperation : a direct force-reflecting control approach," Ph.D. dissertation, TU Eindhoven, 2015.
- [67] P. G. Griffiths and R. B. Gillespie, "Sharing Control Between Humans and Automation Using Haptic Interface: primary and secondary task performance benefits," *Human Factors: The Journal of the Human Factors and Ergonomics Society*, vol. 47, no. 3, pp. 574–590, 2005.
- [68] D. A. Abbink, M. Mulder, and E. R. Boer, "Haptic shared control: smoothly shifting control authority?" *Cognition, Technology & Work*, vol. 14, no. 1, pp. 19–28, 2012.
- [69] G. Baxter, J. Rooksby, Y. Wang, and A. Khajeh-Hosseini, "The ironies of automation: still going strong at 30?" in *Proceedings of the 30th European Conference on Cognitive Ergonomics*, Edinburgh, 2012, pp. 65–71.
- [70] M. Olivari, F. M. Nieuwenhuizen, H. H. Bülthoff, and L. Pollini, "Pilot Adaptation to Different Classes of Haptic Aids in Tracking Tasks," *Journal of Guidance, Control, and Dynamics*, vol. 37, no. 6, pp. 1741–1753, Nov. 2014.
- [71] D. A. Abbink, M. Mulder, F. C. T. van der Helm, M. Mulder, and E. R. Boer, "Measuring Neuromuscular Control Dynamics During Car Following With Continuous Haptic Feedback," *IEEE Transactions on Systems, Man, and Cybernetics, Part B: Cybernetics*, vol. 41, no. 5, pp. 1239 –1249, Oct. 2011.
- [72] P. W. Merlin, *Crash Course: Lessons Learned from Accidents Involving Remotely Piloted and Autonomous Aircraft*, ser. NASA Aeronautics Book Series. National Aeronautics and Space Administration, 2013.
- [73] S. M. Alaimo, L. Pollini, M. Innocenti, J. P. Bresciani, and H. H. Bülthoff, "Experimental comparison of direct and indirect haptic aids in support of obstacle avoidance for remotely piloted vehicles," *Journal of Mechanics Engineering and Automation*, vol. 2, pp. 2159–5275, 2012.
- [74] T. M. Lam, M. Mulder, and M. M. van Paassen, "Haptic Interface For UAV Collision Avoidance," *The International Journal of Aviation Psychology*, vol. 17, no. 2, pp. 167–195, 2007.

- [75] T. M. Lam, H. W. Boschloo, M. Mulder, and M. M. van Paassen, "Artificial Force Field for Haptic Feedback in UAV Teleoperation," *IEEE Transactions on Systems, Man and Cybernetics, Part A: Systems and Humans*, vol. 39, no. 6, pp. 1316–1330, 2009.
- [76] D. A. Abbink and M. Mulder, "Neuromuscular analysis as a guideline in designing shared control," *Advances in haptics*, vol. 109, pp. 499–516, 2010.
- [77] E. Sunil, "Tuning of a haptic collision avoidance system for UAV teleoperation," MSc thesis, Delft University of Technology, Tech. Rep., Aug. 2013.
- [78] D. A. Abbink, "Neuromuscular Analysis of Haptic Gas Pedal Feedback during Car Following," PhD thesis, Delft University of Technology, Delft, 2006.
- [79] W. Mugge, D. A. Abbink, A. C. Schouten, J. P. A. Dewald, and F. C. T. van der Helm, "A rigorous model of reflex function indicates that position and force feedback are flexibly tuned to position and force tasks," *Experimental Brain Research*, vol. 200, no. 3-4, pp. 325–340, Jan. 2010.
- [80] M. D. Penna, M. M. van Paassen, D. A. Abbink, M. Mulder, and M. Mulder, "Reducing steering wheel stiffness is beneficial in supporting evasive maneuvers," in *IEEE International Conference on Systems Man and Cybernetics*, Istanbul, 2010, pp. 1628–1635.
- [81] T. Tsuji, P. G. Morasso, K. Goto, and K. Ito, "Human hand impedance characteristics during maintained posture," *Biological Cybernetics*, vol. 72, no. 6, pp. 475–485, 1995.
- [82] W. Mugge, D. A. Abbink, and F. C. T. van der Helm, "Reduced power method: how to evoke low-bandwidth behaviour while estimating full-bandwidth dynamics," in *International Conference on Rehabilitation Robotics*, Noordwijk, 2007, pp. 575–581.
- [83] A. C. Schouten, E. de Vlugt, and F. C. T. van der Helm, "Design of Perturbation Signals for the Estimation of Proprioceptive Reflexes," *IEEE Transactions on Biomedical Engineering*, vol. 55, no. 5, pp. 1612–1619, May 2008.
- [84] J. S. Bendat and A. G. Piersol, *Random data: analysis and measurement procedures*, 2nd ed. New York: Wiley, 1986.
- [85] F. C. T. van der Helm, A. C. Schouten, E. De Vlugt, and G. G. Brown, "Identification of intrinsic and reflexive components of human arm dynamics during postural control," *Journal of Neuroscience Methods*, vol. 119, no. 1, pp. 1–14, 2002.
- [86] E. J. Perreault, R. F. Kirsch, and P. E. Crago, "Effects of voluntary force generation on the elastic components of endpoint stiffness," *Experimental Brain Research*, vol. 141, no. 3, pp. 312–323, 2001.

- [87] J. Smisek, E. Sunil, M. M. V. Paassen, D. A. Abbink, and M. Mulder, "Human operator limb neuromuscular admittance identified on a spring-centered control interface," [Dataset], DOI: 10.4121/uuid:cb7ddb1c-0bda-4434-a0b6-e8a31a071ac7, TU Delft, 2016.
- [88] J. Lasschuit, T. Lam, M. Mulder, M. M. van Paassen, and D. A. Abbink, "Measuring and Modeling Neuromuscular System Dynamics for Haptic Interface Design," in *AIAA Modeling and Simulation Technologies Conference*, Honolulu, 2008.
- [89] S. G. Hart and L. E. Staveland, "Development of NASA-TLX (Task Load Index): Results of Empirical and Theoretical Research," *Human Mental Workload*, vol. 1, no. 3, pp. 139–183, 1988.
- [90] E. Jeannot, C. Kelly, and D. Thompson, *The development of situation awareness measures in ATM systems*. Brussels: Eurocontrol, 2003.
- [91] A. Field, *Discovering Statistics using IBM SPSS Statistics*. London: Sage, 2013.
- [92] P. Marayong, A. Bettini, and A. M. Okamura, "Effect of virtual fixture compliance on human-machine cooperative manipulation," in *Intelligent Robots and Systems, 2002. IEEE/RSJ International Conference on*, vol. 2, 2002, pp. 1089–1095.
- [93] P. Marayong and A. M. Okamura, "Speed-Accuracy Characteristics of Human-Machine Cooperative Manipulation Using Virtual Fixtures With Variable Admittance," *Human Factors: The Journal of the Human Factors and Ergonomics Society*, vol. 46, no. 3, pp. 518–532, 2004.
- [94] F. Mars, M. Deroo, and C. Charron, "Driver adaptation to haptic shared control of the steering wheel," in *Systems, Man and Cybernetics (SMC), 2014 IEEE International Conference on*. IEEE, 2014, pp. 1505–1509.
- [95] D. A. Abbink, M. Mulder, and E. R. Boer, "Haptic shared control: smoothly shifting control authority?" *Cognition, Technology & Work*, vol. 14, no. 1, pp. 19–28, Nov. 2011.
- [96] J. C. de Winter and D. Dodou, "Preparing drivers for dangerous situations: A critical reflection on continuous shared control," in *Systems, Man, and Cybernetics (SMC), 2011 IEEE International Conference on*. IEEE, 2011, pp. 1050–1056.
- [97] D. W. v. d. Wiel, M. M. van Paassen, M. Mulder, M. Mulder, and D. A. Abbink, "Driver Adaptation to Driving Speed and Road Width: Exploring Parameters for Designing Adaptive Haptic Shared Control." IEEE, Oct. 2015, pp. 3060–3065.
- [98] C. Passenberg, A. Glaser, and A. Peer, "Exploring the Design Space of Haptic Assistants: the Assistance Policy Module," *IEEE Transactions on Haptics*, pp. 1–1, 2013.
- [99] C. Passenberg, N. Stefanov, A. Peer, and M. Buss, "Enhancing task classification in human-machine collaborative teleoperation systems by real-time evaluation of an agreement criterion," in *World Haptics Conference (WHC), 2011 IEEE*, 2011, pp. 493–498.

- [100] C. Passenberg, R. Groten, A. Peer, and M. Buss, "Towards real-time haptic assistance adaptation optimizing task performance and human effort," in *2011 IEEE World Haptics Conference (WHC)*, Jun. 2011, pp. 155–160.
- [101] H. U. Yoon, "Assistive HRI interface with perceptual feedback control: an approach to customizing assistance based on user dexterity," Ph.D. dissertation, University of Illinois at Urbana-Champaign, 2014.
- [102] Y. Tanaka, N. Yamada, T. Tsuji, and T. Suetomi, "Vehicle Active Steering Control System Based on Human Mechanical Impedance Properties of the Arms," *IEEE Transactions on Intelligent Transportation Systems*, vol. 15, no. 4, pp. 1758–1769, Aug. 2014.
- [103] D. Aarno, S. Ekvall, and D. Kragić, "Adaptive virtual fixtures for machine-assisted teleoperation tasks," in *Robotics and Automation, 2005. ICRA 2005. Proceedings of the 2005 IEEE International Conference on*. IEEE, 2005, pp. 1139–1144.
- [104] S. Ekvall, D. Aarno, and D. Kragic, "Online task recognition and real-time adaptive assistance for computer-aided machine control," *IEEE Transactions on Robotics*, vol. 22, no. 5, pp. 1029–1033, Oct. 2006.
- [105] D. A. Abbink, "Task Instruction: the largest Influence on Human Operator Motion Control Dynamics," in *IEEE EuroHaptics Conference*, 2007, pp. 206–211.
- [106] H. Nakamura, D. Abbink, and M. Mulder, "Is grip strength related to neuromuscular admittance during steering wheel control?" in *Systems, Man, and Cybernetics (SMC), 2011 IEEE International Conference on*, 2011, pp. 1658–1663.
- [107] A. Tran, D. Liu, R. Ranasinghe, M. Carmichael, and C. Liu, "Analysis of Human Grip Strength in Physical Human Robot Interaction," *Procedia Manufacturing*, vol. 3, pp. 1442–1449, 2015.
- [108] M. C. Baltzer, D. López, M. Kienle, and F. Flemisch, "Dynamic distribution of control via grip force sensitive devices in cooperative guidance and control," in *11. Berliner Werkstatt Mensch-Maschine-Systeme Conference*, Berlin, 2015.
- [109] K. K. Tsoi, M. Mulder, and D. A. Abbink, "Balancing safety and support: Changing lanes with a haptic lane-keeping support system," in *Systems Man and Cybernetics (SMC), 2010 IEEE International Conference on*. IEEE, 2010, pp. 1236–1243.
- [110] M. Li and A. M. Okamura, "Recognition of operator motions for real-time assistance using virtual fixtures," in *Haptic Interfaces for Virtual Environment and Teleoperator Systems, 2003. HAPTICS 2003. Proceedings. 11th Symposium on*, 2003, pp. 125–131.
- [111] Y. Li, J. C. Huegel, V. Patoglu, and M. K. O'Malley, "Progressive shared control for training in virtual environments," in *EuroHaptics conference, 2009 and Symposium on Haptic Interfaces for Virtual Environment and Teleoperator Systems. World Haptics 2009. Third Joint*, 2009, pp. 332–337.

- [112] A. Bettini, P. Marayong, S. Lang, A. M. Okamura, and G. D. Hager, "Vision-assisted control for manipulation using virtual fixtures," *Robotics, IEEE Transactions on*, vol. 20, no. 6, pp. 953–966, 2004.
- [113] A. R. Peon, C. Pacchierotti, and D. Prattichizzo, "Vibrotactile stimuli for augmented haptic feedback in robot-assisted surgery," in *World Haptics Conference (WHC), 2013*. IEEE, 2013, pp. 473–478.
- [114] E. Nuno and L. Basanez, "Haptic guidance with force feedback to assist teleoperation systems via high speed networks," *VDI Berichte*, vol. 1956, p. 213, 2006.
- [115] M. Mihelj and J. Podobnik, "Virtual Fixtures," in *Haptics for Virtual Reality and Teleoperation*. Springer, 2012, pp. 179–200.
- [116] J. G. W. Wildenbeest, D. A. Abbink, H. Boessenkool, C. J. M. Heemskerk, and J. F. Koning, "How operator admittance affects the response of a teleoperation system to assistive forces—A model analytic study and simulation," *Fusion Engineering and Design*, vol. 88, no. 9, pp. 2001–2005, 2013.
- [117] J. J. Abbott and A. M. Okamura, "Analysis of virtual fixture contact stability for telemanipulation," in *Intelligent Robots and Systems, 2003.(IROS 2003). Proceedings. 2003 IEEE/RSJ International Conference on*, vol. 3. IEEE, 2003, pp. 2699–2706.
- [118] W. Kim, F. Tendick, S. Ellis, and L. Stark, "A comparison of position and rate control for telemanipulations with consideration of manipulator system dynamics," *J. of Rob. and Automation*, vol. 3, no. 5, pp. 426–436, 1987.
- [119] F. Mobasser and K. Hashtrudi-Zaad, "Transparent Rate Mode Bilateral Teleoperation Control," *The International Journal of Robotics Research*, vol. 27, no. 1, pp. 57–72, Jan. 2008.
- [120] I. Williams, R.L., F. Harrison, and D. Soloway, "Naturally-transitioning rate-to-force controller for manipulators," in *ICRA*, vol. 1, 1996, pp. 299–304 vol.1.
- [121] S. Tachi and T. Sakaki, "Impedance controlled master-slave manipulation system. Part 1. Basic concept and application to the system with a time delay," *Advanced Robotics*, vol. 6, no. 4, pp. 483–503, Jan. 1991.
- [122] T. Kotoku, "A Predictive Display With Force Feedback And Its Application To Remote Manipulation System With Transmission Time Delay," in *Proceedings of the 1992 IEEE/RSJ International Conference on Intelligent Robots and Systems, 1992*, vol. 1, 1992, pp. 239–246.
- [123] W.-K. Yoon, T. Goshozono, H. Kawabe, M. Kinami, Y. Tsumaki, M. Uchiyama, M. Oda, and T. Doi, "Model-Based Space Robot Teleoperation of ETS-VII Manipulator," *IEEE Transactions on Robotics and Automation*, vol. 20, no. 3, pp. 602–612, Jun. 2004.
- [124] Y. Tsumaki and M. Uchiyama, "A model-based space teleoperation system with robustness against modeling errors," in *ICRA*, vol. 2, 1997, pp. 1594–1599.

- [125] Y. Tsumaki, T. Goshozono, K. Abe, M. Uchiyama, R. Koeppe, and G. Hirzinger, "Verification of an advanced space teleoperation system using Internet," in *IROS*, vol. 2, 2000, pp. 1167–1172.
- [126] L. Huijun and S. Aiguo, "Virtual-Environment Modeling and Correction for Force-Reflecting Teleoperation With Time Delay," *IEEE Transactions on Industrial Electronics*, vol. 54, no. 2, pp. 1227–1233, Apr. 2007.
- [127] F. Mobasser and K. Hashtrudi-Zaad, "Predictive teleoperation using laser rangefinder," in *CCECE*, 2006, pp. 1279–1282.
- [128] A. Achhammer, C. Weber, A. Peer, and M. Buss, "Improvement of model-mediated teleoperation using a new hybrid environment estimation technique," in *ICRA*, 2010, pp. 5358–5363.
- [129] P. Mitra, D. Gentry, and G. Niemeyer, "User perception and preference in model mediated telemanipulation," in *EuroHaptics Conference*, 2007, pp. 268–273.
- [130] B. Willaert, H. Van Brussel, and G. Niemeyer, "Stability of model-mediated teleoperation: discussion and experiments," *Haptics: Perception, Devices, Mobility, and Communication*, pp. 625–636, 2012.
- [131] B. Willaert, J. Bohg, H. Van Brussel, and G. Niemeyer, "Towards Multi-DOF model mediated teleoperation: Using vision to augment feedback," in *HAVE*, 2012, pp. 25–31.
- [132] I. Xu, U. Cizmeci, and C. Steinbach, "Point-cloud-based model-mediated teleoperation," in *2013 IEEE International Symposium on Haptic Audio Visual Environments and Games (HAVE)*, Oct. 2013, pp. 69–74.
- [133] N. Hogan, "Impedance Control: An Approach to Manipulation," in *American Control Conference, 1984*, Jun. 1984, pp. 304–313.
- [134] J. E. Colgate and N. Hogan, "Robust control of dynamically interacting systems," *International Journal of Control*, vol. 48, no. 1, pp. 65–88, 1988.
- [135] R. Bischoff, J. Kurth, G. Schreiber, R. Koeppe, A. Albu-Schaeffer, A. Beyer, O. Eiberger, S. Haddadin, A. Stemmer, G. Grunwald, and G. Hirzinger, "The KUKA-DLR Lightweight Robot arm - a new reference platform for robotics research and manufacturing," *German Conference on Robotics*, pp. 1–8, 2010.
- [136] L. Bainbridge, "Ironies of automation," *Automatica*, vol. 19, no. 6, pp. 775–779, 1983.
- [137] T. Xia, S. Léonard, I. Kandaswamy, A. Blank, L. L. Whitcomb, and P. Kazanzides, "Model-based telerobotic control with virtual fixtures for satellite servicing tasks," in *Robotics and Automation (ICRA), 2013 IEEE International Conference on*. IEEE, 2013, pp. 1479–1484.

- [138] T. Xia, S. Léonard, A. Deguet, L. Whitcomb, and P. Kazanzides, "Augmented reality environment with virtual fixtures for robotic telemanipulation in space," in *2012 IEEE/RSJ International Conference on Intelligent Robots and Systems*. IEEE, 2012, pp. 5059–5064.
- [139] J. Smisek, E. Sunil, M. M. van Paassen, D. A. Abbink, and M. Mulder, "Neuromuscular-System-Based Tuning of a Haptic Shared Control Interface for UAV Teleoperation," *IEEE Transactions on Human-Machine Systems*, vol. PP, no. 99, pp. 1–13, 2016.
- [140] J. Smisek, M. M. van Paassen, and A. Schiele, "Naturally-Transitioning Rate-to-Force Controller Robust to Time Delay by Model-Mediated Teleoperation," in *IEEE International Conference on Systems Man and Cybernetics*, Kowloon, 2015, pp. 3066–3071.
- [141] J. J. Abbott and A. M. Okamura, "Stable forbidden-region virtual fixtures for bilateral telemanipulation," *Journal of Dynamic Systems, Measurement, and Control(Transactions of the ASME)*, vol. 128, no. 1, pp. 53–64, 2006.
- [142] N. Diolaiti, G. Niemeyer, F. Barbagli, and J. Salisbury, "Stability of Haptic Rendering: Discretization, Quantization, Time Delay, and Coulomb Effects," *IEEE Transactions on Robotics*, vol. 22, no. 2, pp. 256–268, Apr. 2006.
- [143] J. Colgate and J. Brown, "Factors affecting the Z-Width of a haptic display," in *Robotics and Automation, 1994. Proceedings., 1994 IEEE International Conference on*, 1994, pp. 3205–3210 vol.4.
- [144] Y. Yokokohji and T. Yoshikawa, "Bilateral control of master-slave manipulators for ideal kinesthetic coupling—formulation and experiment," *IEEE transactions on robotics and automation: a publication of the IEEE Robotics and Automation Society*, vol. 10, no. 5, pp. 605–620, Oct. 1994.
- [145] R. C. Dorf and R. H. Bishop, *Modern Control Systems*, 7th ed. Boston, MA, USA: Addison-Wesley Longman Publishing Co., Inc., 1994.
- [146] J. van Oosterhout, D. A. Abbink, J. F. Koning, H. Boessenkool, J. G. W. Wildenbeest, and C. J. M. Heemskerk, "Haptic shared control improves hot cell remote handling despite controller inaccuracies," *Fusion Engineering and Design*, vol. 88, no. 9, pp. 2119–2122, 2013.
- [147] N. Mol, J. Smisek, R. Babuska, and A. Schiele, "Nested compliant admittance control for robotic mechanical assembly of misaligned and tightly toleranced parts," in *IEEE International Conference on Systems, Man, and Cybernetics*, Budapest, Oct. 2016.
- [148] C. Perez-del Pulgar, J. Smisek, V. F. Muñoz, and A. Schiele, "Using Learning from Demonstration to Generate Real-time Guidance for Haptic Shared Control," in *IEEE International Conference on Systems, Man, and Cybernetics*, Budapest, Oct. 2016.

- [149] X. Xu, B. Cizmeci, C. Schuwerk, and E. Steinbach, "Model-Mediated Teleoperation: Toward Stable and Transparent Teleoperation Systems," *IEEE Access*, vol. 4, pp. 425–449, 2016.
- [150] J. J. Abbott and A. M. Okamura, "Pseudo-admittance bilateral telemanipulation with guidance virtual fixtures," *The International Journal of Robotics Research*, vol. 26, no. 8, pp. 865–884, 2007.

ABBREVIATIONS

4CH	Four channel teleoperation architecture
ANOVA	Analysis of Variance
ASME	American Society of Mechanical Engineers
CAD	Computer-aided Design
DOF	Degrees of Freedom
ESA	European Space Agency
F/T	Force/Torque (Sensor)
HSC	Haptic Shared Control
IEEE	Institute of Electrical and Electronics Engineers
JAXA	Japan Aerospace Exploration Agency
LCD	Liquid-crystal Display
LWR	Lightweight Robot
NASA	National Aeronautics and Space Administration
NMS	Neuromuscular System
PD	Proportional–derivative controller
PF	Teleoperation architecture with position command and force feedback
PID	Proportional–integral–derivative controller
PN	Teleoperation architecture with position command and no feedback
PP	Teleoperation architecture with position command and position feedback
TLX	NASA Task Load Index
UAV	Unmanned Aerial Vehicle

SAMENVATTING

Systematic Framework for Teleoperation with Haptic Shared Control

Jan Smíšek

Teleoperatie, het uitvoeren van taken op afstand door het besturen van een robot, maakt het mogelijk om belangrijke taken uit te voeren die anders onhaalbaar zouden zijn voor mensen. Enkele van de vele mogelijkheden zijn het doen van herstelwerkzaamheden bij nucleaire ongevallen, activiteiten onder water en satelliet onderhoud. Het uitvoeren van taken op afstand kan gedaan worden door middel van hoofdzakelijk twee uiterste besturingsmethoden: *directe telemanipulatie*, welke flexibiliteit biedt, maar continue aandacht van de gebruiker vereist, en *automatisering*, welke flexibiliteit mist, maar superieure prestaties bij voorspelbare en herhalende taken biedt (in het laatste geval is het de rol van de gebruiker om toezicht te houden). Dit proefschrift verkent een derde mogelijkheid, genaamd *haptische gedeelde sturing* (in het Engels: “Haptic Shared Control”, afgekort: HSC), welke tussen de twee uitersten in ligt en in welke de sturingskrachten die de gebruiker uitoefent continue aangevuld worden met automatisch gegenereerd geleidende krachten. In een systeem met haptische gedeelde sturing dragen de gebruikers continu bij aan het uitvoeren van de taak en hierdoor behouden ze hun vaardigheden en blijven ze bewust van de omgeving. Het is gebruikelijk om systemen met haptische gedeelde sturing heuristisch te ontwerpen door middel van iteratief bijstellen tot de ontwerper hier tevreden mee is. Dit is voornamelijk gebaseerd op experimenten waarbij de mens als onderdeel van de besturingscyclus wordt beschouwd.

In dit proefschrift richten we ons op het verbeteren van dit ontwerp en evaluatie proces. Ons doel is het volgen van een systeemtheoretische aanpak en het formaliseren van ontwerp procedures voor systemen met haptische gedeelde sturing voor teleoperatie. Een dergelijke formalisering zou ontwerpers van toekomstige HSC systemen een beter begrip geven en meer controle over het ontwerpproces, met het einddoel om HSC systemen veiliger, eenvoudiger, en intuïtiever te maken en de algehele prestatie te verhogen.

Het onderzoeksdoel in dit proefschrift is opgedeeld in drie onderdelen:

- (1) *Ontwikkeling van methoden die het mogelijk moeten maken om te gaan met onzekerheden die verwant zijn aan de gebruiker en de reactie van de gebruiker op conflicten tussen de mens-machine doelen en verstoringen van buitenaf.*

Gedurende het onderzoek bleek de reactie van de gebruikers op haptische geleidende krachten van significante invloed. De gebruiker en het geautomatiseerde systeem delen de controle over de taak door middel van een gezamenlijke besturingsinterface.

Zodoende zijn de effecten van de haptische krachten op het 'master' input apparaat sterk afhankelijk van de neuromusculaire admittantie toestand van de arm van de gebruiker die de interface vasthoudt en om deze reden is gezocht naar een systematische methode om een optimale schaling van de haptische geleidende krachten te selecteren. Om dit te bereiken is een nieuwe methode voor het identificeren van de gewenste neuromusculaire toestand van gebruikers en de toepassing hiervan op haptische gedeelde sturing gepresenteerd en gevalideerd. Vergeleken met haptische oplossingen die het neuromusculaire systeem buiten beschouwing laten, minimaliseert het voorgestelde systeem de benodigde fysieke werklast van de gebruiker en verbetert tevens het omgevingsbewustzijn.

Het schalen van de haptische geleidende krachten bepaalt het niveau van gezag dat het automatische geleidingssysteem heeft over de sturing van de taken. In de praktijk kunnen taken veranderen als gevolg van externe verstoringen, of door interne conflicten tussen de doelen van het ondersteunende systeem en de gebruiker. Om deze reden zal één niveau van schaling van de geleidende krachten waarschijnlijk onvoldoende zijn en het aanpassen van het gezag over de sturing zal noodzakelijk zijn om deze veranderlijkheid beter te ondersteunen. Derhalve is een strategie voor een geleiding met aanpasbaar gezag, afhankelijk van de grijpkracht van de gebruiker, voorgesteld. Ook worden twee tegengestelde aanpakken voor het verdelen van het gezag over de sturing getest, namelijk het verhogen of het verlagen van de geleidingskrachten afhankelijk van de grijpkracht van de gebruiker. De resultaten tonen aan dat deze nieuwe greep-aanpasbare methode gebruikers in staat stelt om hun prestatie bij handmatige sturing te verhogen en tevens bij systemen met haptische gedeelde sturing met zwakke schaling van de geleidende krachten. Op hetzelfde moment vermindert deze methode de fysieke inspanning van de gebruiker voor het uitoefenen van de sturing die nodig is voor het omgaan met conflicten en verstoringen.

- (2) *Verminder de onzekerheden, behorende bij een teleoperatiesysteem, die veroorzaakt worden door onnauwkeurige kennis van de geometrie van de omgeving op afstand en vertragingen op de communicatie.*

Bij het uitvoeren van contact taken via teleoperatie zorgt de omgeving van de taak voor natuurlijke beperkingen op de handelingen. Systemen met haptische gedeelde sturing baseren de ondersteuning die ze geven op de beschikbare geometrische modellen van de omgeving van de taak. In de praktijk kunnen deze modellen echter een onnauwkeurige vertegenwoordiging van de werkelijke taak en objecten zijn, wat resulteert in foutieve situaties. Hoewel zeer relevant, is deze onderzoeksrichting tot nu toe voor een groot deel verwaarloosd, met enkel een aantal empirische onderzoeken waarin het effect van deze onnauwkeurigheden is geanalyseerd tijdens experimenten met de mens als onderdeel van de sturingscyclus. Derhalve wordt in dit proefschrift een systeemtheoretische methode ontwikkeld om de consequenties van deze onnauwkeurigheden op het teleoperatiesysteem te bestuderen. Een nieuwe systeem beschrijving – die een veelgebruikt framework, ontwikkeld door Dale Lawrence, uitbreidt – wordt voorgesteld om de effecten van onnauwkeurigheden op de veiligheid van taken en de prestatie te quantificeren. De interactie van natuurlijke krachtterugkoppeling (bijv. terugkoppelkrachten gebaseerd op de meting van de krachtsensor op de robothand of gripper)

met haptische geleidende krachten is geanalyseerd. Het bleek dat deze interactie niet triviaal is en mogelijk van groot praktisch belang.

Een tweede doel was het ontwerpen van een systeem met gedeelde sturing om gebruikers te ondersteunen bij het uitvoeren van contact taken via teleoperatie met grote tijdsvertraging op het communicatiekanaal. Om onveilige interacties met de omgeving op afstand te voorkomen moet de stabiliteit van het systeem gewaarborgd worden, terwijl ook de behoefte van de gebruiker om de vertraagde reactie van de slave robot te anticiperen beperkt moet worden. Een nieuwe uitbreiding op het principe van model-bemiddelde teleoperatie voor systemen waarbij de snelheid geregeld wordt, wordt voorgesteld om robuustheid tegen vertragingen te bereiken, vooral voor langere tijdsvertragingen tussen 0.1 en 2 seconden. In plaats van directe uitwisseling van opdrachten en terugkoppeling tussen het aansturende en uitvoerende systeem wordt een model gemaakt van de omgeving op afstand dat continu actueel gehouden wordt aan de kant van het master systeem. De krachtterugkoppeling naar de gebruiker is dan gebaseerd op het lokale model, welke per definitie niet vertraagd is.

(3) *Ontwikkeling van een unificerend kader voor de analyse van haptische systemen met gedeelde sturing.*

In dit derde deel concentreert dit proefschrift zich meer op de ‘machine’ kant van het ontwerpprobleem van HSC systemen. Hier is het streven naar het formaliseren van haptische gedeelde sturing om de effecten te bestuderen die de gebruiker, het communicatiekanaal, en de mogelijke onnauwkeurigheid van de taakmodellen op het gehele systeem kunnen hebben. Een geünificeerd kader wordt voorgesteld om deze uitdagingen aan te pakken. Dit kader maakt de analyse van HSC systemen mogelijk bij alle conventionele teleoperatiearchitecturen en biedt manieren om de effecten van de gebruiker en het teleoperatiesysteem op de algehele prestatie te bestuderen. Theoretische resultaten worden ondersteund door numerieke simulaties en worden experimenteel geverifieerd op een 6-DOF haptische teleoperatieopstelling.

In dit proefschrift zijn experimenteel geverifieerde systematische methodes ontwikkeld om haptische systemen met gedeelde sturing voor teleoperatie te verifiëren. De voornaamste conclusies zijn:

- (1) De aanpak om de sterkte van de haptische terugkoppeling af te stellen op basis van de ‘ontspannen taak’ toestand van het neuromusculaire systeem heeft geleid tot instellingen die gewaardeerd werden door de gebruikers, terwijl ze een bevredigend niveau van taakprestatie behielden met vermindering van zowel fysieke als mentale inspanning.
- (2) Een haptische gedeelde sturing met aanpasbaar gezag, gebaseerd op de grijpkracht van de gebruiker, kan taakprestaties verhogen vergeleken met suboptimaal afgestelde geleidende systemen zonder aanpasbaar gezag. Verder kan de inspanning van de gebruiker voor het overwinnen van incorrecte geleiding significant worden verminderd vergeleken met systemen zonder aanpasbaar gezag.
- (3) De geleidende krachten en de natuurlijke krachtterugkoppeling van HSC systemen werken op een niet-triviale manier op elkaar in. Dit maskeert effectief de mogelijke

onnauwkeurigheden van het geleidende systeem zodat de gebruiker hier niet van op de hoogte is, wat onveilig kan zijn.

- (4) De gepresenteerde systematische methoden kunnen werkelijk gebruikt worden om nauwkeurige voorspellingen te maken over de prestatie van het bestudeerde tele-operatiesysteem met toegevoegde haptische geleiding, aangezien de voorspellingen door zowel numerieke simulaties als experimentele testronden bevestigd zijn.

De volgende aanbevelingen kunnen gedaan worden voor vervolgonderzoek:

- (a) De gepresenteerde methoden zouden uitgebreid moeten worden door verder te kijken dan haptische gedeelde sturing tot een nog algemener kader van gedeelde sturing, bijvoorbeeld door het opnemen van benaderingen uit de literatuur die het automatiseringsproces direct de input van het bestuurd systeem laten aanpassen.
- (b) De toepasbaarheid van de gepresenteerde bevindingen zou verder onderzocht moeten worden in alledaagse taken en op de rand van het ontwerpgebied van HSC systemen.
- (c) Een volgende stap zou moeten zijn om van systematische analyse richting systematisch ontwerp te gaan, d.w.z. het inzicht dat vergaard is door het gebruik van de gepresenteerde methoden zou direct in het ontwerpstadium toegepast moeten worden om controllers met haptische gedeelde sturing af te stellen.

ACKNOWLEDGEMENTS

This dissertation could not have been imagined, let alone conceived, without the help of my supervisory team, my great colleagues at ESA and TU Delft, my fellow H-Haptics project researchers, my friends, my parents, and my partner. I would like to express a warm *thank you* to all of you!

More specifically, I would like to thank André for giving me the opportunity to pursue this exciting research in his lab. Perhaps even more so, thank you for taking me along for this amazing journey that led to performing real teleoperation experiments from onboard of the International Space Station.

I am grateful to René for his valuable guidance, support, and feedback throughout this research project. Thank you for always having the patience to answer my (admittedly at times not so well defined) questions.

I would like to thank Max for supporting my work and being a great promotor. Thank you for always knowing what to do, especially in the final (i.e., most critical and stressful) parts of the work on the thesis!

I am grateful for the support of my friends and colleagues of the ESA Telerobotics and Haptics Lab. Your help has truly been essential for this work. For the last busy years working on space robots, I hardly could have hoped for a better team! Namely, I would like to thank Eloise, Thomas, Frank, Emiel, Thom, and Alex for their professional support and friendship throughout the past years. A particular ‘thanks’ goes to my fellow Ph.D. candidates in the lab, both former and current, João, Stefan, and Manuel. I very much enjoyed our discussions, both while traveling together to give demos or presentations at conferences, but also during more social occasions (e.g., Friday beers). Furthermore, I would also like to acknowledge all the people at ESA who have directly or indirectly supported my research.

My gratitude also goes to my TU Delft colleagues at the Control and simulation department: Bertine, Daan, Ajenk, João, Tommaso, Jaime, Sophie, Jacco, Clark, Joost, Olaf, Erik-Jan, Ping, Marilena, Xander, Hans, Ferdinand, Andries, Harold, Alwin, Gijsbert, Herman, Maarten, Rolf, Gustavo, Deniz, Jan, Rita, Herman, Yazdi, Henry, Tim, Ivan, Kirk, Emmanuel, Kasper, Annemarie, Isabel, Julia, Kimberly, Dirk, Matěj, Kevin, Lodewijk, Andries, Roland, Jerom, Peng, Haibo, Shaojie, Jia, Ligu, Tao, Ye & Ye, Hann, Yingzhi, Junzi, Sherry, Shuo. Thank you for your help and support, for making me feel welcome each time I was passing by, and generally for the many enjoyable moments over the years.

I would like to thank my fellow shared control researchers of the H-Haptics project: Frans, David, Tricia, Femke, Irene, Jack, Teun, Denis, Patrice, Jeroen, Henri, Nick, Arvid, Roel, Bram, Debjyoti, and Winfred. I very much enjoyed the time spent together at the Autumn symposia and during various conference across the globe. I also appreciate the support of the Dutch Technology Foundation STW to the H-Haptics project.

I am grateful to the M.Sc. students I have the opportunity to work with during my Ph.D., Emmanuel, Mats, and Nicky. Thank you for the great experience of learning from each other. I am also very grateful to the many volunteers that offered their time to participate in our human-in-the-loop experiments.

I would like to thank the ‘Czechoslovak group’ of ESA ESTEC for their friendship and support; namely, my gratitude goes to Markéta, Maria, Anna, Dagmar, Katarina, Petra, Dušan, Marek, Milan, Přemysl, Václav, Zdeněk, Adam, Dan, Jakub, and both Jans. Thank you for making me feel ‘at home’ and for providing the most welcome distraction during the more stressful parts of my research. I especially enjoyed our nice Friday lunch discussions, with topics ranging widely from the effects we humans have on our planet’s ecosystem to the importance of Jimmy Choo for the footwear industry.

I would like to thank my friends and family, especially my parents, for their continuous support while I am away chasing my dreams. Finally, my biggest thanks go to Klara. Thank you for your loving support, patience, and encouragement!

CURRICULUM VITÆ

Jan Smíšek was born on 19th of August 1986, in Městec Králové, Czech Republic. He grew up in Poděbrady, a small spa town in the midst of Czech Republic, where he attended the Gymnázium Jiřího z Poděbrad grammar school.

Since 2006, he studied at the Faculty of Electrical Engineering, Czech Technical University in Prague, Czech Republic, where he, in 2009, obtained his Bachelor's degree in Cybernetics and Measurements, specializing in Control Engineering.

After graduating, he decided to combine the background in control engineering with his life-long fascination for space exploration and enrolled to the *SpaceMaster* program, a Joint European Master in Space Science and Technology. During the program, he studied at Julius-Maximilians-Universität, in Würzburg, in northern Bavaria, Germany and at Luleå Tekniska Universitet, at the Kiruna Space campus, in the very north of Sweden. In 2011, he graduated with a double Master's degree, with an M.Sc. in Systems and Control (*cum laude*) from Czech Technical University in Prague and with an M.Sc. with a Major in Space Technology from Luleå Tekniska Universitet.

Since 2012, he started working toward his Ph.D. degree at the Control and Simulation Department, Faculty of Aerospace Engineering, Delft University of Technology, in Delft, The Netherlands. Also in 2012, he joined, as a Robotics Engineer, the Telerobotics and Haptics Laboratory at the European Space Research and Technology Centre (ESTEC), European Space Agency (ESA), in Noordwijk, The Netherlands. So far, Jan contributed to the development of three ESA teleoperation flight experiments performed by astronauts from onboard the International Space Station.



PROFESSIONAL ACTIVITIES

- Reviewer for the IEEE Transactions on Human-Machine Systems (THMS)
- Reviewer for the IEEE Robotics and Automation Letters (RA-L)
- Reviewer for the Journal of Human-Robot Interaction (JHRI)
- Reviewer for the IEEE International Conference on Intelligent Robots and Systems (IROS)
- Reviewer for the IEEE International Conference on Robotics and Automation (ICRA)
- Reviewer for the IEEE International Conference on Systems, Man, and Cybernetics (SMC)
- Reviewer for the IEEE/ASME International Conference on Advanced Intelligent Mechatronics (AIM)
- Member of the IEEE SMC Technical Committee on Shared Control

LIST OF PUBLICATIONS

- **Jan Smisek**, Winfred Mugge, Jeroen B. J. Smeets, Marinus M. van Paassen, and Andre Schiele, “Operator adaptable haptic guidance: A modeling approach to predict performance under external disturbances”, IEEE Transactions on Haptics, 2017 (in revision)
- **Jan Smisek**, Emmanuel Sunil, Marinus M. van Paassen, David Abbink, and Max Mulder, “Neuromuscular-System-Based Tuning of a Haptic Shared Control Interface for UAV Teleoperation”, IEEE Transactions on Human-Machine Systems, 2016 (in press)
- Nicky Mol, **Jan Smisek**, and Andre Schiele, “Nested compliant admittance control for robotic mechanical assembly of misaligned and tightly toleranced parts”, IEEE International Conference on Systems, Man, and Cybernetics, Budapest, 2016
- Carlos Perez-del-Pulgar, **Jan Smisek**, Victor Munoz, and Andre Schiele, “Using Learning from Demonstration to Generate Real-time Guidance for Haptic Shared Control”, IEEE International Conference on Systems, Man, and Cybernetics, Budapest, 2016
- Andre Schiele, Thomas Krueger, Stefan Kimmer, Manuel Aiple, Joao Rebelo, **Jan Smisek**, Emiel den Exter, Eloise Matheson, Alejandro Hernandez, and Frank van der Hulst, “Haptics-2 – A system for bilateral control experiments from space to ground via geosynchronous satellites”, IEEE International Conference on Systems, Man, and Cybernetics, Budapest, 2016
- Andre Schiele, Manuel Aiple, Thomas Krueger, Frank van der Hulst, Stefan Kimmer, **Jan Smisek**, and Emiel den Exter “Haptics-1: Preliminary Results from the First Stiffness JND Identification Experiment in Space”, Haptics: Perception, Devices, Control, and Applications, Springer International Publishing, 2016
- **Jan Smisek**, Marinus M. van Paassen, and Andre Schiele, “Haptic guidance in bilateral teleoperation: Effects of guidance inaccuracy”, IEEE World Haptics Conference, Evanston, 2015
- **Jan Smisek**, Marinus M. van Paassen, and Andre Schiele, “Naturally-transitioning Rate-to-Force Controller Robust to Time Delay by Model-mediated Teleoperation”, IEEE International Conference on Systems, Man, and Cybernetics, Kowloon, 2015
- Stefan Kimmer, **Jan Smisek**, and Andre Schiele, “Effects of Haptic Guidance and Force Feedback on Mental Rotation Abilities in a 6-DOF Teleoperated Task”, IEEE International Conference on Systems, Man, and Cybernetics, Kowloon, 2015
- **Jan Smisek** and Andre Schiele, “A New Free Floating Satellite Dynamics Test-bed for Hardware-in-the-Loop Docking Experiments”, Symposium on Advanced Space Technologies in Robotics and Automation, Noordwijk, 2015
- Carlos Perez-del-Pulgar, **Jan Smisek**, Victor Munoz, and Andre Schiele, “Haptic guidance to solve the peg-in-hole task based on learning from demonstration”, Machine Learning in Planning and Control of Robot Motion (Workshop at IROS 2015), Hamburg, 2015

- Joao Rebelo, Stefan Kimmer, Eloise Matheson, Emiel Den Exter, **Jan Smisek**, Thomas Krueger, and Andre Schiele, "A System for Space-to-ground Multi-dof Bilateral Teleoperation", Symposium on Advanced Space Technologies in Robotics and Automation, Noordwijk, 2015
- **Jan Smisek**, Winfred Mugge, Jeroen B. J. Smeets, Marinus M. van Paassen, and Andre Schiele, "Adapting Haptic Guidance Authority based on User Grip", IEEE International Conference on Systems, Man, and Cybernetics, San Diego, 2014
- Emmanuel Sunil, **Jan Smisek**, Marinus M. van Paassen, and Max Mulder, "Validation of a Neuromuscular Analysis Based Tuning Method for Haptic Shared Control Systems", IEEE International Conference on Systems, Man, and Cybernetics, San Diego, 2014
- Andre Schiele, Maneul Aiple, Frank van der Hulst, Thomas Krueger, Joao Rebelo, **Jan Smisek**, Stefan Kimmer, and Emiel Den Exter, "Toward the First Force-Reflection Experiment on the International Space Station", International Symposium on Artificial Intelligence, Robotics and Automation in Space, Montreal, 2014
- **Jan Smisek**, Marinus M. van Paassen, David Abbink, and Max Mulder, "Neuromuscular analysis based tuning of haptic shared control assistance for UAV collision avoidance", IEEE World Haptics Conference, Daejeon, 2013
- **Jan Smisek**, Michal Jancosek, and Tomas Pajdla, "3D with Kinect", Consumer Depth Cameras for Computer Vision, Springer International Publishing, 2013
- **Jan Smisek**, Michal Jancosek, and Tomas Pajdla, "3D with Kinect", IEEE International Conference on Computer Vision, Barcelona, 2011



ISBN: 978-94-028-0612-0